57

1. SAMPLE ILLUMINATION OPTICS FOR RAMAN SPECTROCSCOPY

2. GAS PHASE RAMAN SPECTRA FOR SOME CF_3OOX COMPOUNDS, (X = H,D,F, and Cl)

by

AJIT SINGH MANOCHA
B.S. University of Delhi, 1969

A MASTER'S THESIS

submitted in partial fulfillment of the

requirements for the degree

MASTER OF SCIENCE

Department of Chemistry

KANSAS STATE UNIVERSITY
Manhattan, Kansas

1978

Approved by:

Robert M. Hammaker
Major Professor

TABLE OF CONTENTS

PART I

SAMPLE ILLUMINATION OPTICS FOR RAMAN SPECTROSCOPY

LIST OF TABLES

PART I

SAMPLE ILLUMINATION OPTICS FOR RAMAN SPECTROSCOPY

LIST OF FIGURES

PART I

SAMPLE ILLUMINATION OPTICS FOR RAMAN SPECTROSCOPY

TABLE OF CONTENTS

PART II

GAS PHASE RAMAN SPECTRA FOR SOME CF_3OOX COMPOUNDS (X = H, D, F, AND Cl)

LIST OF TABLES

PART II

GAS PHASE RAMAN SPECTRA FOR SOME CF_3OOX COMPOUNDS (X = H,D,F, AND Cl)

LIST OF FIGURES

PART II

GAS PHASE RAMAN SPECTRA FOR SOME CF_3OOX COMPOUNDS (X = H, D, F, AND Cl)

APPENDIX A

I. Sample Illumination Optics for Raman Spectroscopy

A. Introduction

In this part the system for Raman spectroscopy in the Department of Chemistry at Kansas State University is described. The emphasis is on the sample illumination optics which are a combination of commercially available items and items designed and constructed at Kansas State University. The system may be divided into four parts as follows: (1) Lasers, (2) Double Monochromator, (3) Detection System, and (4) Sample Illumination Optics.

The first three parts are commercially available systems and are described briefly in the Sections B, C, and D. The sample illumination optics are designed with convenience and versatility as a major consideration. The objective is to allow easy interchange between accessories for gases, liquids (including a low temperature cell, and sample rotating spinning devices) and solids (including a sample rotating device). The sample illumination optics are described in Section E and the sources of optical and mechanical components used are listed in Section F. Section G describes components fabricated in the Department of Chemistry Shop. Some examples of the performance of the system are given in Section H.

B. Lasers

The illumination source in this work is a Spectra-Physics, Model 164-03 Ar^+ laser. The main output lines are 488.0 nm and 514.5 nm. The maximum output power at 514.5 nm is 2.2 watts and the beam width is about 1-2 mm. The system includes a Spectra-Physics, Model 375 CW dye-laser. Both lasers are placed on the alignment plate supplied by Spectra-Physics. The Ar^+ laser has multi-line output-power of approximately 4.0 watts and

is used to pump the dye-laser system. The dye-laser can be tuned throughout the visible range; however, in this research we are mainly interested in the orange-red region. For this region, the common dyes used are Rhodamine-B and Rhodamine-6G. Rhodamine-B is good for the range 590-690 nm with maximum output at about 620 nm of about 350 mW. For Rhodamine-6G the output is in the range 560-660 nm with maximum power of about 600 mW at about 590 nm. The band width of the dye laser is about 0.3 nm using a standard tuning etalon; however, a fine-tuning etalon is available to further reduce the band width to 0.05 nm.

A Metrological Instruments, Model 60-530 laser-power radiometer is used to measure the output power of the dye laser. The power range of this radiometer is from 0 to 30 watts with flat response less than 10%. The frequency range of this radiometer is 400-800 nm.

C. Double Monochromator

The monochromator is a Spex 14018, 0.85 Meter Czerny-Turner Double Monochromator Spectrometer, f/7.8, with wave-number Compudrive which consists of Stepper-motor and TTL-compatible digital control unit. The monochromator ia able to accomodate JOBIN-YVON 1800 gr/mm holographic gratings (110 x 110 mm ruled area). The gratings are fixed in a kinematic mount for easy interchange. Entrance, intermediate and exit slits open bilaterally to 3 mm width and 20 mm height. The entrance slit has a 3-step height adjustment. This monochromator also has the Spex 1450 periscope viewer, for accurate positioning of micro-size sample and single cryatal by viewing from the inside of the entrance slit toward the sample. The minimum resolution specification is 0.5 cm^{-1} or better at 19436 cm^{-1} (without mask and at full aperature). Spectral range is 11,000-31,000 cm^{-1}.

D. Detection System

The detection system utilizes the RCA C31034 Ga-As cathode, photomultiplier tube with the Spex 1730RF water-cooled thermoelectric cryostat to detect the Raman scattering. The dark count is less than 30 pps at $-30^{\circ}C$. The Spex 1425 Photomultiplier Protector is mounted in the Spex 14018 Double Monochromator to protect against the exposure of the photomultiplier tube to dangerously high intensity light. The counting system is a Princeton Applied Research Quantum Photometer, Model 1140 AC. Count rate sensitivity is 10^1 to 10^6 cts/sec full scale. Discriminator output is positive pulse TTL compatible and the output is linear as well as logrithmic with 100 mV full scale deflection. The addition of two 62 ohm resistors to the Princeton Applied Research 1140 A/C is specified by Spex to reduce the PAR 1140 A/C output from 1.0 V to 100 mV DC. The model 1140 C remote preamplifier/discriminator is contained in an extruded aluminum box with the power/signal connector at one end and the input (BNC connector) at the other.

The signal is recorded by a Toshin Recorder Model T02NI-L with 100 mV full scale deflection. Sensitivity is $\pm$ 0.15% of full scale. Chart speeds are 10, 20, 30, 50, 60, 100, 120, 150, 300, and 600 mm/min, hour. Accuracy is $\pm$ 0.3% of full scale.

The other important part of the equipment is the Spex Compudrive which monitors the forward and the reverse slew, wavenumber marker and 15 different scan speeds. The lower and upper limits of the drive are 0.002 cm^{-1}/sec and 100 cm^{-1}/sec respectively. An event marker provides a mark every 1 cm^{-1}, 10 cm^{-1} or 100 cm^{-1}, preselected for the experiment.

E. Sample Illumination Optics

In this section the sample illumination optics are discussed in detail.

First the major optical requirements are listed and a general diagram for their arrangement is shown. Then some information about sampling and sample positioning is presented. Discussion of some details of various special optical components completes this section. All mechanical components which are not commercially available were built in the Department of Chemistry Shop by Mr. Al Nielson.

1. Major Optical Requirements

In this thesis the term sample illumination optics includes the optical components between the laser head and the monochromator slit. The required functions of the optical section are the following:

(1) Elimination of nonlasing plasma lines from the Ar^+ laser and the fluorescent background of the dye laser.

(2) Rotation of the plane of polarization of the incident laser beam.

(3) Focusing the laser beam to a spot on the sample.

(4) Collection of the scattered radiation and focusing on the monochromator slit.

The configuration chosen is shown in Figure 1. The output beam of either the Ar^+ laser or the dye laser passes through a constant deviation (Pellin Broca) prism and changes direction by 90°. The beam leaving the prism in a downward direction changes direction by 90° to horizontal and by 90° to vertical upward by 45° incidence on two plane mirrors (M1 and M2). Following passage through an aperture, a polarization rotator and a focusing lens, the beam impinges on the sample from below. A collection lens receives and focuses the radiation scattered at 90° in a horizontal direction onto the monochromator slit.

Explanation of Figure 1

Block diagram of the configuration for Raman sample illumination optics

S is the slit of Spex 14018 double monochromator.

C is the collection lens.

FL is the focussing lens.

PR is the polarization rotator.

AP is the aperture.

W_1 and W_2 are 45 degrees angle wedges.

M_1 and M_2 are plane mirrors in mirror holders mounted on wedges W_1 and W_2, respectively.

PBP is the constant deviation prism supported on a special mount with X, Y, Z translational and one rotational degrees of freedom.

SP-375 is the Spectra Physics Model 375 c.w. dye laser.

SP-164-03 is the Spectra Physics Model 164-03 Ar^+ laser.

The choice of axes is shown in the upper right hand corner of the figure.

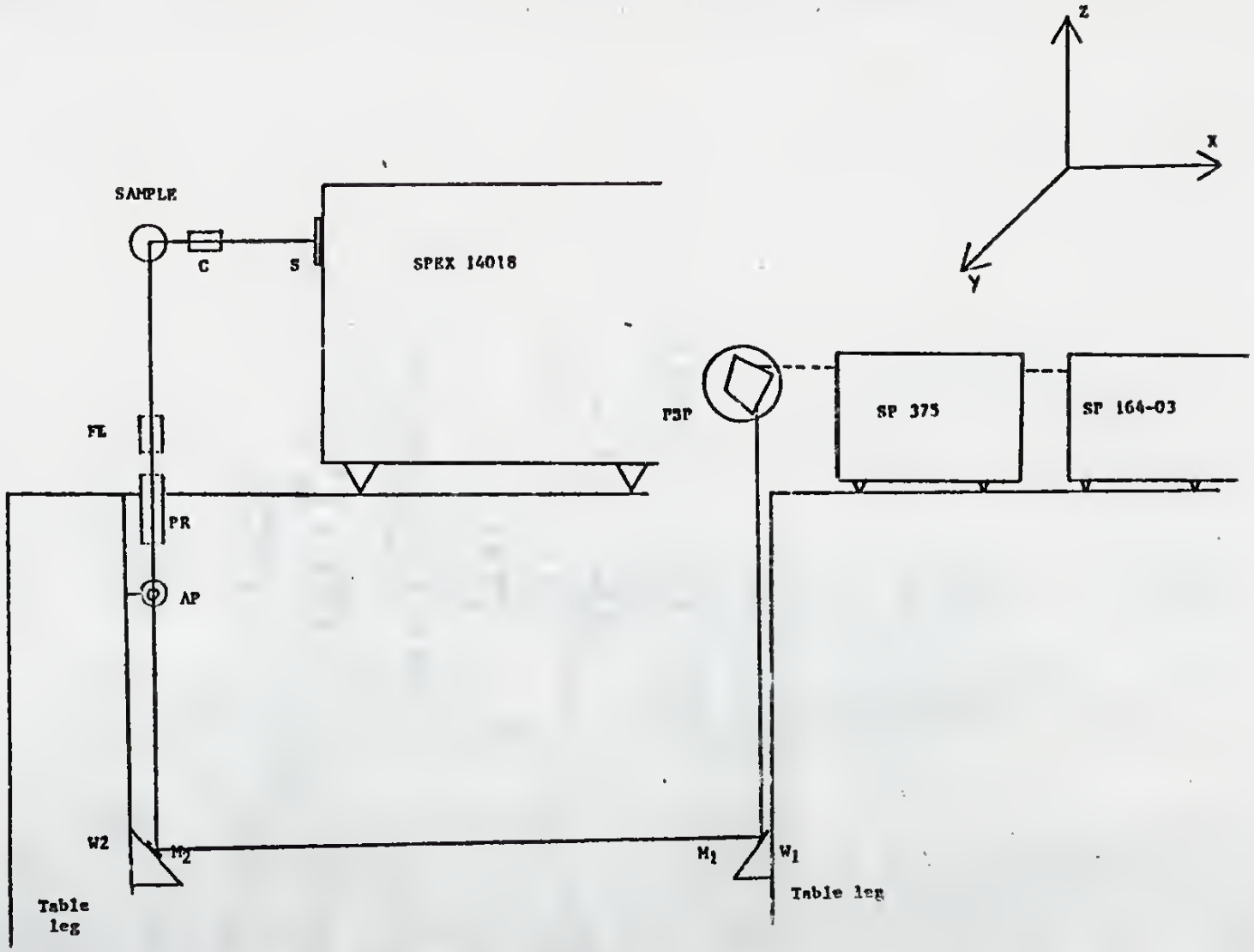
Z
X
Y
SAMPLE
C
S
SPEX 14018
P3P
SP 375
SP 164-03
FL
PR
AP
W2
M2
M1
W1
Table leg
Table leg

Figure 1

2. Sampling

a. Solids

Solids to be examined may be placed in capillary tubes or pressed into pellets. A spinning device has been constructed to rotate colored samples thus minimizing the local heating of the sample due to the laser beam (1). A description of the spinning device built in the machine shop is given in Section G-3. Various solid samples (colored as well as white or colorless) have been successfully examined with this system. A few of the spectra are described briefly in Section H. Figure 2 shows the arrangements in the case of solid samples in the form of pellets. For single crystal samples more sophisticated arrangements are necessary.

b. Liquids

Liquids are examined in conventional liquid cells, capillary cells, a special low temperature cell, and rotating cells. Practically any glass or quartz container can be used depending upon the properties of liquids to be studied. The liquid cell used in these experiments is the cell supplied by the Japan Spectroscopic Company (JASCO) for use with the JASCO Model R-300 Laser Raman Spectrophotometer. The capacity of this cell is 0.3 ml and it has quartz windows and a filling arm which accepts a teflon stopper. Similarly a capillary cell can be used provided the liquid is stable at room temperature. However, for liquids having very low boiling points, a low temperature cell was constructed. The description of this cell is given in Section G-3 and Figures 12 and 12A. The design closely follows that of Brown, Hopkins and Daly (2). This cell has been used successfully for various samples having low boiling points. An adapter for a rotating liquid cell holder has also been constructed. See Section G-3, Figure 11. The results using this rotating

Explanation of Figure 2

Schematic of the spinning arrangement for solids

SM is the spinning motor.

U is the universal sample holder discussed in Section G-3.

S is the entrance slit of the Spex 14018 double monochromator.

P is the sample in the form of a pellet fastened to a disc attached to the shaft of SM.

Note for the colored sample the beam must strike the pellet off the axis of rotation so that as the sample spins the beam traces a circle around the axis rather than striking the same spot on the sample.

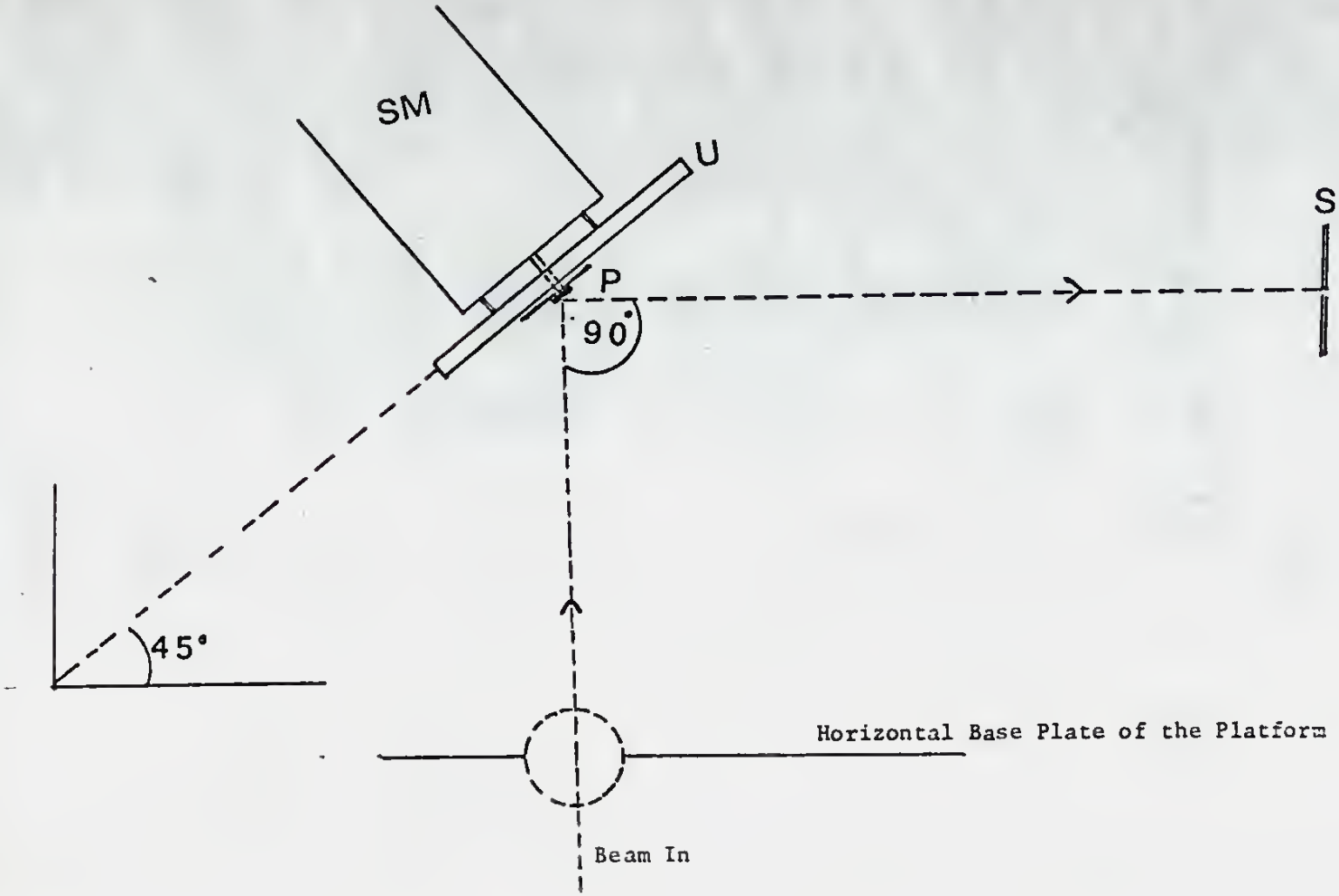

Figure 2

liquid cell have been satisfactory.

c. Gases

The study of gases involves addition modifications. Our apparatus is designed around the Spex 1443 A External Resonating Cavity (ERC) accessory (7). The ERC has a set of two spherical mirrors arranged parallel to each other so each mirror returns a ray of light to the other mirror. The gas cell is constructed so that the windows are at an angle of 57^{o} (the Brewster angle) to the entering laser radiation. This cell is placed between the two mirrors (see Figure 3). The laser beam is reflected between the two mirrors several times and each beam passes through the same point in the center of the cell. This arrangement increases the light flux at the cell center and thus increases the intensity of the Raman scattering (see Figure 3).

3. Sample Positioning

The sample handling system has X, Y, and Z degrees of freedom. These directions are defined in Figure 4. Having these degrees of freedom to align a sample has proved to be a significant convenience. Details of the device which allows X, Y, and Z direction motion are presented in Section G-3.

Rotation as well as translation of the sample is important in viewing pellets where the beam impinges onto the front surface of a pellet glued to a rotating disc (Figure 2). Here the scattered beam is collected at 90^{o} to the incident beam. In most of the cases the pellet is kept at 45^{o} to the horizontal plane but other angles may be selected. Details of the device for rotation of the sample are presented in Section G-3.

Another degree of freedom in positioning the sample is the depth

Explanation of Figure 3

Multipass arrangement in gas cell using the Spex ERC

M_1 and M_2 represent the spherical mirrors of the ERC (External Resonating Cavity).

G is the gas cell having windows at the Brewster angle.

S is the entrance slit of the Spex 14018 double monochromator.

Note that the scattered light goes to the slit in the X direction.

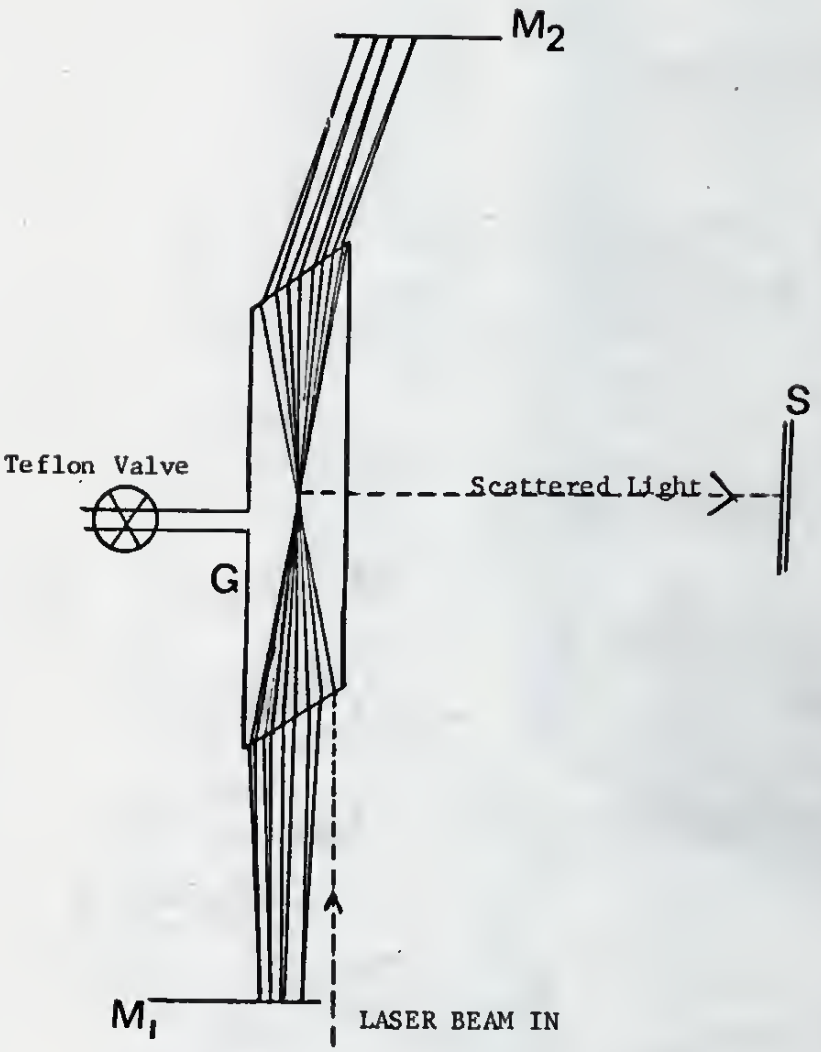

Figure 3

Explanation of Figure 4

The choice of axes

This figure shows the choice of axes to fully describe the operation of the sample illumination optics.

The Y-axis is coming out of the plane of the paper.

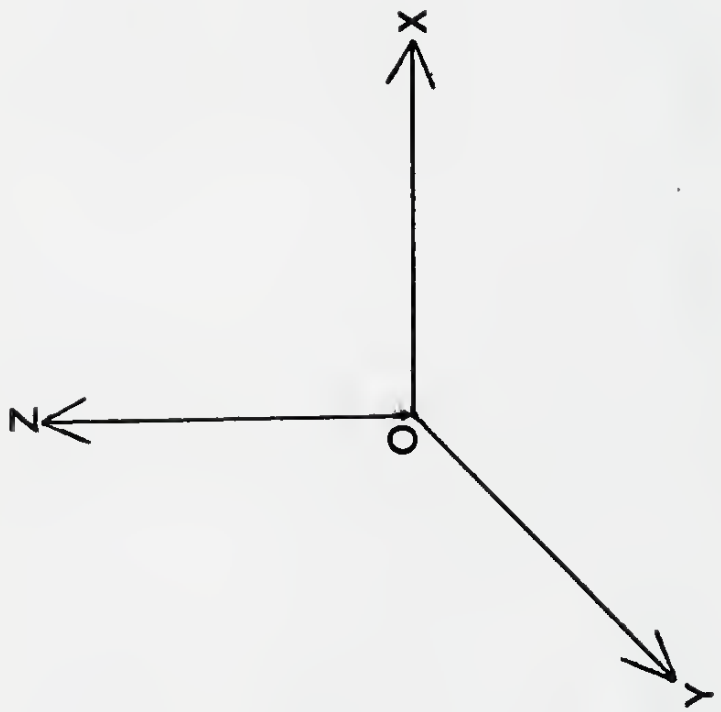

Figure 4

adjustment in the focal plane of the monochromator. For different samples the collection lens is moved to different poaitions due to different sizes of sample holding devices. This motion of the collection lens results in poor matching of light cones at the entrance slit of the monochromator. To minimize this loss of efficiency, the distance between the monochromator slit and whole system consiating of sample cell and collection lens can be varied. Details of the mechanical components to vary this distance are presented in Section G-2. Figure 5 ahowa details of matching light cones or f/number between the collection lena and the monochromator.

4. Optical Components

a. Constant deviation (Pellin-Broca) prism

It is important to reject non lasing plasma linea from the Ar^+ laser and fluorescent background from the dye-laser. A constant deviation prism as shown in Figure 6 is employed for this purpose. This prism works on the principle of total internal reflection (3). If the polarization vector of the incident radiation is in the plane of incidence it will remain in the plane of incidence upon reflection and if the polarization vector is perpendicular to the plane of incidence it will remain so upon reflection. After the beam emerges from the prism, the non lasing lines are slightly displaced in space from the laser line of interest. (The angle of refraction will be different for lines of different wavelengths)(4). The dispersed beam travels approximately 6 to 7 feet from the prism to an aperature after twice changing direction by 90° from 45° incidence on plane mirrors. The deviation of the different wavelengths in this distance is sufficient that only the desired

Explanation of Figure 5

Positioning of the collection lens CC with respect to the slit S

CC is the collection lens.

mm is the first collimating mirror inside the Spex 14018 double monochromator.

S is the entrance slit.

LOM is the optical axis (collinear with X-axis shown in Figure 4).

The f/number of the monochromator is 7.8.

For CC, the f/number = do/Do, where do is the distance LO and Do is the diameter of the lens CC.

Do = 36 mm for the Automatic Miranda lens.

In order to match the cones COC and mOm, the f/number of the external optics should be 7.8 also.

Therefore, LO = do = 7.8 x 36 mm = 280.8 mm.

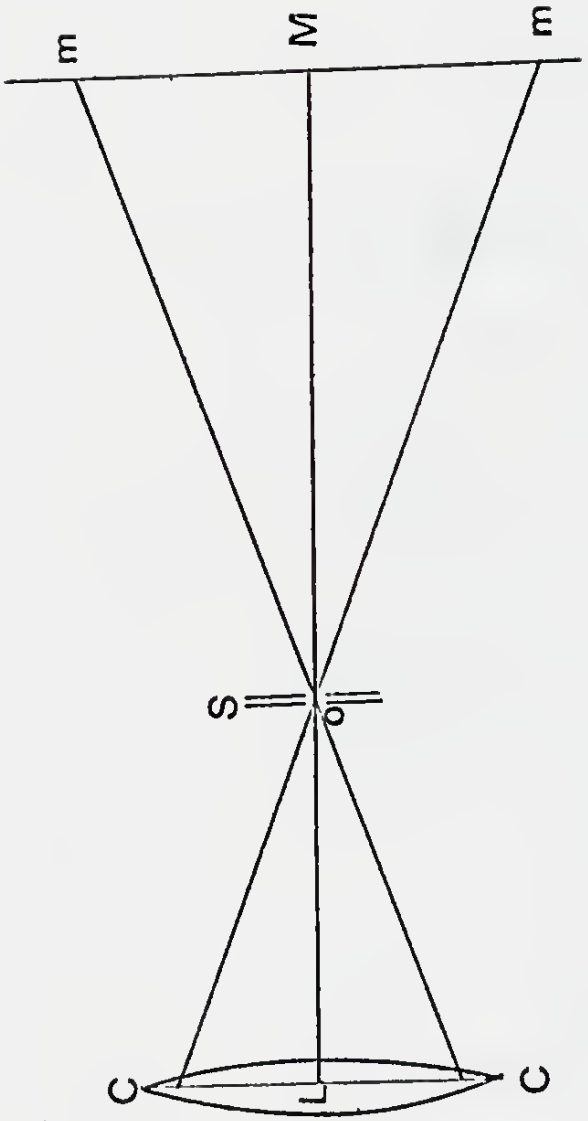

Figure 5

Explanation of Figure 6

The constant deviation (Pellin Broca) prism

RD is the revolving disc.

PBP is the Pellin Broca prism.

ϕ is an angle between the laser beam and the normal to the refracting surfaces.

The choice of axes (Figure 4) is shown in the upper right hand corner.

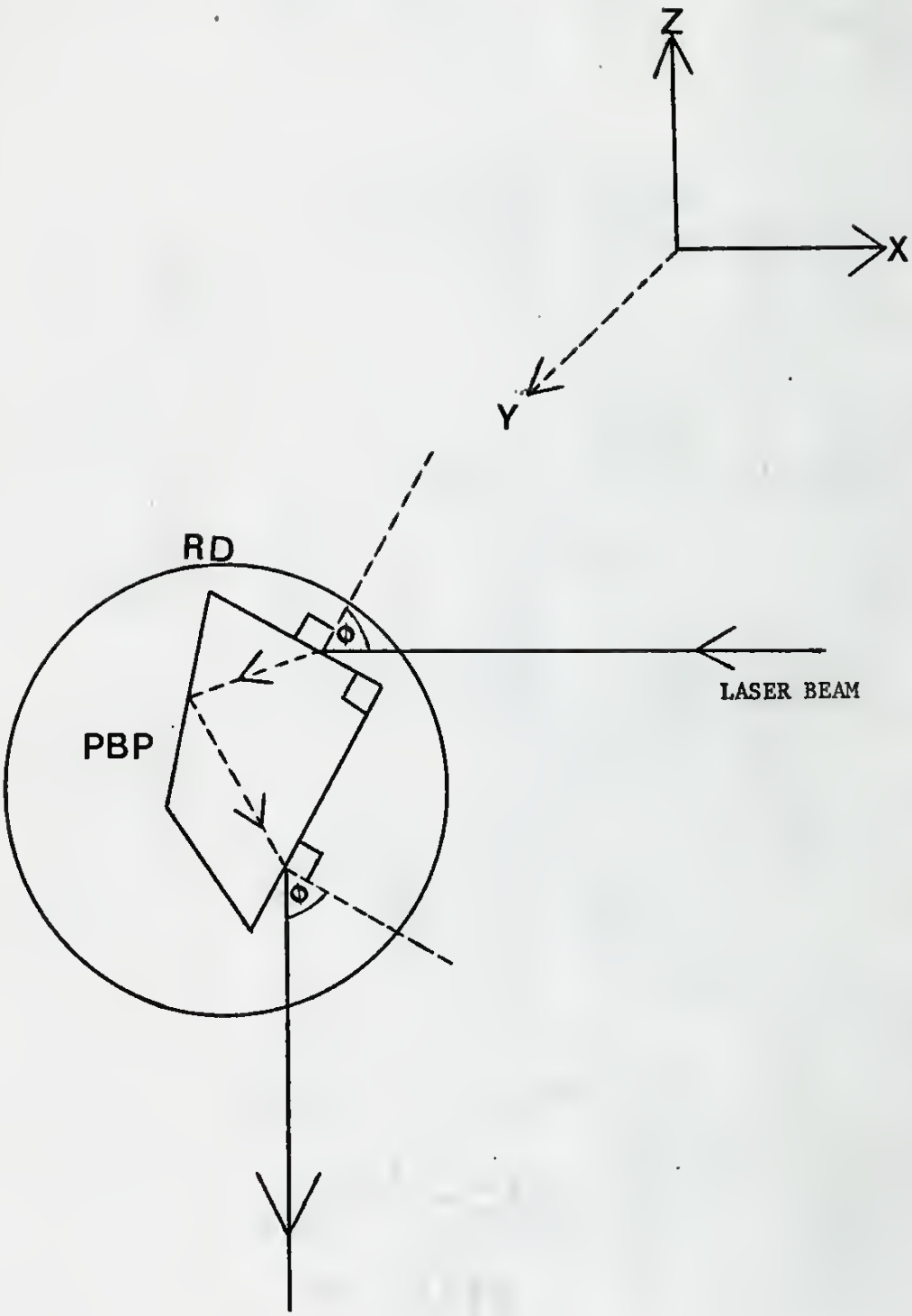

Figure 6

laser line will pass through the aperture (see Figure 1). The other wavelengths are rejected by beam stops.

b. Polarization rotator

The Spectra-Physics Model 310-21 Broadband Polarization Rotator is used to rotate the plane of polarization of the incident laser beam. The constant deviation prism transmits different polarizations with different efficiencies; but the most efficiently transmitted polarization is vertical. Comparable with this is the laser output which also has vertical polarization. Consequently, the polarization is not to be rotated from vertical until after the beam has passed through the constant deviation prism. In the configuration shown in Figure 1, a convenient location for the polarization rotator is between the aperture and the focussing lens. With this configuration and no analyzer or scrambler between the sample and the monochromator slit, depolarization measurements are made by method IV of Claassen, Selig, and Shamir (5). With the polarization rotator in this position, it is possible to use all eight methods of measuring depolarization ratios outlined by Claassen, Selig, and Shamir (5) and by Allemand (6) when the appropriate additional optical components are properly located. For routine survey spectra where polarized lines have their maximum intensity, the beam emerging from the aperture (Figure 1) must have its polarization plane rotated by 90^{o}. If the broadband polarization rotator were not located here, the required rotation of the plane of polarization of the incident beam would necessitate a half-wave plate at this location for each laser line used.

c. Focussing lens

The Spex External Resonating Cavity (ERC) is equipped with a 192 mm

focal length lens. In the Spex 1419 A Raman Illuminator a 60 mm focal length lens is used to focus the laser beam to a spot on solid and liquid samples, therefore, this lens must be removed and replaced by the 192 mm focal length lens to allow the mounting of the ERC accessory for studying gases. It is most convenient to use the 192 mm focal length lens for all samples. Then it is not necessary to change focussing lenses for various solids, liquids or gases. In addition, this 192 mm focal length lens makes the design of mechanical components much simpler. Consequently, the 192 mm focal length lens can be regarded as a permanent part of our configuration and is mounted along with the polarization rotator on an L shape plate (see Figure 7). This L shaped plate is bolted to a stack of translation stages having motion in the X, Y, and Z directions as defined in Figure 4. One disadvantage of this arrangement is that the longer focal length lens is not expected to give as sharp a spot on the sample from the focussed laser beam as would the 60 mm focal length lens. In practice, this effect is not serious as good quality spectra of solids and liquids are obtained. It is possible that at some future time it will be advantageous to make provisions to use a 60 mm focal length lens with liquids and/or solids.

d. Collection lens

Three different camera lenses are available for use as collection lenses as follows: (1) Automatic Miranda, focal length 50 mm, minimum f-stop 1.4; (2) Pentax Super Multi-coated Takumar, focal length 50 mm, minimum f-stop 1.4; (3) Leitz Wetzlar Noctilux, focal length 50 mm, minimum f-stop 1.2.

The work described in this thesis used the Automatic Miranda lens

Explanation of Figure 7

Raman sample illumination system

S is the entrance slit of the Spex 14018 double monochromator.

C is the collection lens.

SD is the device for sliding the whole platform with respect to the monochromator.

HBP is the horizontal base plate.

T_1, T_2, T_3, & T_4 are the translation stages providing X, Y, Z degrees of freedom to the accessories supported on them.

FP is the front plate.

VP_1 is the vertical plate of the main platform.

VP_2 is the vertical plate fixed on HBP in the -Z direction supporting a mount for aperture AP and wedge W for mirror M_2.

U is the universal sample holder.

HSP is the horizontal slide plate.

CR is the circular ring to give an angular degree of freedom.

VSP is the vertical slide plate.

HMP is the horizontal moving plate.

BP is the back plate.

VFP is the vertical fixed plate.

FL is the focusing lens.

PR is the polarization rotor.

The choice of axes is the same as Figure 4.

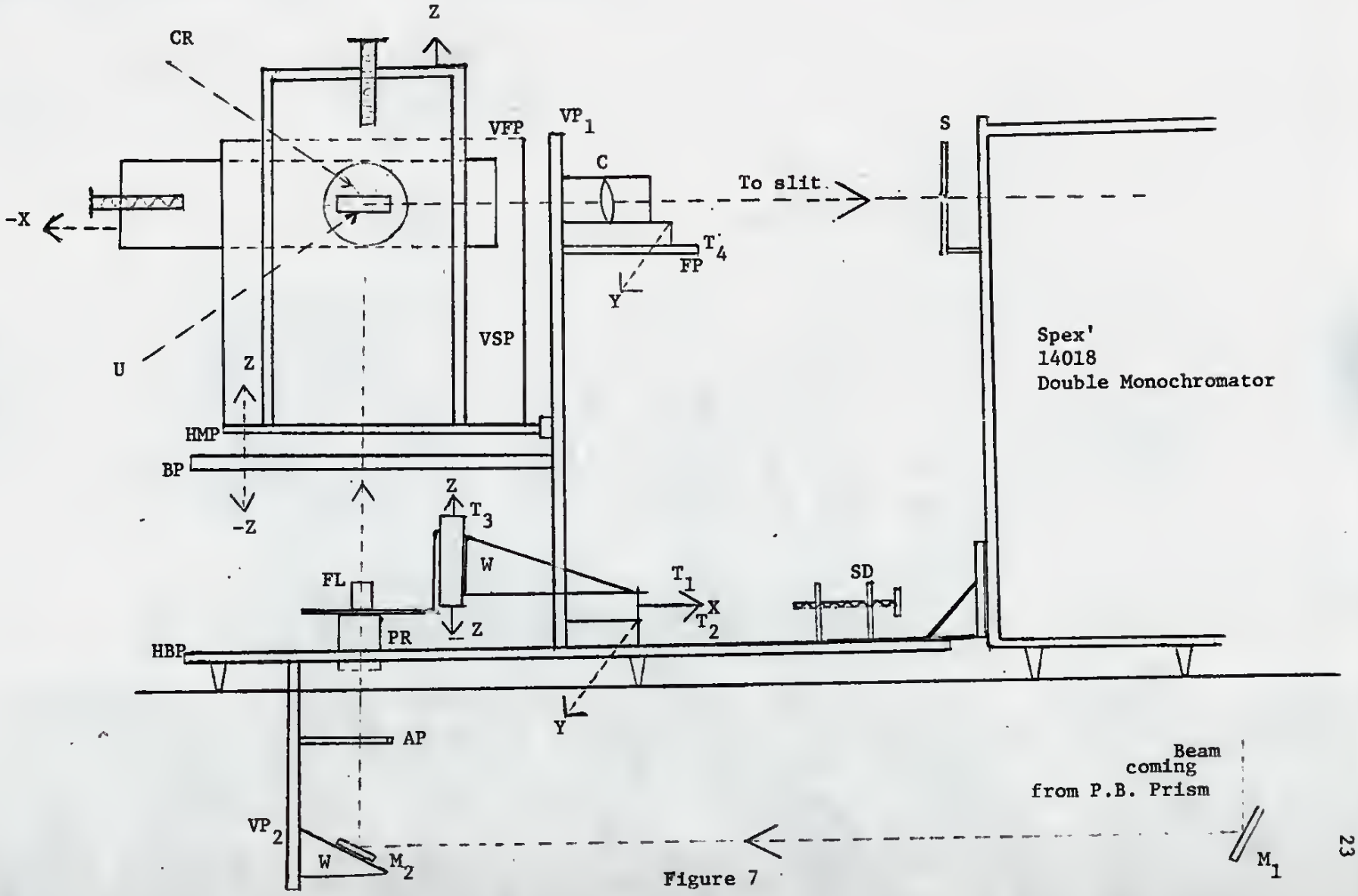
Z
CR
VFP
VP1
S
C
To slit
-X
T4
FP
Y
U
VSP
Spex'
14018
Double Monochromator
Z
HMP
BP
-Z
Z
T3
W
FL
T1
SD
X
T2
PR
Z
HBP
Y
AP
Beam
coming
from P.B. Prism
VP2
W
M2
M1

Figure 7

(focal length 50 mm, minimum f-stop 1.4). The diameter of this lens is 36 mm and the choice of a distance from the slit of about 280 mm matches the light cone from this lens with the monochromator f/number of 7.8 (See Figure 5). The collection lens is mounted on a translation stage having motion perpendicular to the optical axis, that is along the Y axis defined in Figure 4. The position of the lens mount on the translation stage may be altered along the optical axis, that is along the X axis defined in Figure 4, since the lens mount is fixed along the optical axis, that is the X axis defined in Figure 4, but the lens itself can be adjusted relative to the mount along the X-direction by means of the focus adjustment on the lens.

e. Mirrors

Two plane mirrors are used at 45° incidence angles to change the direction of the laser beam by 90° in two places between the constant deviation prism and the aperture as shown in Figure 1. These mirrors can be dielectric coated for high reflectivity for either the red or the blue-green regions. To have maximum reflectivity in both regions requires a change of mirrors. There are some inexpensive mirrors available (from Edmunds Scientific Company) which can be used for a broad spectral range. It should be noted that these mirrors have reflectivity of only 90-95% throughout the entire range.

A concave spherical mirror of focal length 60 mm and diameter 2.5 inches can be placed on the optical axis, that is the X axis defined in Figure 4, on the side of the sample opposite to the monochromator slit. This mirror serves to collect the back scattered radiation and return it to the collection lens. This mirror is fixed in a mount which has the capability for movement in the X, Y or Z directions. Since it is

easily removed, this mirror is used only when needed to increase the amount of scattered radiation collected.

A concave spherical mirror of focal length 60 mm and diameter one inch can be located above the sample provided the sample container is small enough. This mirror can increase the intensity of scattered radiation by reflecting the laser beam back through the sample. This mirror would only be used for liquids or solids since the ERC accessories for gases is designed to multipass the laser beam through a gas cell. This mirror has not been incorporated into the system as yet.

f. Filters

Five neutral density filters of approximately 1, 10, 25, 50 and 80 percent transmission, respectively, are available. The filters are mounted in aluminum frames and fit in a specially constructed housing mounted on an ordinary buret clamp. These filters are positioned just before the plane mirror M2 in Figure 1 and Figure 7. The filters are very convenient for recording signals of quite different strength without changing settings of the laser power supply or the detection system. The filters are especially convenient when using dye laser excitation as one cannot easily change the power of the dye laser.

g. Others

For making depolarization measurements of the types other than method IV described by Claassen, Selig and Shamir (5), a polarization analyzer and/or a polarization scrambler are required. These componenets can be mounted on a semi-circular holder and bolted to the slit housing of the monochromator. However, such an arrangement has not yet been incorporated in this system.

F. Sources of Optical and Mechanical Components for Sample Illumination Optics

Table 1, lists the suppliers and descriptions, price and year of purchase for the commercially available optical and mechanical components used in the sample illumination optics.

G. Components Fabricated in the Department of Chemistry Shop

The mechanical components associated with the sample illumination optics may be divided into three general categories as follows: (1) the device for the holding and positioning the constant deviation (Pellin-Broca) prism, (2) the basic frame to hold the various sampling accessories and optical components, and (3) the universal sample holder for liquids and solid samples.

A rotating disc in the device for holding and positioning the constant deviation prism, the four translational stages used on the basic frame, and some mirror mounts and brackets are commercially available items (see Section F). The remainder of the items in the three categories were constructed in the Department of Chemistry Shop by Mr. Al Nielson. Mr. Nielson also contributed to the design of many of these items.

1. Device for Holding and Positioning the Constant Deviation (Pellin-Broca) Prism

A schematic diagram is shown in Figure 6, where the X, Y and Z directions are as defined in Figure 4. The rotating disc (Ealing Corporation) has its shaft held in a frame so that there is some adjustment of positioning in the Y direction. The whole device is bolted to the table on which the lasers are mounted. The lasers are set on an alignment plate (Spectra Physics Model 377) which is also bolted to the

Table 1: Sources of Optical and Mechanical Components for Sample Illumination Optics

Item:	Supplier's Name and Address:	Description, Price and Year of Purchase
Automatic Miranda camera (collection) lens	Metro Photo, 95th & Antioch, Overland Park, KS 66212	Focal length 50 mm, f-stop 1.4, $149.95 (1975)
Pentax super muticoated Takumar lens	Felix Camera, 2317 Independence Blvd., Kansas City, MO 64124	Focal length 50 mm, f-stop 1.4, $124.80 (1975)
Leitz Wetzlar Noctilux lens	NASA Texas	Focal length 50 mm, f-stop 1.2, (1976)
Neutral density filters	Baird-Atomic, Inc., 125 Middlesex Turnpike, Bedford, MA 01730	S-582M, 79.4 $\pm$ 1.9 % T, $5.00; S-585, 50 $\pm$ 1.0 % T, $11.00; S-589, 25 $\pm$ 1.0 % T, $11.00; S-590M, 10.3 $\pm$ 2.4 % T, $5.00; S-592, 1.11 $\pm$ 0.48 % T, $5.00 (1976)
Liquid Raman cell	JASCO Inc., 218 Bay Street, Easton, MD 21601	0.3 ml. volume for Model R-300 Laser Raman Spectrophotometer, $60.00
External resonating cavity	SPEX Industries, Inc., 3880 Park Avenue, Metuchen, NJ 08840	Model 1443A ERC, $880.00 (1975)
Constant deviation prism (Pellin Broca)	Continental Optical Corporation 176 Central Avenue, Farmingdale, NY 11735	B-P-AA Brewster angle prism, type A, 90° deviation, material BK-7, $120.00 (1974)
Revolving disc for mounting constant deviation prism	Ealing Corporation, 2225 Massachusetts Avenue, Cambridge, MA 02140	22-7918 Graduated rotating table $118.00 (1974)

Table 1 continued:

Item:	Supplier's Name and Address:	Description, Price and Year of Purchase:
Polarization rotator	Spectra Physics, 1250 West Middlefield Road, Mountain View, CA 94040	310-21, $600.00 (1973)
Aperture (Iris diaphragm)	Edmund Scientific, 1777 Edscorp Building, Barrington, NJ 08007	C41970, $13.50 (1975)
Front surface plane mirrors	Edmund Scientific, 1777 Edscorp Building, Barrington, NJ 08007	30621, Broad band mirrors (x2) $4.50 @ (1976)
Translation stages	Newport Research Corp., 18235 Mt. Baldy Circle. Fountain Valley, CA 92708	TSX-1 (one) $55.00 @ 420-1 (one) $85.00 @ 420-0.5 (two)$75.00 @ (1975)
Laser plane mirrors	Newport Research Corp., 18235 Mt. Baldy Circle, Fountain Valley, CA 92708	10D10DM.2 (two) $44.00 @ 10D10DM.4 (two) $31.00 @ (1976) 05D10DM.2 (two) $23.00 @ (1975)
Mirror mounts	Newport Research Corp. 18235 Mt. Baldy Circle Fountain Valley, CA 92708	MM1-B1 (two) $28.00 @ (1975) MM2-B3,BP-2 (two) $39.00 @ (1976)
Angle brackets (wedges)	Newport Research Corp. 18235 Mt. Baldy Circle Fountain Valley, CA 92708	360-90, 90^{o} wedge (one) $28.00 @ 360-45, 45^{o} wedge (two) $32.00 @ (1975)
Pyrex window for low temperature cell	SGA Scientific, 2375 Pratt Blvd. Elk Grove Village, Ill 60007	P-7150, 1/8" thickness, 1" diameter, (four) $1.27 @ (1976)

Table 1 continued:

Item:	Supplier Name and Address:	Description, Price, and Year of Purchase:
Concave spherical mirrors	Miken Optical Co. 53 Abbott Avenue Morristown, NJ 07960	1" diameter, 60 mm focal length, $20.00 @ 2½" diameter, 60 mm focal length, $50.00 @
Silver coating on above mirrors	Denton Vaccum System, Cherry Hill Industrial Park, Cherry Hill, NJ 08003	Denton FS99, Protected silver coating of above two mirros, $75.00 (1976)

table. The location of the device holding the constant deviation prism relative to the lasers is fixed by the position where the device is bolted to the table. Adjustment in the vertical or Z direction is available so that the prism can be moved up and down to match the different beam heights of the two lasers. Adjustment along the beam direction or X axis is provided so that the beam leaving the prism in the downward direction can be centered on M1 in Figure 1. The adjustments are made by a moving aluminum sliding plate with respect to a stationary aluminum plate. The sliding plate is bevelled to fit between bevelled brass guide rails screwed to the stationary aluminum plate. The motion of the moving plate is controlled by a screw held in a stationary collar turning in a threaded hole in the moving plate. The rotating disc really consists of two separate discs one of which rotates with respect to the other. The stationary disc is fixed to the shaft. The prism is attached to the moving disc. A micrometer is positioned at the top of the unit to give fine control of the disc rotation which changes the angle between the laser beam and the prism face (see Figure 6). The micrometer is mounted on a bar which is clamped to the shaft of the rotating disc.

2. Basic Frame

A schematic diagram of the basic frame is shown in Figure 7, and a photograph appears in Figure 8, with the universal sample holder in position and the X, Y, and Z directions are defined in Figure 4. The basic frame has the following functions: (1) to support the plane mirror M2 and the aperture AP, (2) to support the polarization rotator PR and the focusing lens FL and provide adjustments in the X, Y, and Z directions for them, (3) to support the universal sample holder for liquid

Explanation of Figure 8

Photograph of the Raman sample illumination system

This photograph shows the Raman sample illumination system described in Figures 1 and 7 with a capillary tube held in the universal sample holder. This photograph was taken after all the work reported in this thesis was completed and after an explosion had destroyed the automatic Miranda lens. Consequently, the collection lens in this photograph is the Pentax Super Multicoated Takumar lens.

Figure 8

and solid samples and to support the ERC accessory for gases, (4) to support the collection lens C and provide adjustment in the Y direction and (5) to allow motion of the whole frame along the optical axis relative to the monochromator using a sliding device SD to match the cone of light from the collection lens C with the monochromator f/number as discussed in Section E-3 and Figure 5.

The major structure of the basic frame consists of six aluminum plates as follows: (1) a horizontal base plate HBP, (2) a vertical plate VP_1, (3) a back plate BP, (4) a front plate FP, (5) a vertical plate VP_2, and (6) an L shaped plate bolted to the monochromator and attached to the horizontal base plate HBP through the sliding device SD. The HBP (20" x 10.5" x 9/16") and the VP_1 (10.5" x 15" x 9/16") are screwed together using gussets (not shown in Figure 7) as are the two pieces of the L shaped plate (7½" x 4¼" x 9/16"). The HBP has a hole of dimensions 4½" x 4¼" with edges ½" from VP_1 and 3¼" from the side towards the reader (along the positive Y axis). Thia hole serves to accommodate the laser beam and motion of the polarization rotator, PR, and focussing lens FL in all three directions. The VP_1 has a hole of dimensions 5.200" x 6.300" in the bottom to accommodate the translation stages T_1, T_2, and T_3 and a hole of dimensions 5" x 4.800" with edges 2" from the top and 4" from the side toward the reader (along the positive Y axis) to accommodate motion of the collection lens C toward and away from the sample along the optical axis (X axis). The FP (3" x 3 5/8" x 3/8") and BP (6" x 9" x 3/8") are screwed to the VP_1 without using gussets. The VP_2 (14" x 3" x ¼") is screwed to the HBP. A hole in the table (9¼" x 4½") accommodates the VP_2 and the laser beam.

The VP_2 supports the mirror M_2 on a 45^o bracket W_1 (Newport Research Corporation #360-45) with a mount (Newport Research Corporation #MM2-B3) having adjustments for the pitch and yaw of the mirror plane with respect to the light beam so that motion of the reflected beam in the X and Y directions is possible. The plane mirror M_1 shown in Figures 1 and 7, is located on an identical mount and bracket. Here the bracket is attached to a support plate (not shown). This support plate is screwed into the leg of the table holding the lasers and constant deviation prism. The mirror mount and bracket for M_2 can be moved vertically (in the Z direction) since the side of the bracket bolted to VP_2 is slotted. The variable aperture AP (Edmund Scientific #C41970) is held in a two piece mount bolted to VP_2. Motion of one piece of the mount relative to the second piece (bolted to VP_2) gives adjustment in the X and Y directions.

The polarization rotor, PR, and focusing lens, FL, are attached to threaded holes in an L shaped holder. This holder has a second side bolted to translation stage T_3 (NRC #420-1). T_3 is attached to translation stages T_1 and T_2 (NRC #420-05) by a 90^o bracket W (NRC #360-90) and T_2 is bolted to HBP. This stack of 3 translation stages which fits thru the hole in the VP_1 provides adjustment in the X, Y, and Z directions for the PR and the FL. The PR and FL move in the hole in the HBP as the stack of T_1, T_2, and T_3 is used to place PR and FL in the optimum positions. Before T_1 and T_2 and T_3 were bolted together, the displacement on each was set at the mid point and the stack of translation stages was located on HBP so that everything was thought to be in the optimum position with respect to the laser beam.

The BP supports the sample handling accessories. A horizontal moving plate, HMP, (7.090" x 4.070" x ¼") rests on BP and moves in the Y

direction. The HMP is the base plate of the universal sample holder, USH, for liquids and solids discussed later in Section G-3. The BP has a hole of dimensions (4 5/8" x 4¼") with edges 2 7/8" from the back and 7/8" from the edge toward the reader (along the positive Y axis) to accommodate the laser beam and the ERC accessory. The HMP has a circular hole of diameter 2" with edges 4.28" from the back and 2.230" from the edge toward the reader (along the positive Y axis) to accommodate the laser beam and the bottom of the low temperature cell. The end of the HMP opposite to the monochromator rests on a screw that sticks above the BP. The bottom of the HMP slides over this screw as the HMP travels in the Y direction. The end of the HMP nearest the monochromator is supported on a rod passing through vertical plates on the sides of the HMP. The plate on the side of the HMP nearest to the reader (along the positive Y axis) is locked to the rod by a set screw. This rod also passes through two small plates mounted on each edge of the VP_1 of the basic frame. One end of the rod is threaded and moves in or out of a stationary handle as the handle is turned. For gaseous samples, the HMP (and consequently the USH) is removed from the BP. Then the ERC accessory is placed on the BP. The ERC has a rod and spring arrangement similar to the one built for the HMP which allows motion of the section of the ERC holding the gas cell and mirrors relative to the ERC frame in the Y direction. The back scatter collection mirror described in Section E-4e can be mounted on the back edge of the BP as needed.

The FP holds the translation stage T_4 (Newport Research Corporation #TSX-1). The lens mount is bolted to the T_4 through slots rather than holes so that the lens holder and collection lens, C, may be placed at different locations along the optical axis or X direction depending on

the sampling accessory in use. The focussing adjustment of C provides some motion relative to the lena mount along the optical axis or X direction. The T_4 is oriented so that its motion is across the optical axis or in the Y direction. The hole in the VP_1 of the basic frame accommodates motion of the C in the X and Y directions. The lens mount for the Automatic Miranda lena (focal length 50 mm, minimum f-stop 1.4) is specially machined so that the lens rotates onto the mount frame and locks in place. The Pentax Super Multicoated Takumar lens (focal length 50 mm, minimum f-stop 1.4) is threaded so a mount with a threaded hole may be used. The Leitz Wetzlar Noctilux lena (focal length 50 mm, minimum f-stop 1.2) is notched rather than threaded so a mount with a notched hole may be used.

The SD allows motion of the HBP relative to the L shaped plate bolted to the monochromator so that the whole frame can move relative to the monochromator. The L shaped plate fits on top of the HBP and the two are held together by two bolts with heads similar to wing nuts. During motion the HBP slides under the L shaped plate and the two feet on the back of the HBP slide across the table which also accommodates the monochromator and the frame. Vertical posts with rectangular cross-section are screwed to both the HBP and the L shaped plate. One edge of the L shaped plste has a slot which just fits the post on the HBP and guides the L shaped plate in its travel on top of the HBP. A shaft of diameter ½" with a wheel on one end passes through the post on the L shaped plate. The other end of the shaft is threaded and turns in a threaded hole in the vertical post on the HBP. The rotation of the shaft by turning the wheel on one end moves the post on the HBP along the shaft so that HBP moves relative to the L shaped plate along the optical axis or X direction.

3. Universal Sample Holder

The universal sample holder, USH, is included in Figure 7. Figure 9 is a photograph of USH with the spinning motor in position. Figures 10a and 10b are photographs of the USH with a liquid cell and a capillary cell in position, respectively. The base plate of the USH is the HMP described in Section G-2. The HMP provides motion of the USH in the Y direction as described in Section G-2. The motion in the X direction is provided by the horizontal sliding plate, HSP, mounted on a vertical fixed plate, VFP. The motion in the Z direction is provided by the vertical sliding plate, VSP, mounted on the horizontal sliding plate, HSP. The HSP and VSP operate on the same principle described in Section G-1 for the device for holding and positioning the constant deviation prism. The HSP can move with respect to the VFP and, for any fixed position of the HSP, the VSP can move with respect to the HSP. The bottom of the VFP is screwed into the HMP. The top of the VFP has a horizontal bevelled ridge with a threaded hole lengthwise through the center of the bevelled ridge. The bevelled ridge on the top of the VFP fits between two horizontal bevelled brass guide rails attached to the back of the HSP. A screw with a knob held against a brass collar at one end of the bevelled brass guide rails on the back of the HSP turns into the threaded hole in the bevelled ridge at the top of the VFP. The travel of this screw provides motion in the X direction by moving the HSP along the ridge at the top of the VFP. The front of the HSP contains two vertical bevelled brass guide rails and a screw with a knob held against a brass collar at the top of the bevelled brass guide rails. The VSP has its edges bevelled to fit snugly between the bevelled brass guide rails on the front of the HSP. A threaded hole in the center of the VSP accepts the screw on the front

Explanation of Figure 9

Photograph of the spinning motor

This photograph shows the spinning motor described in Figure 2 mounted on the universal sample holder described in Figures 7 and 8. The collection lens is the same as described in Figure 8.

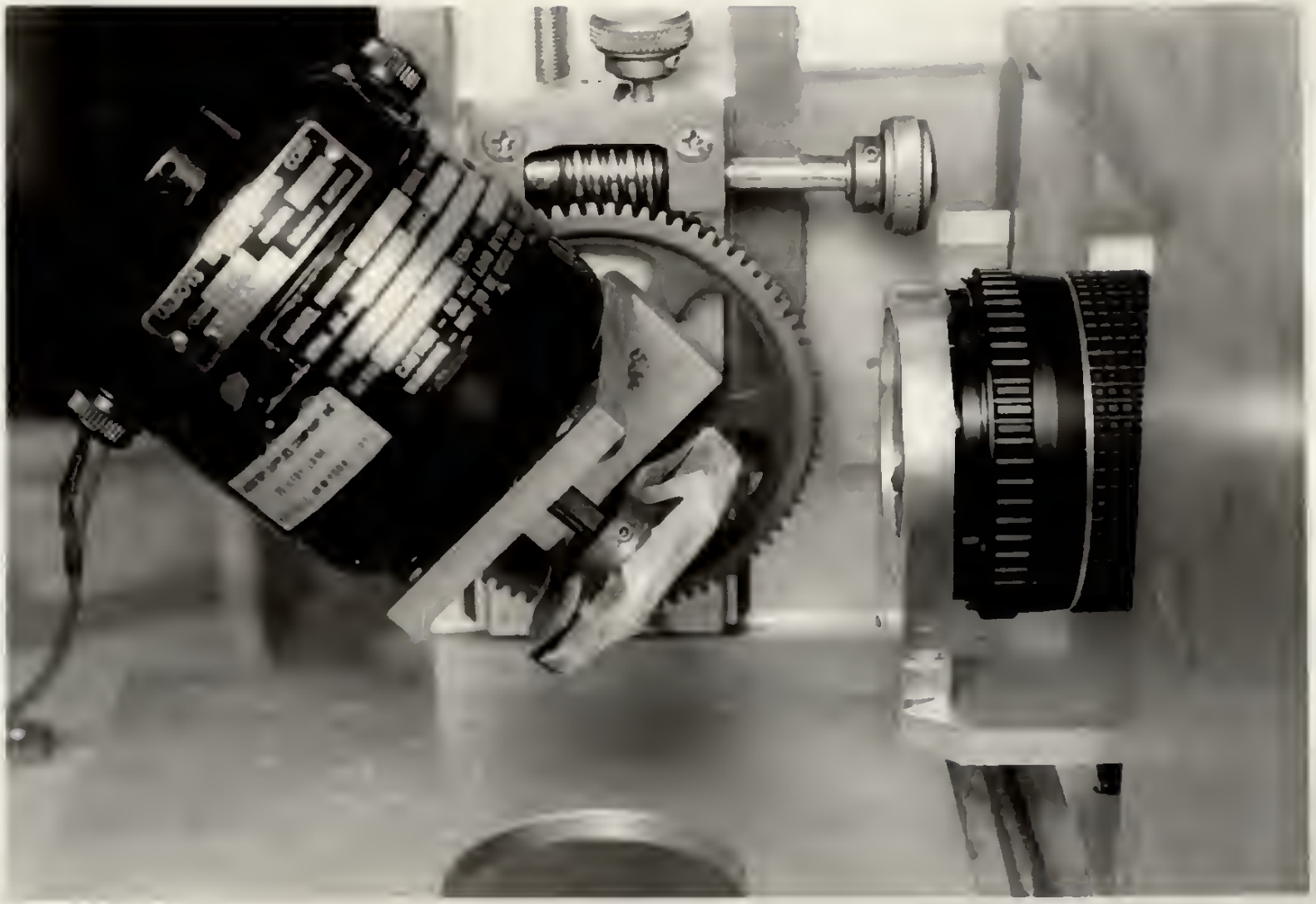

Figure 9

Explanation of Figure 10a

Photograph of a conventional liquid cell

This photograph shows a conventional liquid cell mounted on the universal sample holder described in Figures 7 and 8. In this case an ordinary liquid vial is used as the cell. The collection lens is the same as described in Figure 8.

Figure 10a

Explanation of Figure 10b

Photograph of a capillary tube cell

This photograph shows a capillary tube mounted on the universal sample holder described in Figures 7 and 8. This arrangement may be used for solids or liquids. The collection lens is the same as described in Figure 8.

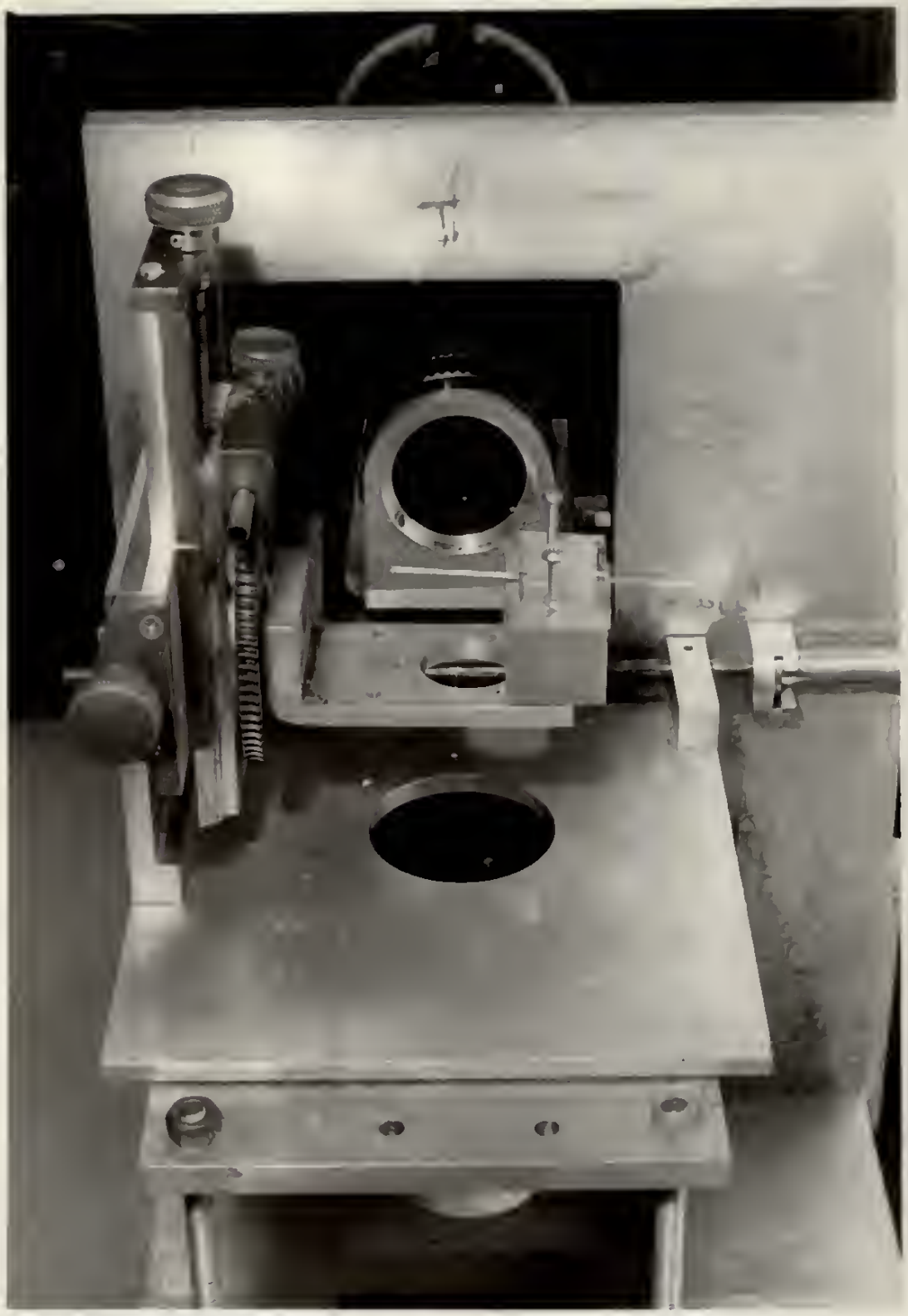

Figure 10b

side of the HSP. The travel of this screw provides the motion in the Z direction by the moving of the VSP with respect to the HSP. Thus the USH has translation in the X, Y and Z directions.

The USH can now be adapted to various sampling devices by proper design of the VSP. At present only two VSP's are needed. One VSP has a large gear wheel bolted to it. A gear attachment mounted on top of the VSP turns the gear wheel. An L shaped plate labelled U in Figure 7, is bolted to the gear wheel. Rotation of the gear wheel changes the angle that the plane of U makes with the incident laser beam. The plate, U, has threaded holes so that the following attachments may be located there: (1) a spinning motor for rotating solids packed into rings (of two different diameters) on a disk, solids in the form of pellets glued or clipped to the disk, and liquids in a cell designed for rotation; (2) a specially machined holder for the 0.3 ml capacity liquid cell purchased from JASCO; and (3) a plexiglass holder for capillaries containing solids or liquids. Thus, the VSP with the gear wheel and U is used a) for spinning both aolids and liquid samples at any angle to the laser beam, b) for holding a pellet either spinning or stationary at any angle to the laser beam, c) for a stationary liquid cell with windows at or near normal incidence to the laser beam, and d) for capillary cells for both solids and liquids. The other VSP is L ahaped and is used to hold the low temperature cell. The horizontal portion of this L shaped plate has a circular hole of diameter 2" to accommodate the bottom window section of the low temperature cell (see Figure 12) and the laser beam.

The rotating liquid cell holder consists of a cylindrical adapter shown in Figure 11. One end of the adapter has a hole to accommodate the

Explanation of Figure 11

Holder for spinning liquid sample cells

S is the shaft of the spinning motor described in Figures 2 and 9.

SS is the set screw to hold the adapter tightly to the shaft S.

AA is the aluminum adapter to hold ordinary liquid sample cells similar to the one shown in Figure 10a. The "O" ring in the cavity in AA holds a liquid sample cell or another adapter for an NMR sample tube sungly in the cavity.

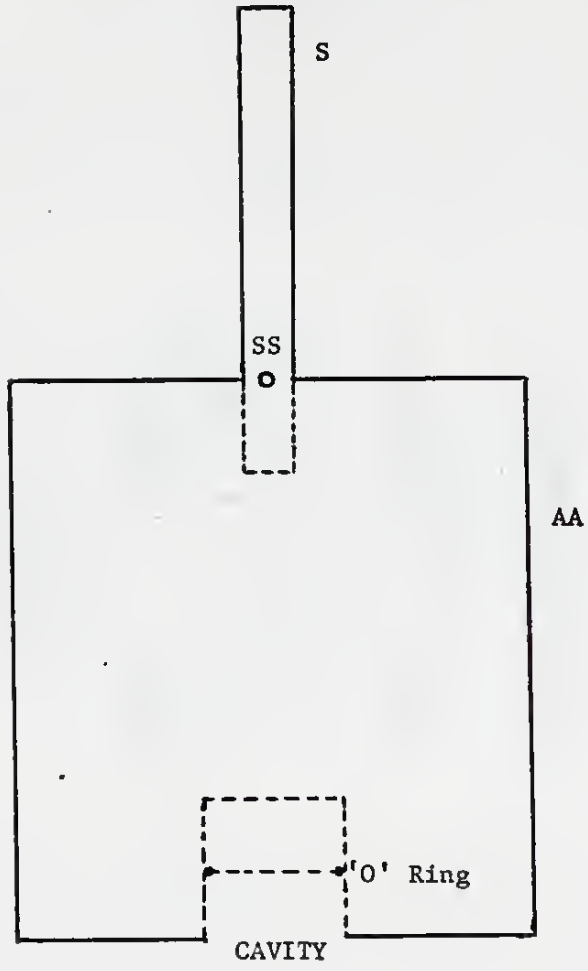

Figure 11

shaft of the spinning motor and the adapter is held in place on the shaft by a set screw. The other end of the adapter has a large hole (about 7/16" diameter) with an "O" ring set in a groove inside. A cell is made by sealing one end of a piece of glass tubing which fits tightly inside the "O" ring. After filling through the open end, the cell is inserted into the adapter and held in place by the "O" ring. Various diameters of tubing can be used with proper packing material to give a tight fit inside the "O" ring of the adapter.

The low temperature cell mentioned in Section E and shown in Figure 12 has some metal parts. S is a brass ring with the outside threaded. A groove is machined on the top of S to fit the end of the glass section of the cell and the glass tubing is glued into the groove in S with Varian Torr-Seal resin. The bottom side of the S has a groove for an "O" ring. R is an aluminum plate with a cylinderical extension with a hole to accommodate the laser beam. The bottom of the extension has a grove for an "O" ring. A glass disc fits against this "O" ring. Two rings with a lip on one end and the inside threaded are used to hold R and the glass disc in position. One ring fits around the edge of R and screws onto S and presses R against the "O" ring between R and S. The other ring fits around the edge of the extension of R and screws onto the extension and press the glass disc against the "O" ring between the glass disc and the extension of R. The arrangement is chosen to make the glass disc small enough that a commercially available glass disc (Scientific Glass Apparatus Co. #P-7150) of good optical quality and nominal thickness (1/8") will be strong enough not to fail under vacuum. TF_1, TF_2, and TF_3 are teflon stopcocks. TF_1 is for sample introduction into and removal from the tube LM where the sample is maintained as a

Explanation of Figure 12

Low temperature cell

TF_1, TF_2, TF_3 are teflon stopcocks. The sample is introduced through TF_1 into tube LM.

Tube XY ia either evacuated or contains freon or some other inert material to facilitate heat exchange between the cooling material in the dewar and the sample in tube LM.

TF_3 allowa the evacuation of the dewar.

R ia an aluminum plate with a cylindrical extenaion having a pyrex window to accomodate the laser beam and S is a brass ring with an "O" ring seal. See the next to last paragraph of Section G-3 for a detailed description.

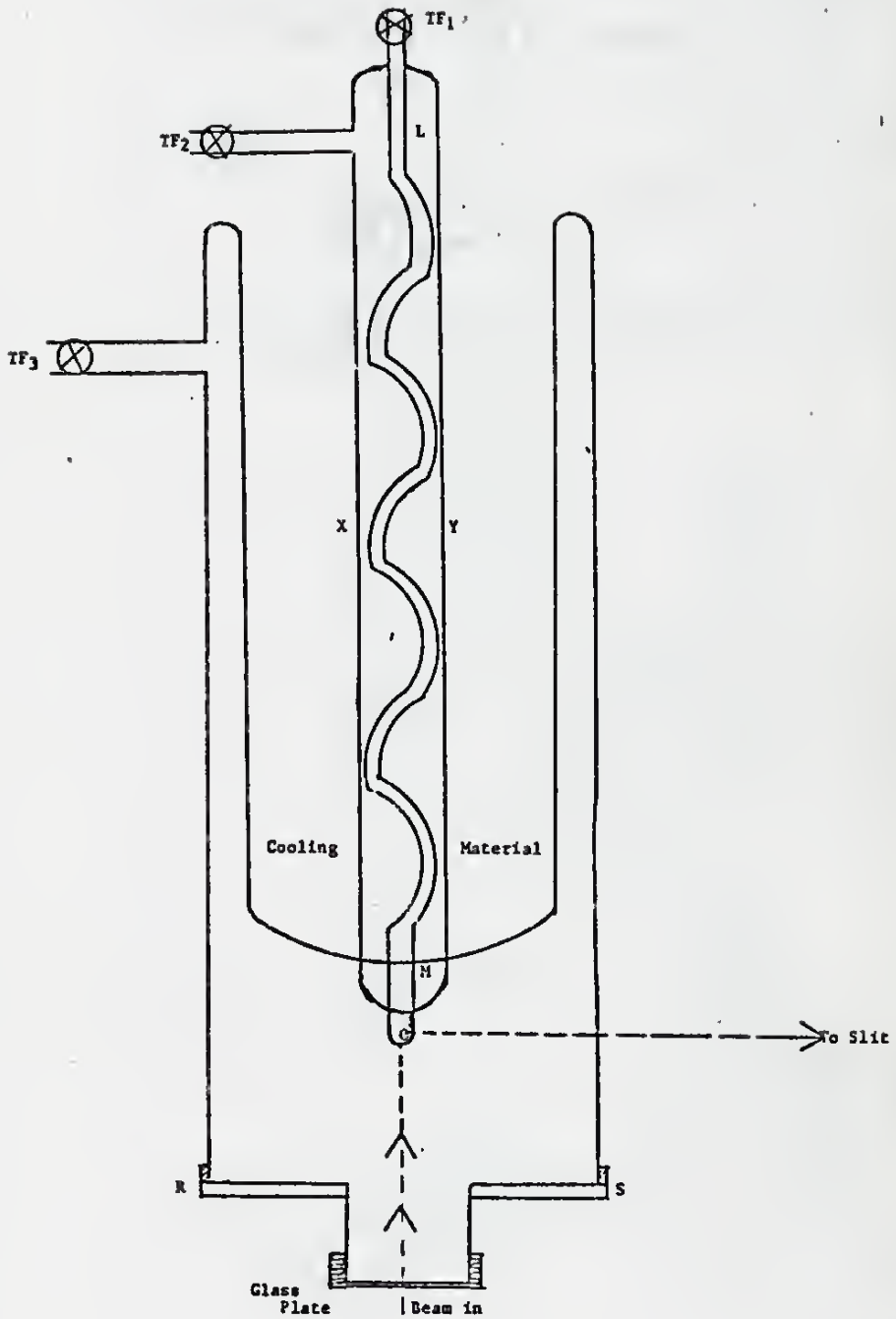
TF1
TF2
TF3
L
X
Y
Cooling
Material
M
To Slit
R
S
Glass
Plate
Beam in

Figure 12

liquid in the tip for Raman studies. TF_2 allows evacuation or introduction of a chosen pressure of gas to facilitate heat exchange in tube XY. TF_3 is for evacuation of the outer section of the cell to make it a dewar flask. In our operation tube XY as well as the dewar sections are evacuated to the lowest obtainable pressure and TF_2 and TF_3 are kept closed.

After all the work reported in this thesis was completed but before the photographs shown in Figures 8, 9, and 10 were taken, an explosion occurred which destroyed the automatic Miranda lens. Consequently, the photographs appearing in Figures 8, 9, and 10 were taken with the Pentex Super Multicoated Takumar lens in position. The explosion occurred with a sample of $CF_2(OF)_2$ in a sealed tube used for nuclear magnetic resonance spectroscopy at room temperature while under irradiation by the Ar^+ laser Note: Figure 12a is a photograph of the low temperature cell resting on the VSP in the USH of the Raman sample illumination system.

H. Performance of the Raman System

This system is showing satisfactory performance as the following examples will illustrate.

1. Solids

To date several solid samples have been recorded and the quality of the spectra has been good. In the summer of 1975, some solid samples supplied by Wright-Patterson Air Force Base, were observed with the JASCO model R-300 Laser Raman Spectrophotomer. The samples were: Gibbsite, Boehmite, Bayerite, and some aluminum metal surfaces. Since the constant deviation prism was not set up at that time the interference from nonlasing plasma lines was a serious problem. In addition stray light rejection was insufficent to allow approach to the Rayleigh line of less than 500-800 cm^{-1}. The work was redone using the Raman system built around the Spex 1401 double monochromator in the Department of Physics

Explanation of Figure 12a

Photograph of the low temperature cell

This photograph shows the low temperature cell, described in Figure 12, on its L shaped vertical sliding plate in the universal sample holder of the Raman sample illumination system described in Figures 1, 7 and 8.

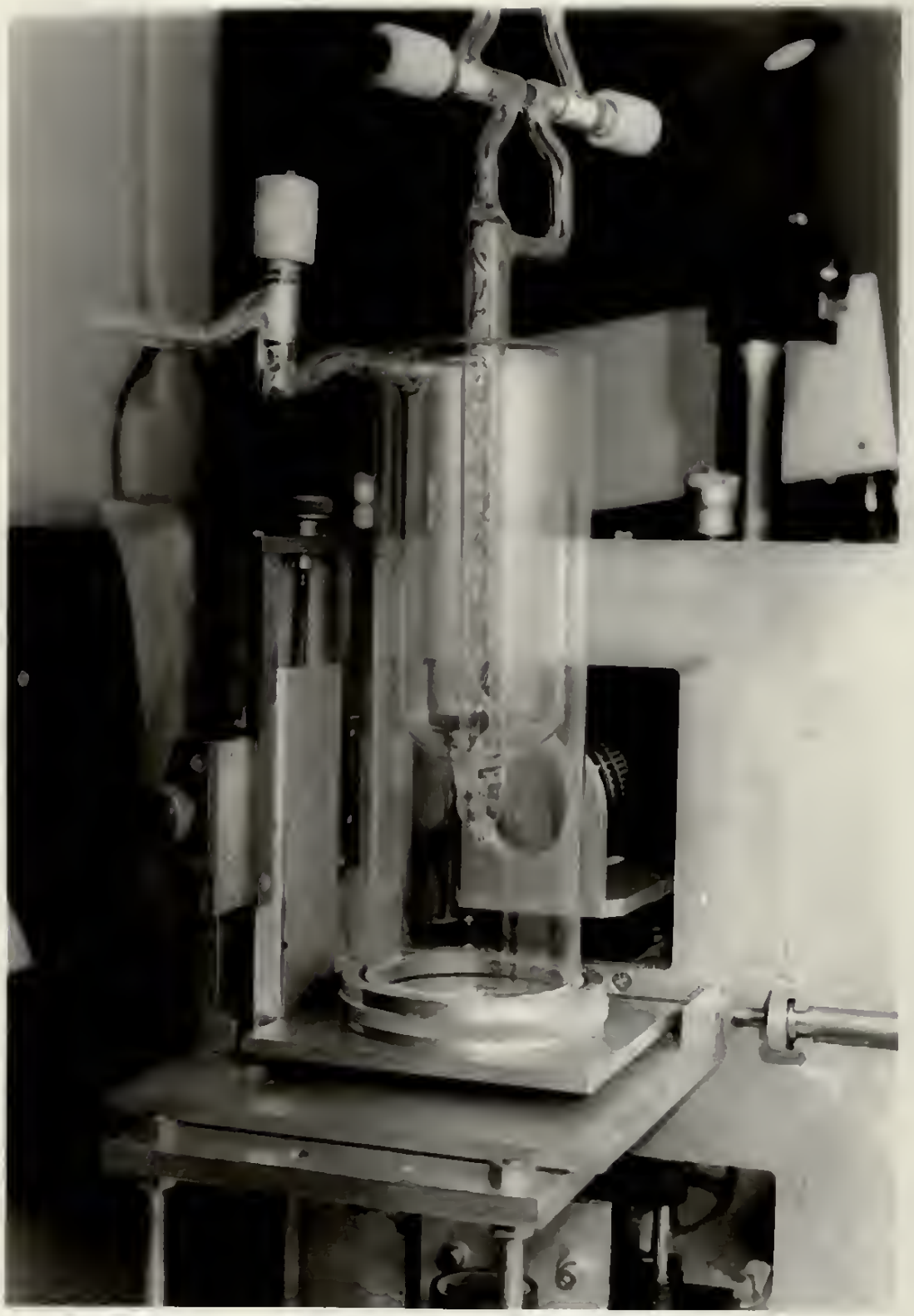

Figure 12a

at Kansas State University. After the installation of the present system in the Department of Chemistry in the summer of 1976, several of the samples were repeated on the new system. The following comparison is consistent with comparable performance expected from the Spex 14018 and the Spex 1401. Figures 13 and 14 represent the spectrum of Gibbsite, $Al(OH)_3$, recorded on the Spex 1401 (Department of Physics) and the Spex 14018 (Department of Chemistry), respectively. Some frequencies for the above samples are summarized in Table 2.

Other solid samples were studied in collaboration with Mr. John Blaha (8). Here, the frequencies for molecular chlorine and bromine in an adduct with 2, 1, 3-benzeneselenadiazole were observed. The spectra of the chlorine and bromine molecule adducts showed peaks for Cl_2 around 530 cm^{-1} and for Br_2 around 295 cm^{-1}. Difficulties arose from the color of these samples and the unstable nature of the compounds, therefore, the CW dye laser was used to excite the spectra. These compounds were slowly decomposing since the color of each adduct disappeared after several hours of irradiation with the laser beam. At the same time the corresponding peaks for Cl_2 and Br_2 in each spectrum disappeared while the rest of the spectrum remained almost unchanged. Details will appear elsewhere (8).

2. Liquid samples

For colorless liquid samples which are stable at room temperature good quality Raman spectra are readily obtained. Spectra of numerous liquid samples in different shaped containers have been recorded. Twenty colorless organic liquids (highly pure) supplied by the American Petroleum Institute have been recorded. These spectra are being published in the API standard tables and the project manager, Dr. Cecil H. Dickson, is

Table 2

Summary of the Observed Raman Frequencies of

Some Solid Samples and Aluminum Metal Surfaces

	Sample	Frequencies, in cm^{-1}
1.	Anodized Aluminum	1775, 1860, 2560, 3415, 3940, 4260, 4365
2.	Untreated Aluminum	1745, 1845, 2550, 3015, 3075, 3235, 3420, 3670, 3945, 4180, 4260, 4385
3.	$Al(OH)_3 \cdot nH_2O$ (black scrap)	575, 1590, 1780, 1860, 2560, 3420, 3940, 4045, 4255, 4370
4.	Gibbsite	220, 305, 360, 410, 530, 555, 705, 810, 900, 1010, 3370, 3440, 3530, 3620
5.	Boehmite	350, 485, 665, 1770, 3110, 3260, 3435, 3945, 4365
6.	Bayerite	No scattering observed.

Explanation of Figure 13

Raman spectrum of Gibbsite powder, Spex 1401

This figure shows the Raman spectrum of Gibbsite powder recorded on the Spex 1401 double monochromator in the Department of Physics. The four peaks at 3371, 3433, 3523, and 3616 cm^{-1} are characteristic of Al-OH stretching.

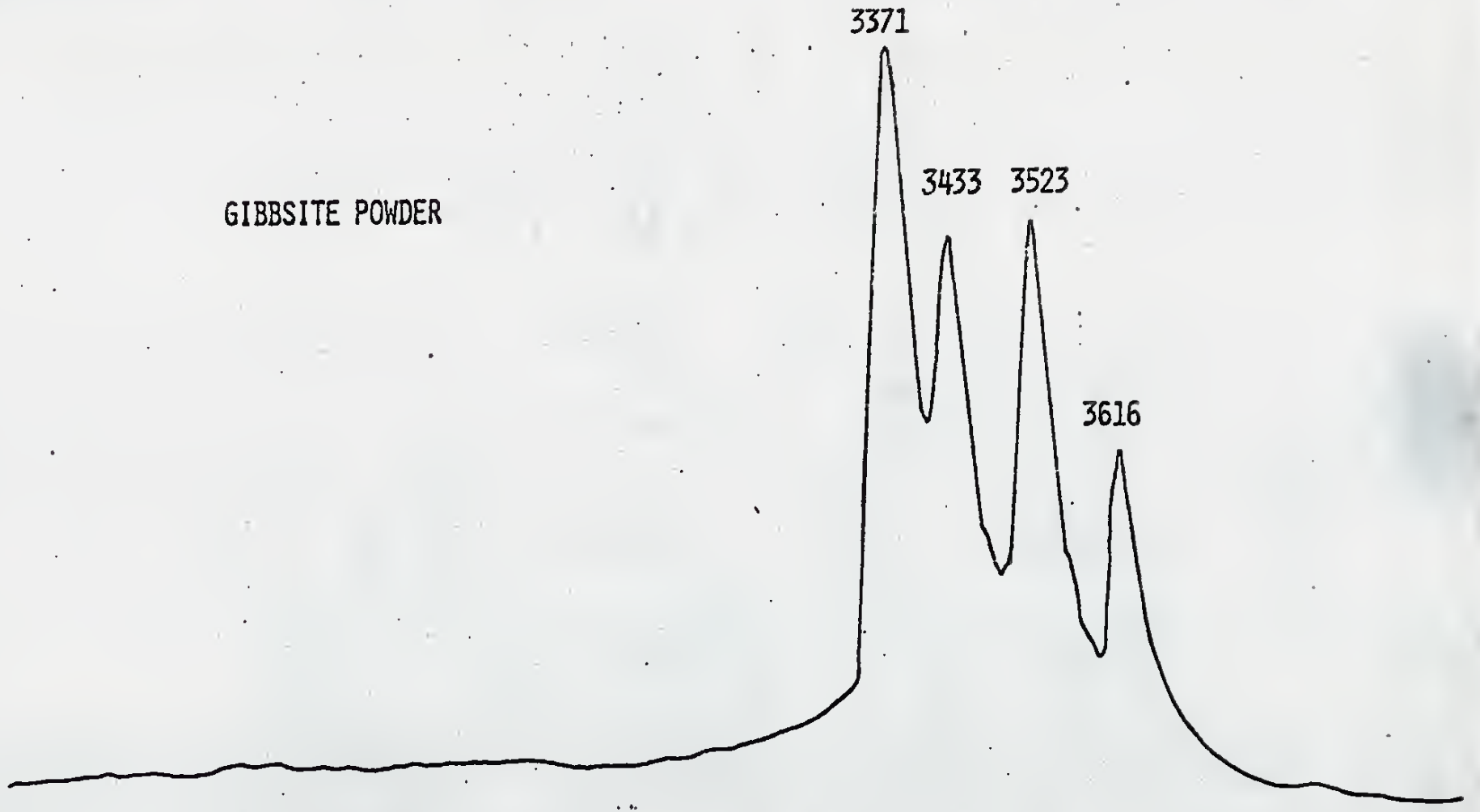

Figure 13

Explanation of Figure 14

Raman spectrum of Gibbsite powder, Spex 14018

This figure shows the Raman spectrum of Gibbsite powder recorded on the Spex 14018 double monochromator in the Department of Chemistry. The four peaks at 3367, 3437, 3526, and 3620 cm^{-1} are the same ones assigned in Figure 13.

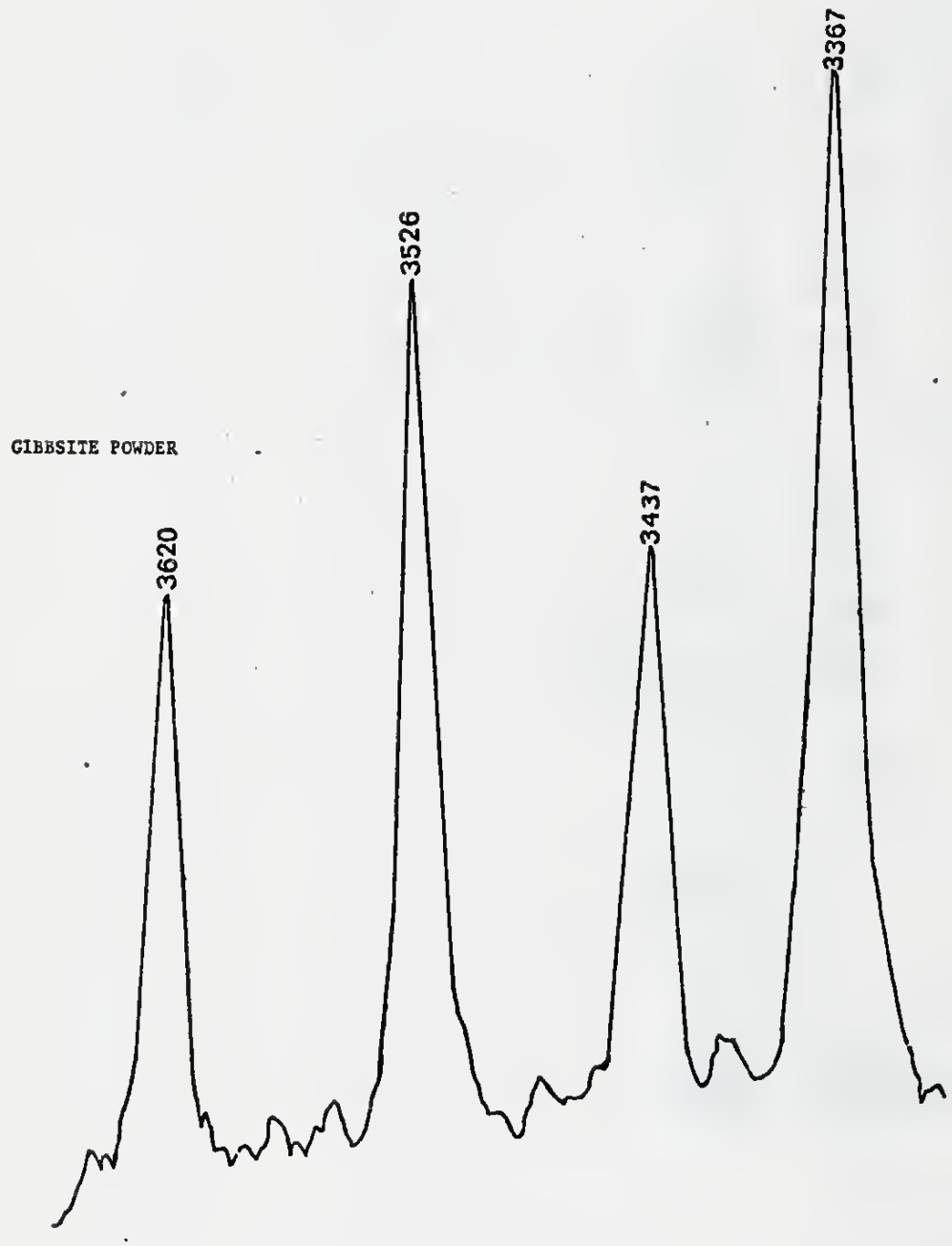

Figure 14

highly satisfied with the quality of each spectrum. This program will continue.

Some liquids with boiling points between 11° C and -69° C (e.g. CF_3OOX, X = H, D, F and Cl) have been successfully studied using the low temperature cell shown in Figure 12. Some data are presented in Part II of this thesis. Note: Figure 15 shows a high resolution spectrum of liquid CCl_4.

3. Gases

Spectra of samples of CF_3OOH, CF_3OOF, CF_3OF, CCl_2F_2 and Cl_2 have been recorded. The spectrum of CF_3OOF was of low quality and partially obscured by O_2 due to the fact that CF_3OOF was continuously decomposing probably due to high laser power. The experimental difficulties encountered in recording spectra of Cl_2 gas and CCl_2F_2 gas gave good experience for future experiments. The spectrum of Cl_2 gas is shown in Figure 16. The peaks at 547 cm^{-1} and 551 cm^{-1} correspond to $^{35}Cl - {}^{37}Cl$ and $^{35}Cl_2$, respectively, and the small shoulder around 543 cm^{-1} is due to $^{37}Cl_2$.

Spectra of gaseous CF_3OOH and CF_3OOF are reported in Part II and spectra of gaseous CF_3OF are reported elsewhere (9).

The quality of spectra in the gas phase is critically dependent on the availability of suitable gas cells. Initially a gas cell purchased from Cary Instruments having quartz windows fused to a quartz cylindrical tube cut at the Brewster angle was used. This cell was used over a period of time and became contaminated and unusable. A second cell was constructed by Mr. M. Ohno, the Kansas State University glass blower. This cell was constructed of pyrex glass with window cuts at the Brewster angle. For this cell disposable windows are cut from microscope slides

Explanation of Figure 15

Raman spectra of liquid CCl_4

This figure shows a high resolution spectrum and a survey spectrum of liquid CCl_4 on the Spex 14018 double monochromator.

Conditions for the survey spectrum:

Laser and the exciting wavelength:	Ar^+, 514.5 nm.
Laser power:	300 mw.
Slit width:	200/200/200 μm
Scan speed:	2.0 cm^{-1}/sec.
Chart speed:	3.0 cm/min.
Gain:	3K.
Filter:	1.3.
Polarization:	0 deg.

Conditions for the high resolution spectrum:

Laser and the exciting wavelength:	Ar^+, 514.5 nm.
Laser power:	300 mw.
Slit width:	50/200/50 μm
Scan speed:	0.1 cm^{-1}/sec.
Chart speed:	2.0 cm/min.
Gain:	1K.
Filter:	1.3.
Polarization:	0 deg.

Note: The conventional liquid cell described in Figure 10a was used at room temperature to record the above spectra.

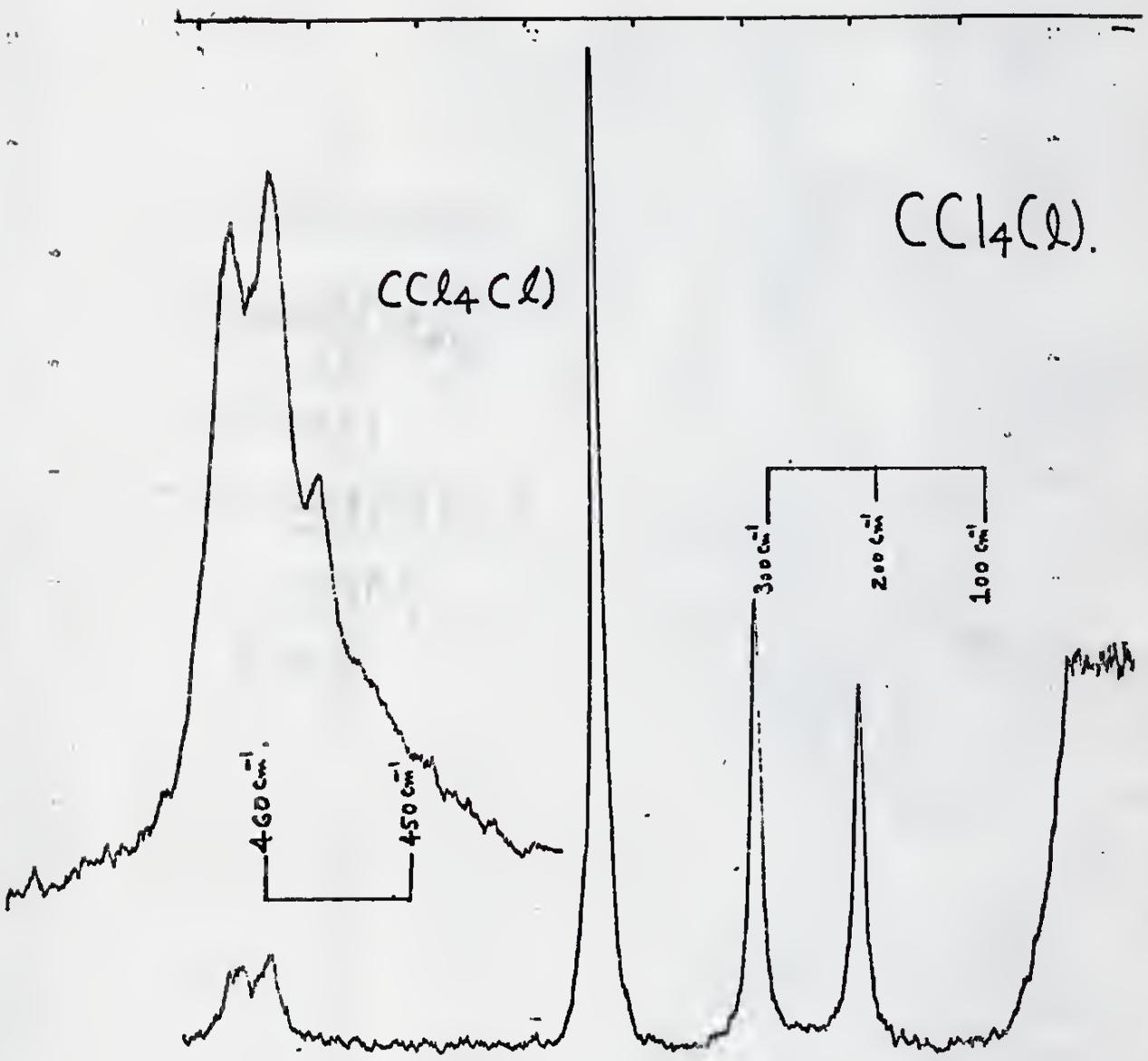

Figure 15

Explanation for Figure 16

Raman spectrum of gaseous Cl_2

This figure shows a high resolution spectrum of gaseous Cl_2 using the Spex ERC and the gas cell described in Figure 3.

Conditions for the spectrum:

Laser and the exciting wavelength:	Ar^+, 514.5 nm.
Laser power:	2.1 watts.
Slit width:	130/150/130 μm
Scan speed:	0.5 cm^{-1}/sec.
Chart speed:	2.0 cm/min.
Gain:	1K.
Filter:	1.3.
Polarization:	0 deg.
Sampling:	Gas cell.
Pressure:	500 torr.

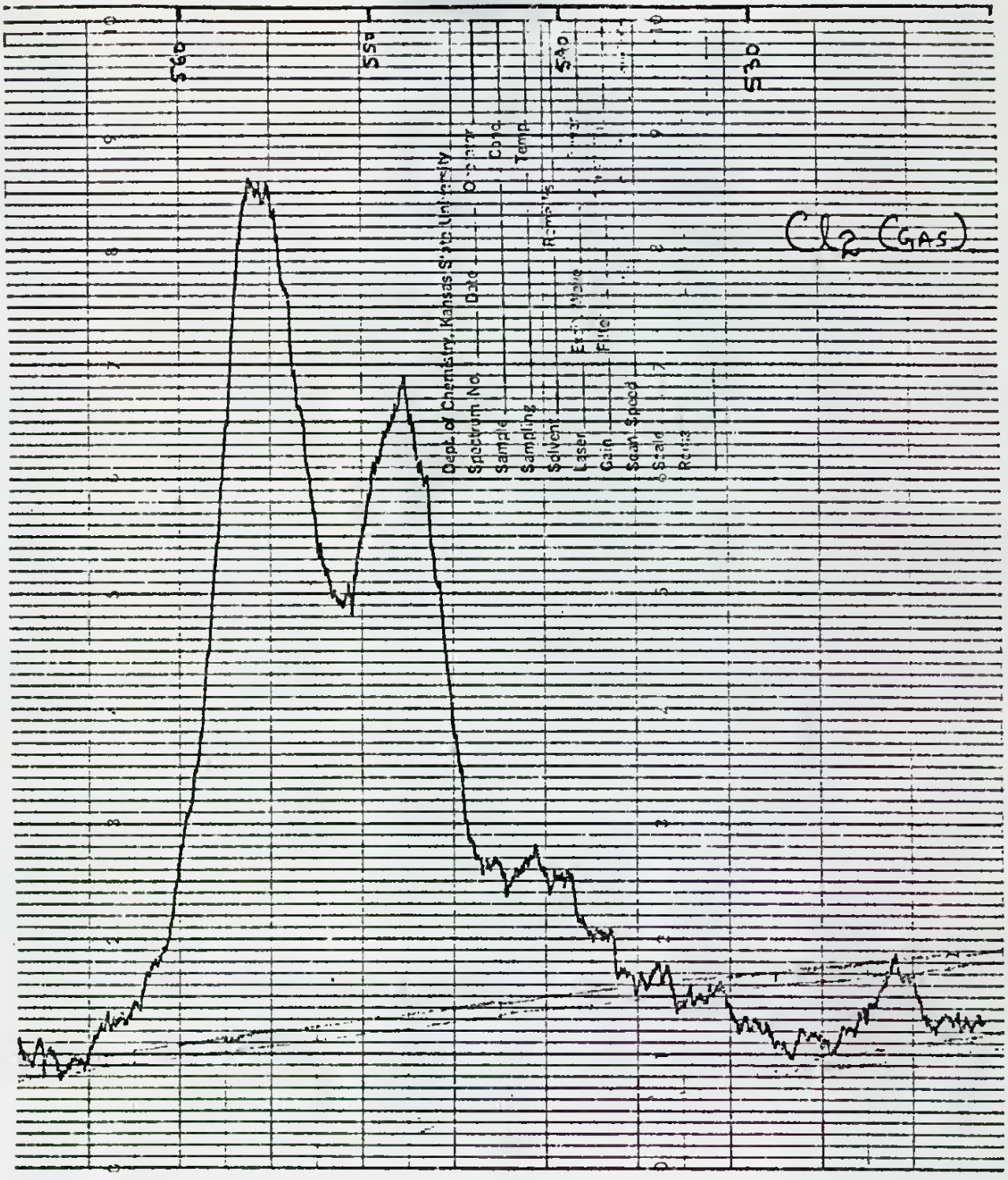
Cl2 (GAS)
Dept. of Chemistry, Kansas State University
Spectrum No.
Date
Sample
Cond.
Temp.
Sampling
Solvent
Laser
Gain
Scan Speed
Scale
Runs

Figure 16

and attached to the cell with halocarbon wax. Whenever one wants to replace bad windows, the exchange of windows is relatively simple. These cells work nicely except that the multipass pattern is distorted due to imperfections in the Brewster angle cut into the cell. More practice and experience may provide solutions to these problems and make the recording of Raman spectra of gas samples with this experimental set-up easier.

LITERATURE CITED

1. W. Kiefer, Appl. Spectry. 28, 115 (1974).
2. C. W. Brown, A. G. Hopkins, and F. P. Daly, Appl. Spectry. 28, 194 (1974).
3. F. A. Jenkins and H. E. White, Fundamentals of Optics, 4th Edition (McGraw Hill Book Company, New York), p. 25.
4. M. Born snd E. Wolf, Principle of Optics (Pergamon Press, 2nd Ed. 1964, New York), p. 177.
5. H. H. Claassen, H. Selig, snd J. Shamir, Appl. Spectry. 23, 8 (1969).
6. C. D. Allemand, Appl. Spectry. 24, 348 (1970).
7. Instructions Mannual for 1443A ERC, Spex Industries (New Jersey), October 1972.
8. J. Blaha, MS Thesis, Kansas State University, Manhattan, KS 66502, (1976).
9. J. C. Kuo, MS Thesis, Kansss State University, Manhattan, KS 66502, (1978).

II. Gas Phase Raman Spectra of Some CF_3OOX Compounds (X = H, D, F, Cl)

A. Introduction

CF_3OOX compounds (X = H, D, F, Cl) are of special interest to the synthetic inorganic chemist (1-7). Along with bis (trifluoromethyl trioxide), CF_3OOOCF_3, (8), they serve as the key reagents for the synthesis of many highly fluorinated peroxides (2, 5-7, 9-11). In fact, an important stimulus to the increase, over the past decade, in the number and variety of known highly fluorinated peroxides was the discovery in 1967 of CF_3OOOCF_3 (8) and in 1968 of CF_3OOH (1), the parent compound of the CF_3OOX series (2-5).

In addition to exploiting the synthetic potential of CF_3OOOCF_3 and the CF_3OOX series (2, 5-7, 9-11), the Fluorine Chemistry group in the Department of Chemistry at Kansas State University has investigated the vibrational spectra of CF_3OOOCF_3 (12) and the structure of the CF_3OOX series by vibrational spectroscopy (13) and electron diffraction (14). The electron diffraction data were taken by Dr. C. J. Marsden in the laboratory of Professor L. S. Bartell at the University of Michigan using samples prepared by Dr. D. D. DesMarteau. The vibrational spectra were recorded at Kansas State University by Dr. D. D. DesMarteau and Dr. R. M. Hammaker and consisted of infrared spectra of the gas phase at ambient temperature and Raman spectra of the liquid phase below ambient temperature. In the analysis of the electron diffraction data, it was desirable to have force constants for the CF_3OOX series members. Dr. R. M. Hammaker had made preliminary frequency assignments for the normal modes using the infrared data for gases and the Raman data for

liquids. These were used by Dr. C. J. Marsden at the University of Michigan to do a normal coordinate analysis and obtain the desired force constants. The present investigation was undertaken to complete this study of the vibrational spectra of the CF_3OOX series by attempting to obtain additional Raman data and to refine further the force constants for the CF_3OOX series.

The gas phase infrared data available (13) covered the frequency range from 4000 to 160 cm^{-1} and included all four CF_3OOX series members X = H, D, F, Cl. The liquid Raman data available (13) included only the three series members X = H, D, F. Only an Ar^+ laser was available at the time these dats were taken and the yellow CF_3OOCl liquid at low temperature was completely decomposed by photolysis within minutes after exposure to the laser beam. It was not possible to do more than locate the two intense bands in CF_3OOCl as near 830 and 290 cm^{-1}. When the system for Raman Spectroscopy built around the Spex 14018 Double Monochromator and described in Part I was completed it was possible to do gas phase Raman spectroscopy with the Ar^+ laser and liquid phase Raman spectroscopy with the CW dye laser. The experimental work selected for inclusion in this part of the thesis is the following:

(1) Gas phase Raman spectra of CF_3OOH and CF_3OOF using the Ar^+ laser

(2) Liquid phase Raman spectra of CF_3OOCl using the CW dye laser

(3) Liquid phase Raman spectra of CF_3OOH, CF_3OOD, and CF_3OOF using the Ar^+ laser.

The available liquid phase Raman spectra of CF_3OOH, CF_3OOD and

CF_3OOF using the Ar^+ laser had been recorded using the JASCO Model R-300 Laser Raman spectrophotometer (13). These data will be redetermined using the Spex 14018 Double Monochomator as a check on consistency and quality of spectra from the two instruments. Since the torsional modes of the CF_3OOX series, τ_{CF_3} and τ_{OX} (with the exception of τ_{OH} and τ_{OD}) are below 160 cm^{-1}, they are not observable with our infrared spectrophotometer (Perkin-Elmer Model 180). Consequently, our only access to these frequencies in the gas phase is Raman spectra. For CF_3OF a large frequency shift on phase change occurs for the CF_3 torsion (15,16). Similar frequency shifts on phase change may occur for the CF_3OOX series. In addition, the Raman spectra for gaseous CF_3OOH and CF_3OOF will complement the infrared data and assist in final frequency assignments to normal modes and possible refinement of the force constants. Since the CW dye laser power will not be sufficient for the observation of gas phase Raman spectra, our investigation of CF_3OOCl will be limited to the liquid phase. It is hoped that comparison of liquid phase and gas phase Raman frequencies for CF_3OOH and CF_3OOF will allow reasonable estimates of gas phase Raman frequencies for CF_3OOCl to be made from liquid Raman frequencies. The estimated gas phase Raman frequencies for CF_3OOCl below and above 160 cm^{-1} will supplement and compliment, respectively, the available infrared data (13). The addition of the Raman measurements listed previously will then complete the study of the vibrational spectra of the CF_3OOX series as all our present capabilities for doing Raman spectroscopy will have been utilized.

B. Experimential Procedures

1. Sources of Compounds

All four CF_3OOX compounds were prepared by Dr. D.D. DesMarteau at Kansas State University using published procedures as follows:

CF_3OOH (1,2);	$CF_3OOC(O)F+H_2O$	→	$CF_3OOH + CO_2 + HF$
CF_3OOF (3):	CF_3OOH+F_2	$\xrightarrow{CsF}$	$CF_3OOF + HF$
CF_3OOCl (4,5):	$CF_3OOH+ClF$	$\xrightarrow{CsF}$	$CF_3OOCl + HF$
CF_3OOD:	$CF_3OOH + D_2O$	→	$CF_3OOD + HDO$

The CF_3OOD formed in the last reaction is always contaminated with CF_3OOH. It is possible to obtain a higher yield of CF_3OOCl from reaction (5) of ClF with $CF_3OOC(O)F$ but it is difficult to separate unreacted $CF_3OOC(O)F$ from CF_3OOCl so the method above was used.

2. Recording the Raman Spectra

All Raman spectra were recorded using the instrument described in Part I. For gases the Spex 1443A External Resonating Cavity (ERC) was used with both commercial and locally fabricated gas cells as noted in Part I Section H-3. The commercial gas cell was one formerly marketed by Cary Instruments but no longer available. It is similar in design to the Spex 1443 Gas Cell (Brewster angle windows, stopcock for convenient filling, diameter 10 mm, length 40 mm). The other gas cell body was made of pyrex with the ends cut at the Brewster angle and a Teflon stopcock near the center of the cell body. Windows were glass microscope slides sealed to the pyrex cell body with a halocarbon wax. The Raman spectra of the liquids were recorded using the low temperature cell described in Part I (Section G-3). The Spectra-Physics Model 164-03 Ar^+ laser was used to obtain the spectra of gaseous CF_3OOH and CF_3OOF as well as liquid CF_3OOH,

CF_3OOD, and CF_3OOF. The spectra of liquid CF_3OOCl were recorded using the Spectra Physics Model 375 CW dye-laser pumped by the Ar^+ laser. The frequency of the dye laser output was 620 nm for these experimenta uaing Rhodamine B as the lasing dye.

C. Raman Spectra

Examples of the Raman spectra recorded are shown in Figures 1, 2, 3, and 4 for CF_3OOH, CF_3OOD, CF_3OOF, and CF_3OOCl, respectively, in the liquid phase and in Figures 5 and 6 for CF_3OOH and CF_3OOF, respectively, in the gas phase. The frequencies from the Raman spectra are presented in Tables 1, 2, 3, and 4 for CF_3OOH, CF_3OOD, CF_3OOF, and CF_3OOCl, reapectively. These tables also contain the unpublished data of D.D. DesMarteau and R.M. Hammaker (13) which consist of infrared spectra of the four gases recorded down to 160 cm^{-1} on a Perkin-Elmer Model 180 infrared apectrophotometer and Raman spectra of liquid CF_3OOH, CF_3OOD, and CF_3OOF in the low temperature cell recorded on the JASCO Model R-300 Laser Raman spectrophotometer using the Ar^+ ion laser. The instrument parameters used in recording Raman spectra with the instrument described in Part I are included in the captions for Figurea 1, 2, 3, 4, 5, and 6. The assignments to be described in subsequent sections are included in Tablea 1, 2, 3, and 4.

The polarization information in Tables, 1, 2, and 3 is from the unpublished data of D.D. DesMarteau and R.M. Hammaker (13) taken with the JASCO instrument. For Table 4, the polarization information comes from the data taken on the instrument deacribed in Part I. Depolarization ratios were determined by method IV of Claassen, Selig, and Shamir (17) but their f has not been determined for the JASCO instrument or the instrument described in Part I. For the JASCO instrument, known depolarized bands gave depolarization ratios between 0.75 and 0.89. Such measurements have

Explanation of Figure 1

Raman spectrum of liquid CF_3OOH

Conditions for the spectrum:

Laser and the exciting wavelength:	Ar^+, 514.5 nm.
Laser power:	130 mw.
Slit width:	150/200/150 μm.
Scal speed:	1.0 cm^{-1}/sec.
Chart speed:	2.0 cm/min.
Gain:	1K.
Filter:	1.3.
Polarization:	0 deg.
Sampling:	Low temperature cell.
Temperature:	-30°C.

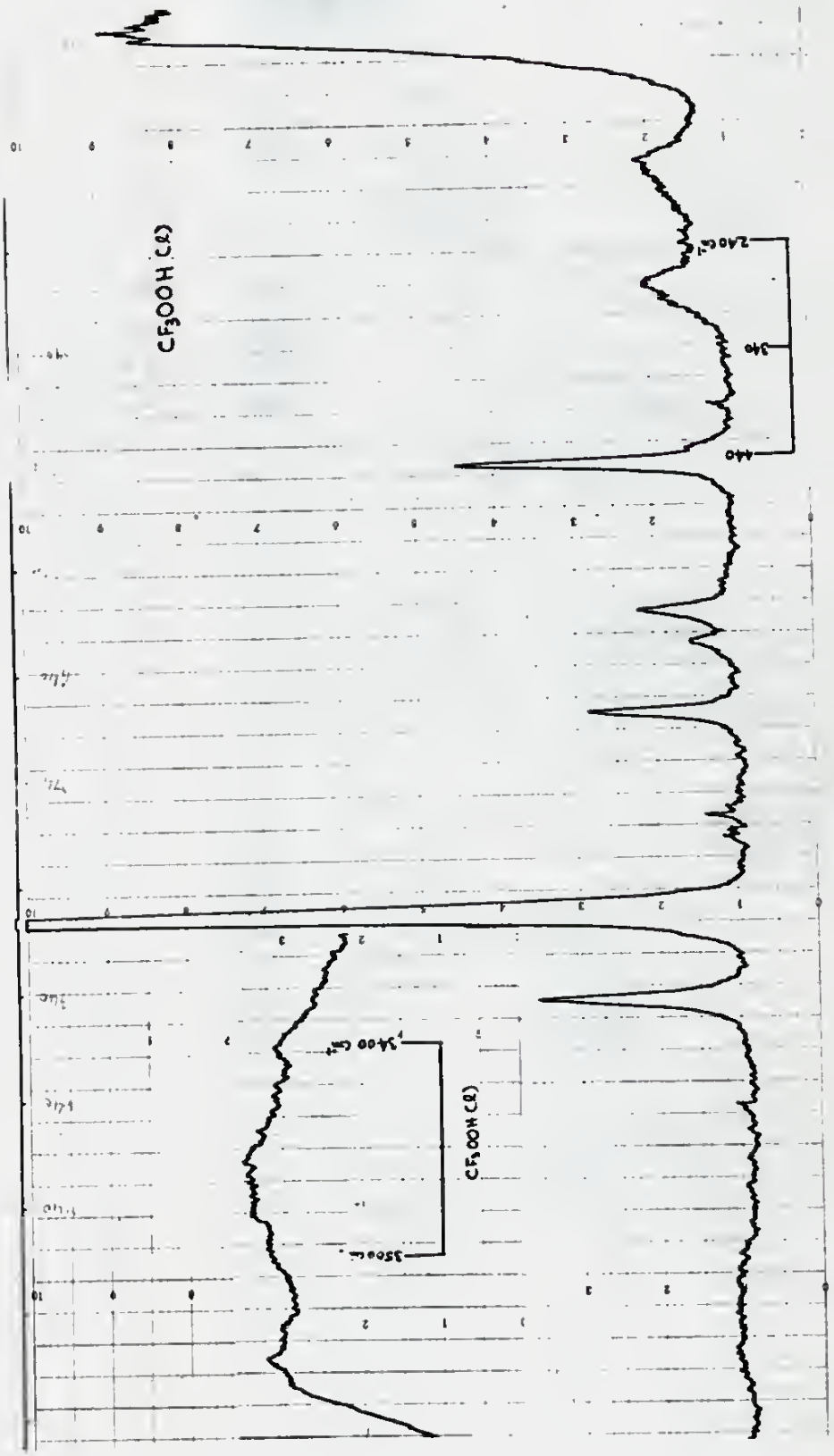

Figure 1

Explanation of Figure 2

Raman spectrum of liquid CF_3OOD

Conditions for the spectrum:

Laser and the exciting wavelength:	Ar^+, 514.5 nm.
Laser power:	250 mw.
Slit width:	180/200/180 μm.
Scan speed:	1.0 cm^{-1}/sec.
Chart speed:	2.0 cm/min.
Gain:	1K.
Filter:	1.3.
Polarization:	Top plots at 0^o and the bottom plots at 90^o, except the insert in range from app. 1200 to 1300 cm^{-1} at 0^o.
Sampling:	Low temperature cell.
Temperature:	About 0^o C.

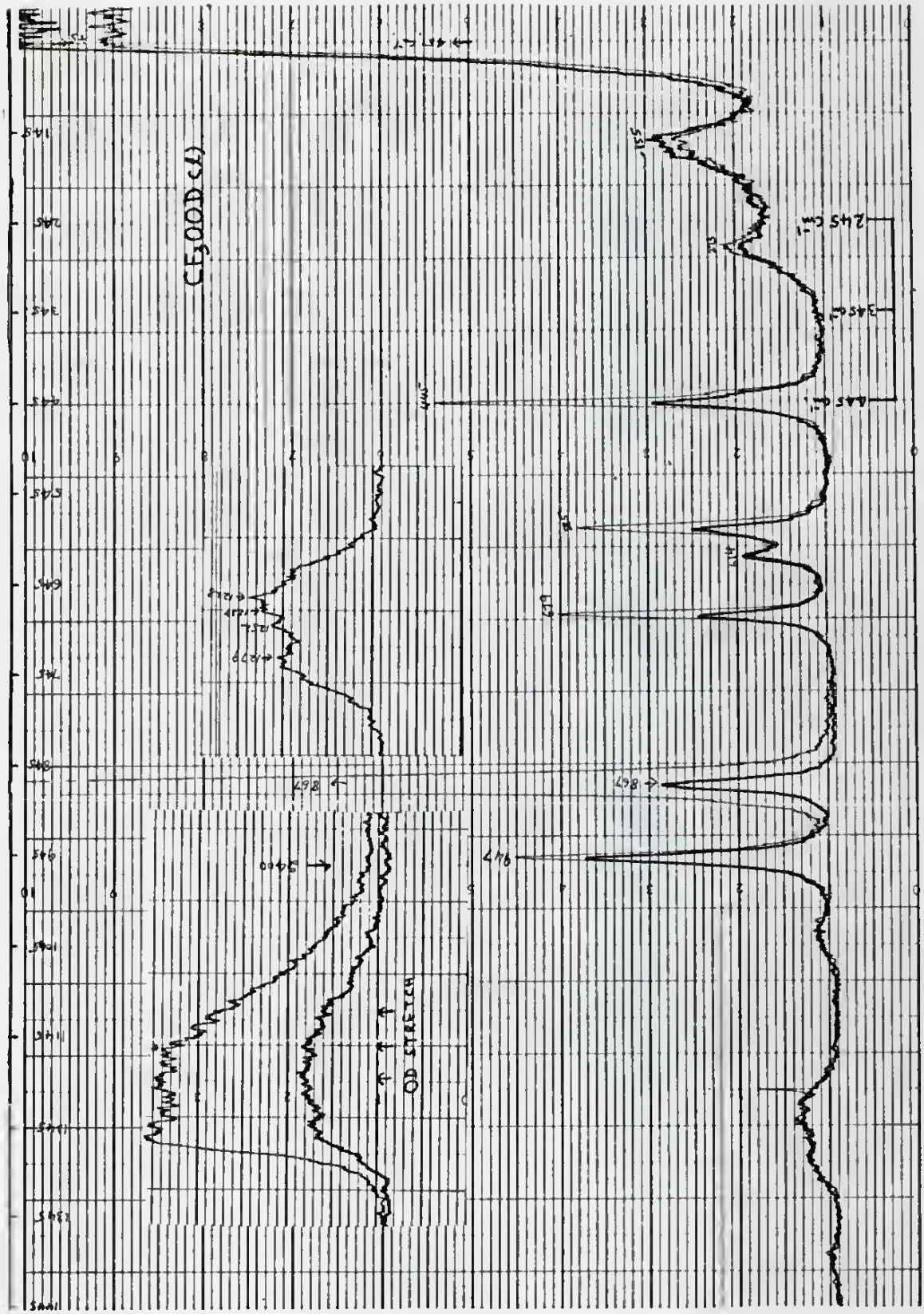

Figure 2

Explanation of Figure 3

Raman spectrum of liquid CF_3OOF

Conditions for the spectrum:

Laser and the exciting wavelength:	Ar^+, 514.5 nm.
Laser power:	200 mw.
Slit width:	180/200/180 μm.
Scan speed:	1.0 cm^{-1}/sec.
Chart speed:	3.0 cm/min.
Gain:	3K.
Filter:	1.3.
Polarization:	0 deg.
Sampling:	Low temperature cell.
Temperature:	-60° C.

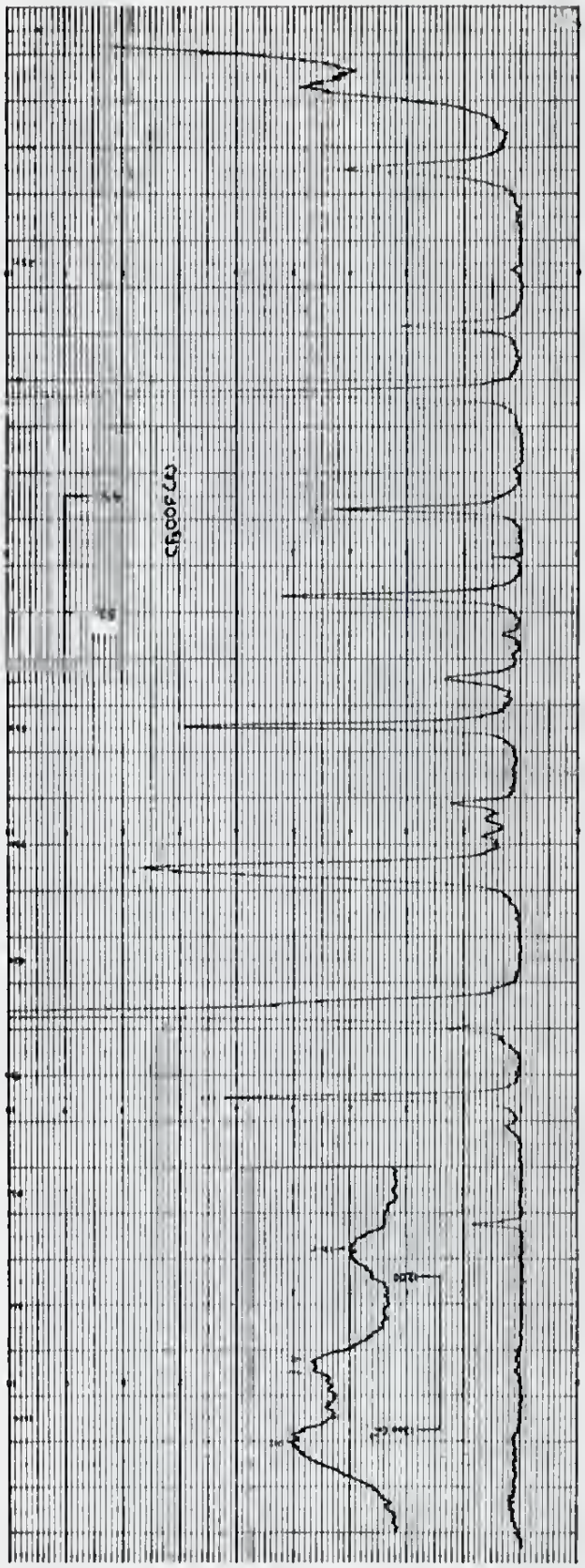

Figure 3

Explanation of Figure 4

Raman spectra of liquid CF_3OOCl

Conditions for the somplete spectrum:

Laser and the exciting wavelength:	Dye laser (Rhodamine B), 620 nm.
Laser power:	100 mw.
Slit width:	200/200/200 μm.
Scan speed:	0.5 cm^{-1}/sec.
Chart speed:	2.0 cm/min.
Gain:	100.
Filter:	2.2.
Polarization:	Top plot at 0°; Bottom plot at 90°.
Sampling:	Low temperature cell.
Temperature:	-20° C.

Conditions for the low frequency insert:

Laser power:	150 mw.
Slit width:	150/150/150 μm.
Scan speed:	1.0 cm^{-1}/sec.
Chart speed:	3.0 cm/min.
Gain:	300.
Filter:	1.3.
Polarizaton:	0 deg.
Other conditions:	Unchanged.

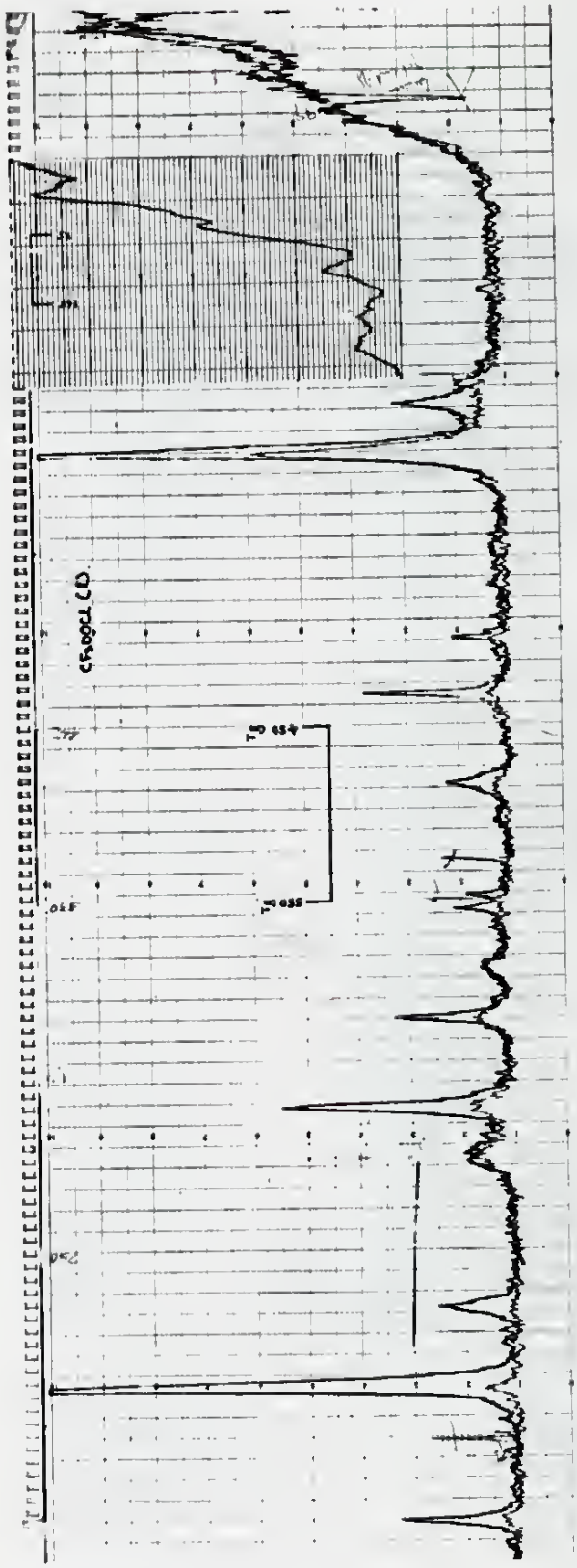

Figure 4

Explanation of Figure 5

Raman spectrum of gaseous CF_3OOH

Conditions for the spectrum:

Laser and the exciting wavelength:	Ar^+, 514.5 nm.
Laser power:	2.2 watts.
Slit width:	200/200/200 μm.
Scan speed:	1.0 cm^{-1}/sec.
Chart speed:	2.0 cm/min.
Gain:	300.
Filter:	1.3.
Polarization:	0 deg.
Sampling:	Gas cell.
Temperature:	Room temperature.
Pressure:	500 torr.

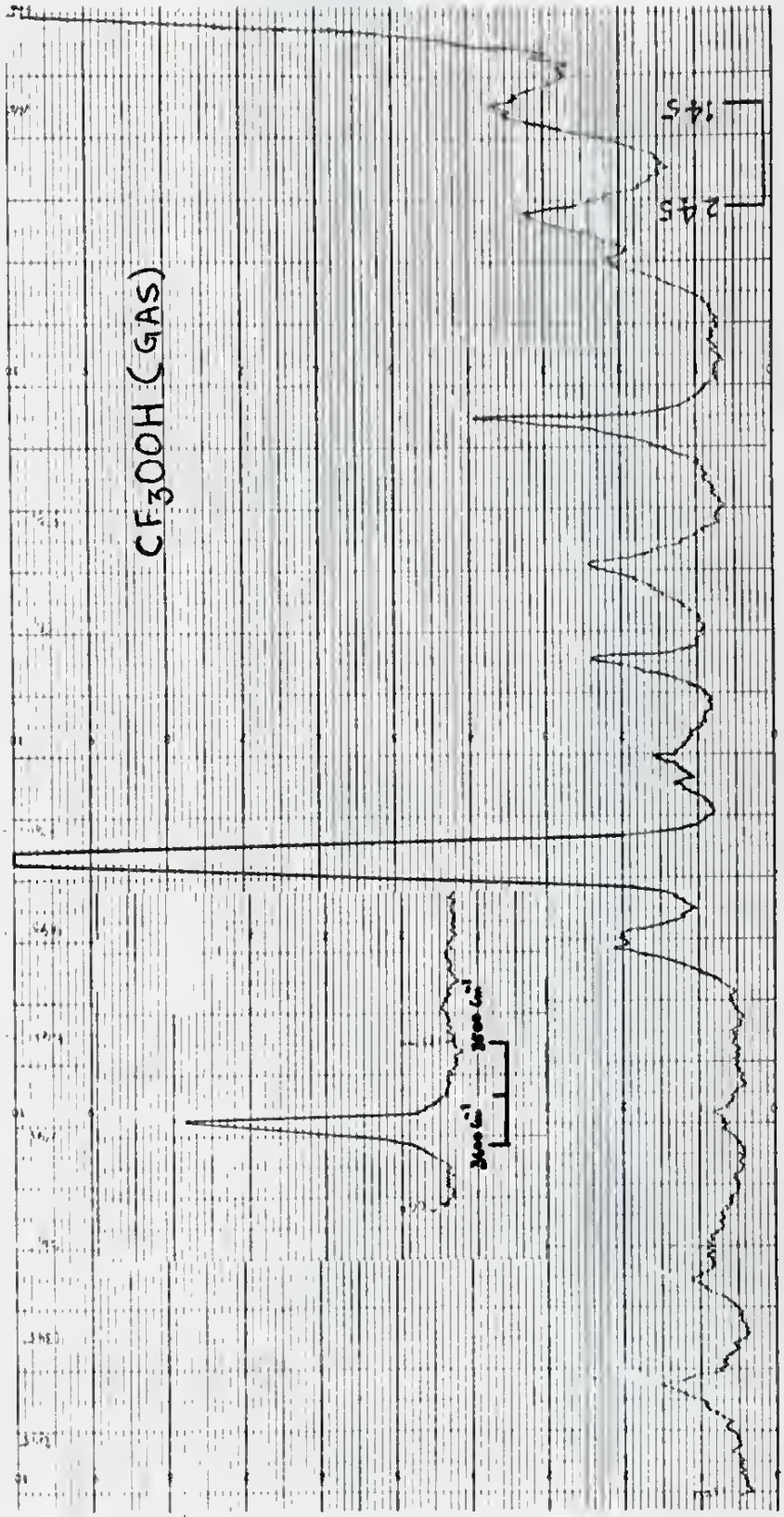

Figure 5

Explanation of Figure 6

Raman spectrum of gaseous CF_3OOF

Conditions for the spectrum:

Laser and the exciting wavelength:	Ar^+, 514.5 nm.
Laser power:	2.1 watts.
Slit width:	200/200/200 μm.
Scan speed:	0.5 cm^{-1}/sec.
Chart speed:	3.0 cm/min.
Gain:	100.
Filter:	1.3.
Polarization:	0 deg.
Sampling:	Gas cell.
Temperature:	Room temperature
Pressure:	600 torr

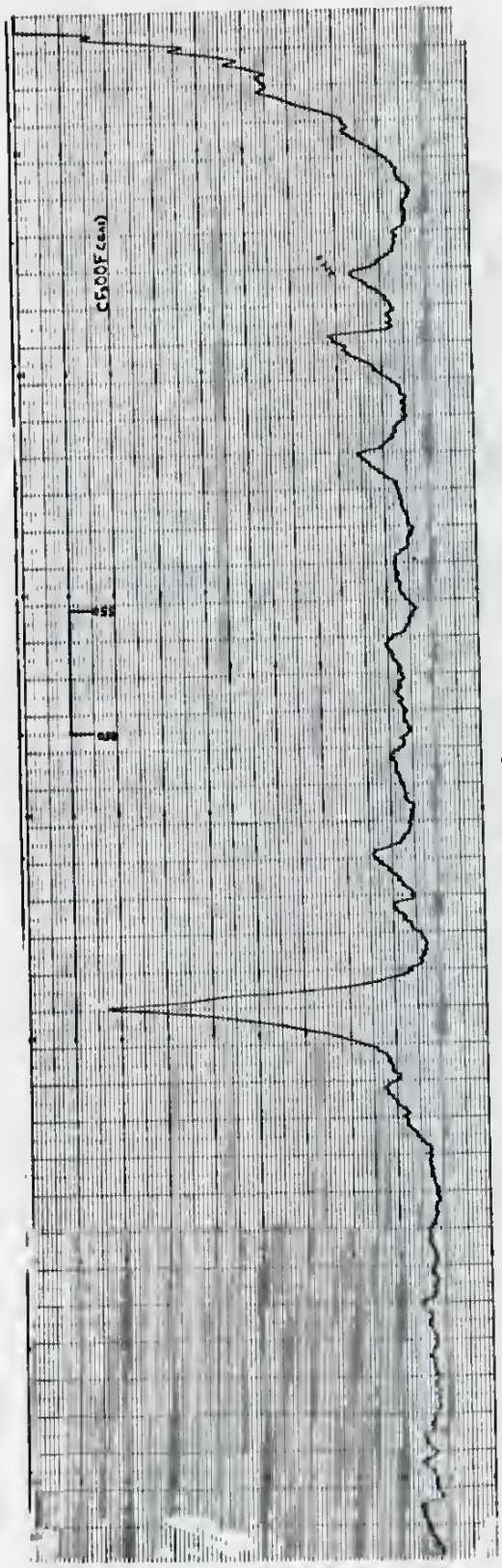

Figure 6

Table 1. Infrared and Raman frequencies for CF_3OOH (in cm^{-1})[a]

I.R. (g) P.E. 180	Raman(g) 14018	Absolute Intensity[b]	Raman(l) 14018	Absolute Intensity[b]	Raman(l) R-300	Relative Intensity[b]	Polarization[c]	Assignments[d]
	141.6	16	155	8	~160	2.4	dp/wp	ν_{15}, τ_{CF}
244	246	20						ν_{14}, τ_{OH}3
	290	4	275	9	~275	3.1	p	ν_8, $\rho_{CF_3}(A')$
370								$\nu_{14} + \nu_{15}$
378								$\tau_{OH} + \tau_{CF_3}$
431(sh)?P?								
440Q	445	33	448	34	446	13.5	p	ν_9, δ_{COO}
451R								
473P								
482Q								$2\nu_{14}$, $2\tau_{OH}$
490(sh)?R?								
576(sh)P?								
587Q?	590	16.5	582	12	584	8.85	p	ν_7, a.$\delta_{CF_3}(A')$
605P								
615Q	617	-	612	4	616	2.4	dp/wp	ν_{12}, a.$\delta_{CF_3}(A'')$
625(sh)?R?								
671P								
677(sh)								
680Q	686	16	679	18	680	12.2	p	ν_6, s.δ_{CF_3}
687R								
865	866	>100	872	>100	868	100	p	ν_4, ν_{OO}

Table 1 continued:

I.R. (g) P.E. 180	Raman(g) 14018	Absolute Intensity[b]	Raman(l) 14018	Absolute Intensity[b]	Raman(l) R-300	Relative Intensity[b]	Polarization[c]	Assignments[d]
939(sh)P 941? 947Q 949(sh) 950(sh) 955R	948	12.5	948	26	949	16.3	p	ν_3, ν_{CO}
1221 1230					~1210			ν_2, a.ν_{CF_3}
1244 1252	~1253	4			~1230	~1.5		ν_{11}, a.ν_{CF_3} (A")
1269 1279 1290(sh)	1285	6			~1280	1.6		ν_1, a.ν_{CF_3} (A')
1375P 1383Q 1391R	1387	10.5			~1400	2.4	p	ν_{10}, δ_{OOH}
3567P 3575Q 3583R	3575	36			~3550	7.7	p	ν_5, ν_{OH}

a. Abbreviations used: I.R., infrared: (g), gas phase; (l), liquid phase; P.E. 180, Perkin-Elmer Model 180 infrared spectrophotometer; 14018, Spex Model 14018 Double Monochromator: R-300, JASCO Model R-300 Laser Raman Spectrophotometer; sh, shoulder; P,Q,R, possible P,Q, and R branches in infrared spectra of gases; dp/wp, depolarized or weakly polarized; p, polarized.

Table 1 continued:

b. All intensity columns refer to the frequency columns to their immediate left (for a specified type of spectrum, phase, and instrument). Absolute intensity does not have its conventional meaning but is used where all Raman spectra were recorded with the most intense band exceeding full scale deflection on the recorder chart. The values given in the absolute intensity columns are the positions of the band maxima on the recorder chart minus the position of the base line on the recorder chart (see Figures 1-6). The recorder chart scale used is 0 to 100. Thus, for the absolute intensity columns values below 100 can be compared with each other but their intensity relative to the most intense band is only known to be < (value listed)/100. Relative intensity is used in the cases where Raman spectra were recorded with the most intense Raman band on scale. The most intense Raman band has been assigned an intensity of 100 and all other band intensities have been put on this scale where the most intense band has an intensity of 100.

c. Polarization measurements were made on the JASCO R-300 Laser Raman Spectrophotometer using method IV of Claassen, Selig, and Shamir (17). Their f value has not been determined for the JASCO instrument; however, known depolarized bands gave depolarization ratios between 0.75 and 0.89 using the JASCO instrument.

d. The symbols used here are based on C_s symmetry (see Table 6) although CF_3OOX compounds possess only C_1 symmetry (see Table 5). For C_s symmetry $\nu_1 - \nu_{10}$ would belong to the A' species and $\nu_{11} - \nu_{15}$ would belong to the A" species (see Table 6).

Table 2. Infrared and Raman frequencies for CF_3OOD (in cm^{-1})[a]

I.R. (g) P.E. 180	Raman(1) 14018	Absolute Intensity[b]	Raman(1) R-300	Relative Intensity[b]	Polarization[c]	Assignments[d]
	155	11	~160	3	dp/wp	ν_{15}, τ_{CF_3}
174[e]						
183						ν_{14}, τ_{OD}
190(sh)						
	273	6	~275	2.3	p	ν_8, $\rho_{CF_3}(A')$
320?						
330?						
340						$2\nu_{14}$, $2\tau_{OD}$
356						$\nu_{14} + \nu_{15}$, $\tau_{OD} + \tau_{CF_3}$
365(sh)?						
427(sh)P?						
431?						
438Q	445	44	445	18	p	ν_9 δ_{COO}
448(sh)R?						
574(sh)?P?						
585Q?	585	28	583	13	p	ν_7, $a.\delta_{CF_3}(A')$
604P						
614Q	614	8	613	2.5	dp/wp	ν_{12}, $a.\delta_{CF_3}(A'')$
624(sh)?R?						
672P						
677(sh)						
680Q	679	20	680	~15	p	ν_6, $s.\delta_{CF_3}$
687R						

Table 2 continued:

I.R. (g) P.E. 180	Raman(1) 14018	Absolute Intensity[b]	Raman(1) R-300	Relative Intensity[b]	Polarization[c]	Assignments[d]
863	~867	>100	867	100	p	ν_4, ν_{OO}
936P 942(sh) 944Q 952R	947	35	947	22	p	ν_3, ν_{CO}
1012(sh)?P? 1020Q 1028(sh)?R? 1033(sh)?	~1033	2	~1035	1.3	p	ν_{10}, δ_{OOD}
1227 1235	~1233	12	~1220	3		ν_2 s. ν_{CF_3}
1246	~1252	11	~1240	3.65		ν_{11}, a. ν_{CF_3}(A")
1257 1271 1280 1290(sh)?	~1279	10	~1280	2.2		ν_1, a. ν_{CF_3}(A')
2634P 2642Q 2650R	~2620	22	~2620	16.3	p	ν_5, ν_{OD}

Table 2 continued:

a. See note a in Table 1.

b. See note b in Table 1.

c. See note c in Table 1.

d. See note d in Table 1.

e. The midpoint of this doublet at 174 cm^{-1} and 183 cm^{-1} is taken as 179 cm^{-1} and the value 179 cm^{-1} is used (Tables 8, 10, 12, and 15) in the discussion of the assignments and in the normal coordinate analysis.

Table 3. Infrared and Raman frequencies for CF_3OOF (in cm^{-1})[a]

I.R. (g) P.E. 180	Raman(g) 14018	Relative Intensity[b]	Raman(l) 14018	Absolute Intensity[b]	Raman(l) R-300	Relative Intensity[b]	Polarization[c]	Assignments[d]
			77.5	14	~75		dp/wp	ν_{15}, τ_{CF_3}
	132	6.5	147	29	147	7.6	dp/wp	ν_{14}, τ_{OF}
278	280	15	283	20	282	6.8	p	ν_8, $\rho_{CF_3}(A')$
330P 336Q 343R	332	22	342	>100	340	49	p	ν_{10}, δ_{OOF}
429P 434Q 440R	430	14.4	441	32	440	12	p	ν_9, δ_{COO}
509(sh)P 512(sh) 514Q 516(sh) 520R			516	41	515	17	p	ν_{13}, $\rho_{CF_3}(A'')$
582P 588Q 595R	584	7.24	587	12	587	~5	dp/wp	ν_7, a. $\delta_{CF_3}(A')$
617(sh) 624P? 630Q? 634R?			628	58	628	26	p	ν_{12}, a. $\delta_{CF_3}(A'')$

Table 3 continued:

I.R. (g) P.E. 180	Raman(g) 14018	Relative Intensity[b]	Raman(l) 14018	Absolute Intensity[b]	Raman(l) R-300	Relative Intensity[b]	Polarization[c]	Assignments[d]
688(sh)P? 693Q 698R	684	6	695	9.5	695	6	dp/wp	ν_6, s.δ_{CF_3}
755P 757 760Q 765R	752	13	750.5	63	750	34	p	ν_5, ν_{OF}
867(sh) 871P? 874Q 879R? 882	875	100	868(sh) ~876	>100	874	100	p	ν_4, ν_{OO}
945(sh)P? 948sh 950Q 955R	946	13	949	51	949	29	p	ν_3, ν_{CO}
1184(sh) 1190 1196			1182	7	1180		dp/wp	ν_2, s.ν_{CF_3}
1222 1230 1257(sh) 1263 1270			1259	8	1255		dp/wp	ν_{11}, a.ν_{CF_3} (A")
1297			1307	12	1310		dp/wp	ν_1, a.ν_{CF_3} (A')

Table 3 continued:

a. See note a in Table 1.

b. See note b in Table 1.

c. See note c in Table 1.

d. See note d in Table 1.

Table 4. Infrared and Raman frequencies for CF_3OOCl (in cm^{-1})[a]

I.R. (g) P.E. 180	Raman(1) 14018	Absolute Intensity[b]	Polarization[c]	Assignments[d]
	80	~6	p	ν_{15}, τ_{CF_3}
	150	~4	dp/wp	$2\nu_{15}$, $2\tau_{CF_3}$
	204	~4	p	$2\nu_{15}+\nu_{14}$; $2\tau_{CF_3}+\tau_{OCl}$
250				
259	266	22	p	ν_8, ρ_{CF_3} (A')
265(sh)				
~290	295	>100	p	ν_{10}, δ_{OOCl}
491P				
424Q	431	28	p	ν_9, δ_{COO}
429R				
474				
478	483	12	p	ν_{13}, ρ_{CF_3} (A")
578P				
583Q	588	5	dp/wp	ν_7, a.δ_{CF_3} (A')
589R				
610P?				
615Q?[e]	617	23	p	ν_{12}, a.δ_{CF_3} A")
620(sh)R?				
661P				
665Q	667	45	p	ν_6, s.δ_{CF_3}
670R				
693(sh)P?				
697Q	696	8.5	dp/wp	ν_5, ν_{OCl}
701(sh)R?				
824P				
828Q	830	>100	p	ν_4, ν_{OO}
832R				
898(sh)?				
900P				
903Q	905	22	p	ν_3, ν_{CO}
904sh				
908R				
1205(sh)?				
1213				ν_2, s.ν_{CF_3}
1230?				

Table 4 continued:

I.R. (g) P.E. 180	Raman(1) 14018	Absolute Intensity[b]	Polarization[c]	Assignments[d]
1241 1247				ν_{11}, a.γ_{CF_3}(A")
1281 1286(sh) 1290(sh)	1296			ν_1, a.ν_{CF_3} (A')

a. See note a in Table 1.

b. See note b in Table 1.

c. Polarization measurements were made on the Spex 14018 Double Monochromator using method IV of Claassen, Selig, and Shamir (17). Their f value has not been determined for the Spex 14018 Double Monochromator.

d. See note d in Table 1.

e. Due to the uncertainty in the shape of this band it is treated as a doublet at 610 cm^{-1} and 615 cm^{-1} and midpoint is taken as 613 cm^{-1} rather than taking 615 cm^{-1} as a possible Q branch frequency. The value 613 cm^{-1} is used (Tables 8, 10, 14, and 15) in the discussion of the assignments and in the normal coordinate analysis.

not yet been made with known depolarized bands for the instrument described in Part I.

D. Geometry and Symmetry Coordinates for the CF_3OOX Series

The geometry used for the normal coordinate analysis reported in Section F was taken from the results of the electron diffraction experiments performed at the University of Michigan (14). The general structure for CF_3OOX is shown in Figure 7 (which is Figure 1 in reference 14). The structural parameters are listed in Table 5 (which is abstracted from Tables IV and VI in Reference 14). The nature of the tilt and twist angles in Table 5 is illustrated in Figure 8. The general molecular model adopted assumed only that the CF_3 group possesses local C_{3v} symmetry and that its axis lies in the O_2O_1C plane. The angle of tilt denotes the deviation of the threefold axis of the CF_3 group away from the $C\text{-}O_1$ direction. For a positive tilt angle F_1 is closer to O_1 than are F_2 and F_3. The angle of twist defines the rotation of the CF_3 group about its threefold axis away from the conformation in which it staggers the $O_1\text{-}O_2$ bond. For a non zero angle of twist, the O_2O_1C plane and the O_1CF_1 plane are no longer coincident. For a positive twist angle F_3 is closer to O_2 than is F_2.

Although, the CF_3OOX structures described in Table 5 have only C_1 symmetry, it is convenient to define symmetry coordinates under C_s symmetry for purposes of comparison with the related CF_3OX series (16, 18) which does possess C_s symmetry. For a structure with a zero angle of twist as shown in Figure 7 only the X atom being out of the $F_1CO_1O_2$ plane prevents C_s symmetry. The deviation from C_s selection rules might depend on the mass of the out of plane atom, X. If so, then CF_3OOH and CF_3OOD might approximate C_s selection rules while CF_3OOF and CF_3OOCl might show increasing deviation from C_s selection rules. The atom numbering system and internal

Explanation of Figure 7

General structure for CF_3OOX

The figure shows a view of the molecule CF_3OOX (X = H, D, F, and Cl) showing the atomic labeling scheme adopted in Table 5. F_1, F_2, F_3, are the three fluorine atoms of the CF_3 rotor which is assumed to possess local C_{3v} symmetry with its C_3 axis in the O_2O_1C plane. X may be H, D, F, or Cl and is not in the O_2O_1C plane.

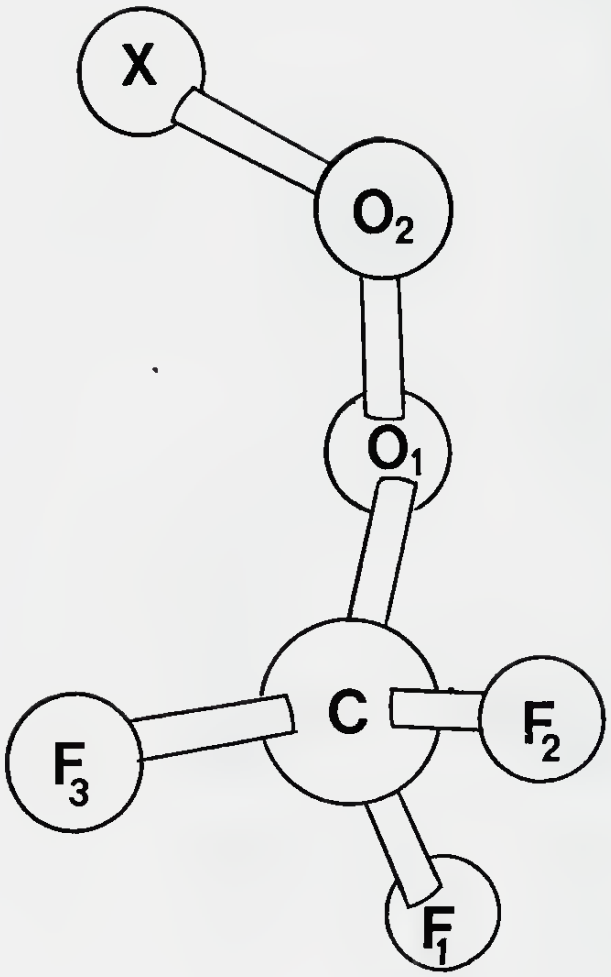

Figure 7

Table 5. Structural Parameters for CF_3OOH, CF_3OOF, and CF_3OOCl (14) as CF_3OOX

Parameter and units[a]	CF_3OOH[b]	CF_3OOF	CF_3OOCl[c,d]
Lengths, Å			
r (O_2-X)	0.974	1.449	1.699
r (O_1-O_2)	1.447	1.366	1.447
r (C-O_1)	1.376	1.419	1.372
r (C-F)	1.324	1.322	1.323
Angles, deg.			
(O_2-O_1-C)	107.6	108.2	108.1
(F_1-C-F_2)	109.2	109.0	110.0
tilt	4.8	3.9	5.1
(X-O_2-O_1)	100.0	104.0	110.8
τ(X-O_2-O_1-C)	95.0	97.1	93.2
twist	0.0	- 2.2	- 15.5 and + 23.6
I_a (amu-Å^2)	91.0	102.3	107.1
I_b (amu-Å^2)	162.6	263.0	371.9
I_c (amu-Å^2)	162.8	274.4	386.6
K[e]	- 0.997	- 0.948	- 0.970

a. Bond lengths are internuclear distances averaged over rotational and vibrational states that are thermally populated. The angle of tilt and the angle of twist and their signs are illustrated in Figure 8.

b. For CF_3OOD the corresponding values are 91.8, 167.4, 168.0, and -0.991 for I_a, I_b, I_c, and K respectively.

c. CF_3OOCl exists as a mixture of conformations with different twist angles. The conformer with a -15.5 deg. angle of twist is 66% abundant and the one with a +23.6 deg. angle of twist is 34% abundant.

Table 5 continued:

d. The values of I_a, I_b, I_c, and K listed are for $CF_3OO^{35}Cl$ with a -15.5 degree angle of twist.

e. Asymmetry parameter, K, defined as $2(I_b^{-1}-(\frac{1}{2})(I_a^{-1}+I_c^{-1}))/(I_a^{-1}-I_c^{-1})$, = -1.0 for a prolate symmetric top.

Explanation of Figure 8a

Illustration of the angle of tilt

X and F_3 are above the $O_2O_1CF_1$ plane and F_2 is below that plane. A positive tilt angle decreases the F_1O_1 distance and increases the F_2O_1 and F_3O_1 distances. Note that the tilt angle is the angle between the C_3 axis of the CF_3 rotor and the O_1C bond.

Explanation of Figure 8b

Illustration of the angle of twist

The figure shows the view along the threefold axis of the CF_3 group (coincident with the $C\text{-}O_1$ bond for a zero angle of tilt). A positive angle of twist moves F_3 (and F_1) closer to O_2 and moves F_2 farther from O_2. Note that for a non zero angle of twist the O_1CF_1 and O_2O_1C planes are not coincident.

a

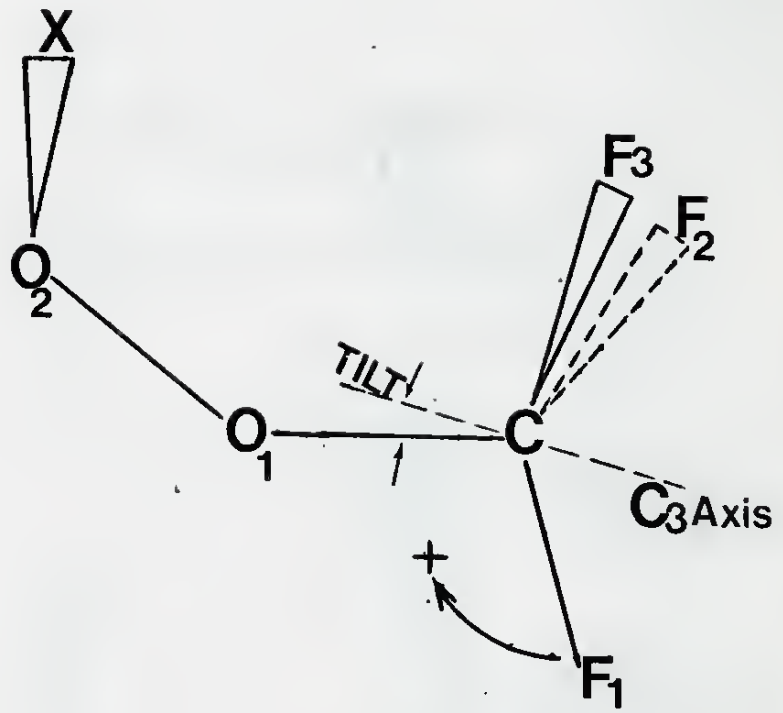

b

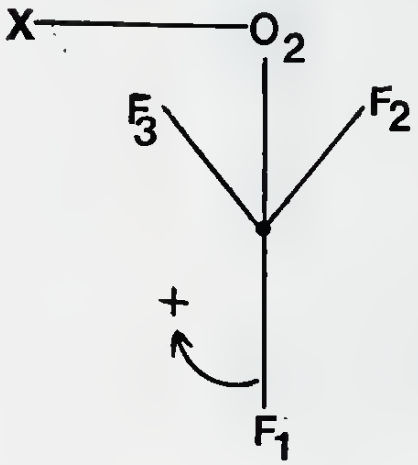

Figure 8a & 8b

coordinate definitions chosen to generate C_s symmetry coordinates are illustrated in Figure 9. The symmetry coordinates are listed in Table 6. The same diagram as shown in Figure 9 could be used for CF_3OX if oxygen atom 3 were deleted and the X atom moved to the oxygen atom 3 position. The numbering system in Figure 9 was used in the CART program (19) as noted in Section F to set up the secular equation but with the X atom out of the COO plane as in Figure 7 and Table 5.

E. Background for Preliminary Assignments

The CF_3OX series where X=F, Cl provides analogy to our CF_3OOX series. Studies of CF_3OF (20) and CF_3OCl (21) and our work on Cl_2O_7 (22) had caused us to do a detailed study of gas phase infrared and liquid phase Raman spectra of CF_3OF and CF_3OCl (16,18). While our work was in progress Smardzewski and Fox (15) reported gas phase Raman spectra for CF_3OF and Raman spectra for both CF_3OF and CF_3OCl in argon matrics at 8 K. The combination of their Raman data with our Raman and infrared data for CF_3OF and CF_3OCl gives a reasonably complete picture of the vibrational spectra of these CF_3OX molecules. In addition the structure of CF_3OF has been determined using election diffraction (23).

Our preliminary assignments for the CF_3OX series were those of Smardzewski and Fox (15). Proposed normal modes approximated by the symmetry coordinates in Table 6 were assigned as follows for the CF_3 group; three CF stretches, 1150-1350 cm^{-1}; three CF_3 deformations, 540-700 cm^{-1}; two CF_3 rocks 200-300 cm^{-1}; and one CF_3 torsion (or CO torsion), 100-150 cm^{-1}. For the COX skeletal modes the assignments were as follows for CF_3OF and CF_3OCl, respectively, using gas phase infrared frequencies: C-O stretch, 947 and 919 cm^{-1}; O-X stretch, 882 and 780 cm^{-1}; and COX bend, 429 and 393 cm^{-1}. By analogy to the results of Durig's group for CH_3

Explanstion of Figure 9

Atom numbering and internal coordinates for CF_3OOX

The figure shows the scheme chosen for numbering the atoms and defining the internal coordinstes.

The X atom is held in the COO plane to give C_s symmetry.

r is CF stretching.

l is CO stretching.

d is OO stretching.

R is OX stretching.

α is FCF bending.

β is FCO bending.

γ is COO bending.

δ is OOX bending.

Note τ_{23} snd τ_{12} in Tsble 6 refer to torsion about the O-O and C-O bonds, respectively.

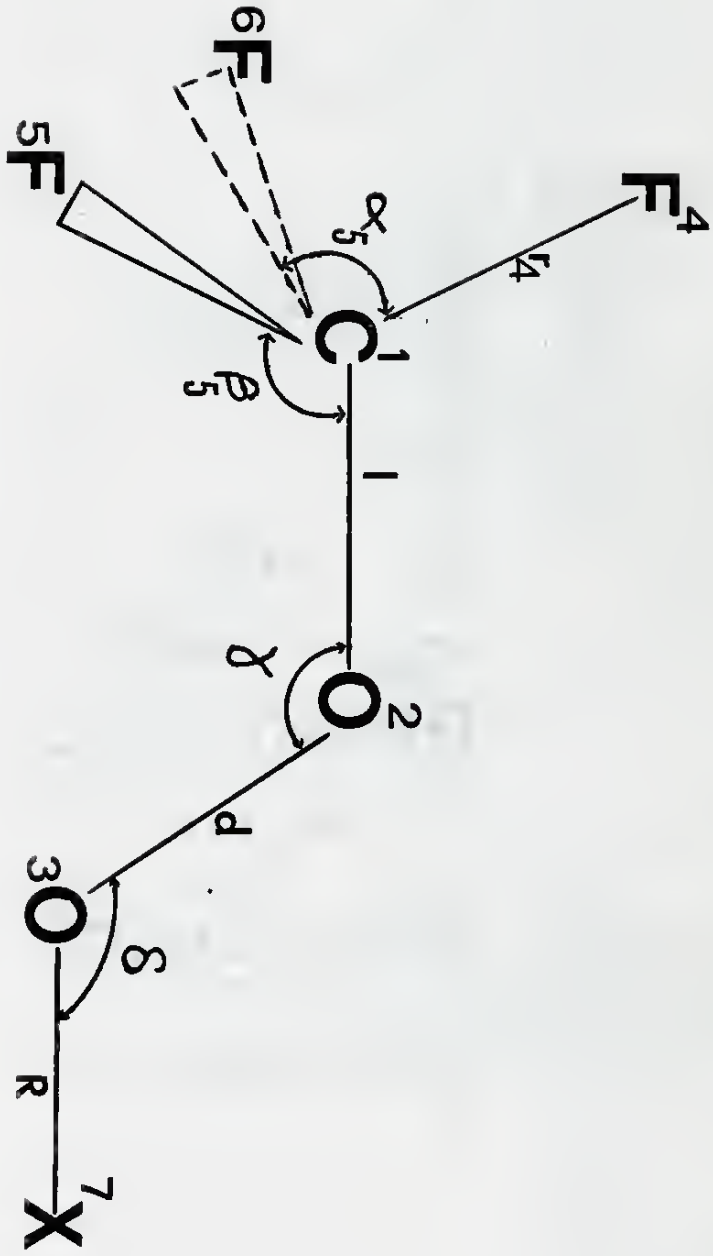

Figure 6

Table 6. Symmetry coordinates for CF_3OOX under C_s symmetry.

Numbers[a]		Coordinate[b]	Symbol[c]	Description[d]
		A' Species		
1	1	$(1/\sqrt{6})(2\Delta r_4-\Delta r_5-\Delta r_6)$	ν_{CF_3}	antisymmetric CF_3 stretch
2	2	$(1/\sqrt{3})(\Delta r_4+\Delta r_5+\Delta r_6)$	ν_{CF_3}	symmetric CF_3 stretch
3	3	$\Delta 1$	ν_{CO}	CO stretch
	4	Δd	ν_{OO}	OO stretch
4	5	ΔR	ν_{OX}	OX stretch
5	6	$(1/\sqrt{6})[\Delta\alpha_4+\Delta\alpha_5+\Delta\alpha_6)$ $-(\Delta\beta_4+\Delta\beta_5+\Delta\beta_6)]$	δ_{CF_3}	symmetric CF_3 deformation
6	7	$(1/\sqrt{6})(2\Delta\alpha_4-\Delta\alpha_5-\Delta\alpha_6)$	δ_{CF_3}	antisymmetric CF_3 deformation
7	8	$(1/\sqrt{6})(2\Delta\beta_4-\Delta\beta_5-\Delta\beta_6)$	ρ_{CF_3}	CF_3 rock
	9	$\Delta\gamma$	δ_{COO}	COO bend
8	10	$\Delta\delta$	δ_{OOX}	OOX bend
		A" Species		
9	11	$(1/\sqrt{2})(\Delta r_5-\Delta r_6)$	ν_{CF_3}	antisymmetric CF_3 stretch
10	12	$(1/\sqrt{2})(\Delta\alpha_5-\Delta\alpha_6)$	δ_{CF_3}	antisymmetric CF_3 deformation
11	13	$(1/\sqrt{2})(\Delta\beta_5-\Delta\beta_6)$	ρ_{CF_3}	CF_3 rock
	14	$\Delta\tau_{23}$	τ_{OX} or τ_{OO}	OX torsion or OO torsion
12	15	$\Delta\tau_{12}$	τ_{CF_3} or τ_{CO}	CF_3 torsion or CO torsion

a. The number at the left refers to the corresponding CF_3OX symmetry coordinate if Figure 9 were for CF_3OX with the oxygen atom 3 deleted and the X atom moved to the oxygen 3 atoms position. The number at the right refers to CF_3OOX.

b. The A' species also includes the redundant symmetry coordinate $1/\sqrt{6}[\Delta\alpha_4+\Delta\alpha_5+\Delta\alpha_6)+(\Delta\beta_4+\Delta\beta_5+\Delta\beta_6)]$ which is not shown but would, of course, be included in the normal coordinate analysis.

Table 6 continued:

c. For CF_3OX, symmetry coordinate 8 would have the symbol δ_{COX}. For CF_3OOX, symmetry coordinate 14 could have symbol either τ_{OX} or τ_{OO} and symmetry coordinate 15 could have symbol either τ_{CF_3} or τ_{CO}.

d. For CF_3OX, symmetry coordinate 8 would be called COX bend. For CF_3OOX, symmetry coordinate 14 could be called either OX torsion or OO torsion and symmetry coordinate 15 could be called either CF_3 torsion or CO torsion.

torsions (24), we had initially concluded that the Raman bands assigned to the CF_3 torsion were $\Delta v=2$ transitions (mainly $0\rightarrow2$) rather than $\Delta v=1$ transitions (mainly $0\rightarrow1$) (16,25). After receiving our preliminary assignments for the CF_3OX and CF_3OOX series, Dr. Marsden brought the microwave investigation of CF_3OF by Buckley and Weber (26) to our attention. Vibrational satellite lines having 0.4 times the intensity of the ground state lines at 194 K in the microwave spectrum of CF_3OF (26) are in good agreement with a population ratio of 0.39 if the v=1 state in the torsional mode is 127 cm^{-1} above the v=0 state (using the gas phase Raman frequency of Smardzewski and Fox (15) of 127 cm^{-1} for the $0\rightarrow1$ transition in the CF_3 torsion). If the band at 127 cm^{-1} were due to a $0\rightarrow2$ transition, then the $0\rightarrow1$ transition would be 65 cm^{-1} giving a population ratio of 0.62 at 194 K. On the basis of this evidence for CF_3OF and analogy for CF_3OCl and the CF_3OOX series, we now assign observed Raman bands to τ_{CF_3} not $2\tau_{CF_3}$.

The normal coordinate analysis done by Dr. Marsden was based on transferring force constants from (hopefully) related molecules and trying to obtain a set which was roughly transferable between all CF_3OX and CF_3OOX series members. The results of this preliminary normal coordinate analysis for the CF_3OX series members were consistent with the assignments of Smardzewski and Fox with one exception. Rather than two CF_3 rocks between 200 and 300 cm^{-1}, the calculations always gave one CF_3 rock (mode 11 for CF_3OX and mode 13 for CF_3OOX in Table 6) above 400 cm^{-1}, and one between 200 and 300 cm^{-1}. For the CF_3OX series, the two Raman bands between 200 and 300 cm^{-1} could be accounted for by one CF_3 rock and the overtone ($\Delta v=2$) of the CF_3 torsion which is intense enough to observe in analogy to the observation of Durig et al (24) for CH_3 rotors. For CF_3OF and CF_3OCl a shoulder in the infrared spectrum and a weak band in the

Raman spectrum, respectively, both near 430 cm^{-1}, could then be assigned to the CF_3 rock (18).

The acceptance of this assignment for the CF_3OX series and the results of the preliminary normal coordinate analysis gave expected ranges of frequencies for the CF_3 fundamentals of the CF_3OOX series. Only modes for the OOX part of CF_3OOX remained uncertain and major bands not readily assigned to the CF_3 part of the structure were attributed to the OOX part of the structure. These assignment (as noted in Section C) are included in Tables 1, 2, 3, and 4. For normal modes expected to be common to all series members, frequency ranges are the following in cm^{-1} units: three CF_3 stretches 1150-1300, one C-O stretch 900-950, three CF_3 deformations 580-695, two CF_3 rocks 250-300 and 420-520, one O-O stretch 825-875, one COO bend 420-445. For the CF_3 torsion the frequency range in cm^{-1} is ∿140-160 (H,D) and ∿70-80 (F,Cl). For normal modes involving the OOX group, frequencies in cm^{-1} units are assigned as follows: stretching: OH∿3575, OD∿2640, OF∿760, OCl∿695; bending: OOH∿1385, OOD∿1020, OOF∿340, OOCl∿295; torsions: OH∿245, OD∿180, OF∿130-150, OCl∿50??. Detailed discussion of these assignments is in Section G.

F. Normal Coordinate Analysis

The normal coordinate analysis done at Kansas State University used the programs CART, GMAT, FPERT and VSEC developed by Schactschneider (19). The program FPERT was used with $1/\lambda^2$ weighting where $\lambda = 4\pi^2c^2\nu^2$ and c and ν are the velocity of light and frequency in cm^{-1} units, respectively. The geometry with C_1 symmetry used to set up the input to CART is shown in Figure 7 and 8 and in Table 5 from Section D. The F matrix used, which is shown in Table 7, was the one adopted by Dr. C. J. Marsden for the

normal coordinate analysis done at the University of Michigan. The experimental frequencies adopted for use in the normal coordinate analysis are listed in Table 8; the majority of these frequencies are from gas phase infrared spectra. In cases where gas phase infrared data were not available, frequencies were taken from gas phase Raman spectra or were estimated from liquid Raman spectra.

The sets of force constants finally selected are listed in Table 9 for the CF_3OOX series with results for the CF_3OX compounds (18) included for comparison purposes. In most cases these value are similar to or identical with the ones finally chosen by Dr. Marsden for the force constants in the normal coordinate analysis at the University of Michigan. An exception is CF_3OOF where two sets of force constants in addition to the one similar to Dr. Marsden's values are listed in Table 9. This situation will be discussed in Section H. As a consequence of the way in which the GMAT program treats the CF_3 torsion, the force constant value for the CF_3 torsion in Table 9 (τ_1) must be multiplied by 9 to give the values appropriate to the program used at the University of Michigan. The frequencies calculated using the force constants in Table 9 are shown in Table 10 and compared there to the experimental frequencies from Table 8. The potential energy distributions for the calculated frequencies in Table 10 are shown in Tables 11, 12, 13, and 14 for CF_3OOH, CF_3OOD, CF_3OOF, and CF_3OOCl, respectively. The results shown in Tables 11 through 14 are presented differently in Table 15 with sections a through n where each section shows the potential energy distributions for all four CF_3OOX compounds (from Tables 11 through 14) and the two CF_3OX compounds (from reference 18) for a given normal mode according to the assignments presented in Section G.

Table 7. F matrix for CF_3OOX

		r_4	r_5	r_6	1	d	α_4	α_5	α_6	β_4	β_5	β_6	γ	τ_1	R	δ	τ_2
		1	2	3	4	5	6	7	8	9	10	11	12	13	14	15	16
r_4	1	r	rr	rr	r1	0	rα	rα'	rα'	rβ	rβ'	rβ'	0				
r_5	2		r	rr	r1	0	rα'	rα	rα'	rβ'	rβ	rβ'	0				
r_6	3			r	r1	0	rα'	rα'	rα	rβ'	rβ'	rβ	0				
1	4				1	1d	1α	1α	1α	1β	1β	1β	1γ				
d	5					d	0	0	0	0	0	0	dγ		Rd	dδ	
α_4	6						α	$\alpha\alpha$	$\alpha\alpha$	$\alpha\beta$	$\alpha\beta'$	$\alpha\beta'$	0				
α_5	7							α	$\alpha\alpha$	$\alpha\beta'$	$\alpha\beta$	$\alpha\beta'$	0				
α_6	8								α	$\alpha\beta'$	$\alpha\beta'$	$\alpha\beta$	0				
β_4	9									β	$\beta\beta$	$\beta\beta$	0				
β_5	10										β	$\beta\beta$	0				
β_6	11											β	0				
γ	12												γ				
τ_1	13													τ_1			
R	14														R	Rδ	
δ	15															δ	
τ_2	16																τ_2

Table 8. Experimental Infrared and Raman Frequencies for Normal Coordinate Analysis

Mode	CF_3OOH			CF_3OOD		CF_3OOF			CF_3OOCl	
	vapor		liq.	vapor	liq.	vapor		liq.	vapor	liq.
	R	IR	R	IR	R	R	IR	R	IR	R
ν_{CF_3}	1285	1269	∿1280	1271	∿1279	-	1297	1307	1281	∿1296
ν'_{CF_3}	∿1253	1244	∿1230	1246	∿1252	-	1270	1259	1241	-
ν''_{CF_3}	-	1230	∿1210	1235	∿1233	-	1190	1182	1213	-
ν_{CO}	948	947[a]	948	944[a]	947	946	950[a]	949	903[a]	905
ν_{OO}	866	865	872	863	867	875	874[a]	∿876	828[a]	830
ν_{OX}	3575	3575[a]	∿3550	2642[a]	∿2620	752	760[a]	751	697[a]	696
δ_{CF_3}	686	680[a]	679	680[a]	679	684	693[a]	695	665[a]	667
δ'_{CF_3}	617	615[a]	612	614[a]	614	-	630[a]	628	613	617
δ''_{CF_3}	590	587	582	585	585	584	588[a]	587	583[a]	588
ρ_{CF_3}	-	-	-	-	-	-	514[a]	516	478	483
δ_{COO}	445	440[a]	448	438[a]	445	430	434[a]	441	424[a]	431
δ_{OOX}	1387	1383[a]	∿1400	1020[a]	∿1033	332	336[a]	342	290[b]	295
ρ'_{CF_3}	290	-	275	-	273	280	278	283	259	266

Table 8 continued:

Mode	CF_3OOH			CF_3OOD		CF_3OOF			CF_3OOI	
	vapor		liq.	vapor	liq.	vapor		liq.	vapor	liq.
	R	IR	R	IR	IR	R	IR	R	IR	R
τ_{OX}	246	244	-	179	-	132	-	147	$\sim 50^b$	$\sim 54^b$
τ_{CF_3}	142	-	155	-	155	$\sim 70^b$	-	78	72^b	80

a. These are Q branch frequencies.

b. These are estimated frequencies rather than experimental ones (see discussion in Section G).

Table 9. Force Constant Values for CF_3OOX and CF_3OX

		FORCE CONSTANT TYPE		FORCE CONSTANT VALUES						
		CF_3OX	CF_3OOX	CF_3OF	CF_3OCl	CF_3OOH CF_3OOD	CF_3OOF	CF_3OOF	CF_3OOF	CF_3OOCl
1.	r	CF	CF	6.95	6.95	6.95	7.0	7.0	7.0	6.95
2.	l	CO	CO	5.20	5.20	5.3	5.3	5.2	5.0	5.2
3.	d	OX	OO	3.85	2.80	3.35	3.2	3.6	3.8	3.35
4.	α	FCF	FCF	2.00	2.05	2.05	1.97	1.97	1.97	2.0
5.	β	FCO	FCO	1.20	1.15	1.25	1.15	1.15	1.15	1.05
6.	γ	COX	COO	1.80	1.70	1.70	1.70	1.70	1.70	1.50
7.	τ_1	CF_3	CF_3	0.0167	0.0161	0.021	0.010	0.010	0.010	0.013
8.	rr	(CF)	(CF)	0.90	0.90	0.95	0.95	0.95	0.95	0.85
9.	rl	(CF)	(CO)	0.85	0.90	0.85	0.95	0.95	0.95	0.60
10.	ld	(CO)(OX)	(CO)(OO)	1.00	0.30	0.60	0.60	0.60	0.60	0.60
11.	rα	(CF)	(FCF)	0.12	0.12	0.12	0.12	0.12	0.12	0.15
12.	rα'	(CF)	(FCF)	0.91	0.91	0.91	0.91	0.91	0.91	0.91
13.	rβ	(CF)	(FCO)	0.75	0.70	0.75	0.75	0.75	0.75	0.72
14.	rβ'	(CF)	(FCO)	0.10	0.10	0.0	0.03	0.03	0.03	0.0
15.	lα	(CO)	(FCF)	0.20	0.20	0.20	0.20	0.20	0.20	0.20

Table 9.continued:

		FORCE CONSTANT TYPE		FORCE CONSTANT VALUES						
				CF_3OX	CF_3OOX	CF_3OF	CF_3OCl	CF_3OOH CF_3OOD	CF_3OOF	CF_3OOF	CF_3OOF	CF_3OOCl
16.	$\ell\beta$	(CO)	(FCO)	0.60	0.60	0.60	0.60	0.60	0.60	0.60
17.	$\ell\gamma$	(CO)(COX)	(CO)(COO)	0.0	0.10	0.0	0.0	0.0	0.0	0.40
18.	$d\gamma$	(OX)(COX)	(OO)(COO)	0.25	0.10	0.25	0.40	0.40	0.40	0.40
19.	$\alpha\alpha$	(FCF)	(FCF)	0.30	0.35	0.35	0.35	0.35	0.35	0.30
20.	$\alpha\beta$	(FCF)	(FCO)	0.0	0.0	0.05	0.0	0.0	0.0	0.0
21.	$\alpha\beta'$	(FCF)	(FCO)	0.15	0.15	0.15	0.15	0.15	0.15	0.13
22.	$\beta\beta$	(FCO)	(FCO)	0.10	0.10	0.10	0.10	0.10	0.10	0.15
23.	R	-	OX			7.15	3.5	3.0	3.0	2.77
24.	δ	-	OOX			0.93	1.4	1.4	1.4	1.35
25.	τ_2	-	OX			0.035	0.23	0.23	0.23	0.05
26.	Rd	-	(OX)(OO)			0.0	0.95	0.50	0.50	0.60
27.	$d\delta$	-	(OO)(OOX)			0.40	0.40	0.40	0.40	0.40
28.	$R\delta$	-	(OX)(OOX)			0.0	0.40	0.40	0.40	0.20

Units: stretching, mdyne Å^{-1}; bending and torsion, mdyne Å rad^{-2}; stretch-bend, mdyne rad^{-1}; bend-bend mdyne Å rad^{-2}.

Table 10. Calculated and Experimental Frequency Comparison[a]

	No	Symbol	CF_3OOH	CF_3OOD	CF_3OOF			CF_3OOCl
C	1	a. ν_{CF_3}	1294	1295	1289	1288	1285	1285
O			1269	1271	1297	1297	1297	1281
C	11	a. ν_{CF_3}	1232	1232	1241	1241	1241	1240
O			1244	1246	1270	1270	1270	1241
C	2	s. ν_{CF_3}	1202	1204	1195	1188	1174	1216
O			1230	1235	1190	1190	1190	1213
C	3	ν_{CO}	938	937	951	950	948	904
O			947	944	950	950	950	903
C	4	ν_{OO}	865	865	873	871	892	832
O			865	863	874	874	874	828
C	5	ν_{OX}	3579	2607	753	759	760	688
O			3575	2642	760	760	760	697
C	6	s. δ_{CF_3}	687	687	692	693	693	668
O			680	680	693	693	693	665
C	12	a. δ_{CF_3}	615	614	631	631	631	611
O			615	614	630	630	630	613
C	7	a. δ_{CF_3}	584	583	582	584	583	584
O			587	585	588	588	588	583
C	13	ρ_{CF_3}	449	447	528	528	528	487
O			-	-	514	514	514	478
C	9	δ_{COO}	431	427	433	433	432	410
O			440	438	434	434	434	424
C	10	δ_{OOX}	1354	1004	330	330	330	278
O			1383	1020	336	336	336	290[b]
C	8	ρ_{CF_3}	291	281[b]	285	286	286	253
O			290	290[b]	278	278	278	259
C	14	τ_{OX}	242	182	131	131	131	50[b]
O			244	179	132	132	132	50[b]
C	15	τ_{CF_3}	143	138[b]	69[b]	69[b]	69[b]	71[b]
O			142	142[b]	70[b]	70[b]	70[b]	72[b]

a. The rows labeled C contain calculated frequencies in cm^{-1}; the rows labeled O contain observed frequencies in the gas phase I.R. or Raman spectra except as noted by b.

b. Estimated frequencies based on liquid Raman spectra (see Discussion in Section G).

G. Discussion of Assignments

1. General Considerations

The CF_3OOX and CF_3OX structures belong to the C_1 and C_s point group, respectively. For a zero angle of twist (Figure 8b) the CF_3OO fragment of CF_3OOX has C_s symmetry but for a non zero angle of twist only the CF_3O fragment of CF_3OOX has C_s symmetry. Thus, CF_3OOH and CF_3OOD fail to have C_s symmetry only by having H and D, respectively, as the odd atom out of the plane of symmetry. Even neglecting the small (-2.2^o) angle of twist (Table 5 and Figure 8b) so the CF_3OO fragment had C_s symmetry, CF_3OOF fails to have C_s symmetry by having F as the odd atom out of the plane of symmetry. For CF_3OOCl both conformations have large nonzero (-15.5^o and $+23.6^o$) angles of twist (Table 5 and Figure 8b) and fail to have C_s symmetry by having both the second O and the Cl as odd atoms out of the plane of symmetry of the CF_3O fragment. Let us assume (as suggested in Section D) that deviation from C_s selection rules and polarization properties depends (among other things) on the mass(es) of the odd atom(s) out of the plane of symmetry. Then CF_3OOH and CF_3OOD would be predicted to approximate C_s selection rules and polarization properties reasonably well while CF_3OOF and CF_3OOCl would not. CF_3OOF and CF_3OOCl might be predicted to deviate from C_s behavior in a different manner due to the different angles of twist as well as different masses of the X atom.

Two cases of isoelectronic and constant or nearly constant mass relations exist between the CF_3OOX and CF_3OX series. CF_3OF, CF_3OOH, and CF_3OOD form an isoelectronic and nearly constant mass series while $CF_3O^{35}Cl$ and CF_3OOF are an isoelectronic and constant mass pair. Since the OH and OD stretching and bending modes are expected to be well localized and CF_3OOH and CF_3OOD might approximate C_s selection rules and polarization properties

Table 11. Potential Energy Distribution for CF_3OOH

Force Constant Number (Table 9)

Obs. ν	3575	1383	1269	1244	1230	947	865	680	615	587	-	440	290	244	142	cm^{-1}
Calc ν	3579	1353.5	1294.5	1232	1202	938	865	687	615	584	449	431	291	242	143	cm^{-1}
1			90	126	53	56		10	8	5						
2			18		55	14		9				6				
3							83	10				10				
4			22	25	28			25	65	82	39	33				
5			13	14	16		10	15	20	6	71	36	47	22	5	
6			11				13	17				18	22	17		
7															95	
8			-11	-17	5	14										
9					-19	13										
10							- 5									
11																
12			-23	-27	-30			11	11	10						
13			-14	-22	6				6							
14																
15					8											
16			- 6		-22			9								
17																
18							- 7									
19					7			8	-11	-11	- 6					
20																
21					- 6			- 7	7		-10	- 7				
22											- 6					
23	100															
24		100														
25													34	62		
26																
27							- 8									
28																

% Error = 1.01%

Table 12. Potential Energy Distribution for CF_3OOD

Force Constant Number (Table 9)

Obs. ν	2642	1271	1246	1235	1020	944	863	680	614	585	–	438	290	179	142	cm^{-1}
Calc.ν	2607	1295	1232	1204	1004	937	865	687	614	583.5	447	427	281	182	138	cm^{-1}
1		90	126	53		54		10	8	5						
2		18		55		14		9				5				
3							83	10				10				
4		22	25	28				25	66	83	38	32				
5		13	14	16			10	15	19	5	70	39	62	6		
6		11					13	17				16	34	5		
7															92	
8		-11	-17	5		13										
9				-19		13										
10							- 5									
11																
12		-23	-27	-30				11	11	10						
13		-14	-22	6					6				- 6			
14																
15				8												
16		- 6		-22				9								
17																
18							- 7									
19				7				8	-11	-12	- 6					
20																
21				- 6				- 7	7		-10	- 7				
22											- 5		- 5			
23	100															
24					98											
25													8	86		
26																
27							- 8									
28																

% Error = 1.50%

Table 13a. Potential Energy Distribution for CF_3OOF using Dr. Marsden's Force Constant Values

Force Constant Number (Table 9)

	Obs. ν	1297	1270	1190	950	874	760	693	630	588	514	434	336	278	132	70	cm^{-1}
	Calc. ν	1289	1241	1195	951	873	753	692	631	582	528	433	330	285	131	69	cm^{-1}
1		97	125	48	55			11	6	5							
2		13		62	14			7				6					
3						37	53	11		6							
4		22	23	27				23	35	72	62	40	14				
5		11	12	15		5	7	13	24	7	7	33	53	75	11		
6		11				8	8	18				16	6	21	10		
7																95	
8		-12	-17	6	14												
9				-23	14												
10																	
11																	
12		-23	-26	-30				12	7	10	5						
13		-15	-21	8					6					- 5			
14																	
15				8													
16				-24				8									
17																	
18							- 7	5									
19				8				8	- 6	-10	-11						
20																	
21				- 7				- 6	6			- 8	- 5				
22														- 6			
23						36	69										
24						13			17	5	36		27				
25												6		10	75		
26						21	-34										
27						- 8											
28						- 8											

% Error = 1.03%

Table 13b. Potential Energy Distribution for CF_3OOF using ℓ = 5.2, d = 3.6, R = 3.0, and Rd = 0.5 (from Table 9)

Force Constant Number (Table 9)

	Obs. ν	1297	1270	1190	950	874	760	693	630	588	514	434	336	278	132	70	cm^{-1}
	Calc.ν	1288	1241	1188	950.5	871	759	693	631	583.5	528	433	330	285.5	131	69	cm^{-1}
1			99	125	47	53			11	6	5						
2			11		63	15			6				7				
3							91										
4			22	23	28				23	35	72	62	40	14			
5			11	12	15		8		14	25	8	8	34	53	75	11	
6			11				12		22				16	6	20	10	
7																	95
8			-13	-17	7	13											
9					-24	15											
10																	
11																	
12			-23	-26	-31				11	7	10						
13			-16	-21	9					6					- 5		
14																	
15					9												
16					-25				7								
17																	
18							-10										
19					9				7	- 6	-10	-11					
20																	
21					- 7				- 6	5			- 8	- 5			
22															- 7		
23								96									
24							6	12		16	5	34		27			
25													6		10	75	
26								- 5									
27							- 8										
28								-13									

% Error = 0.97%

Table 13c. Potential Energy Distribution for CF_3OOF using ℓ = 5.0, d = 3.8, R = 3.0 and Rd = 0.5 (from Table 9)

Force Constant Number (Table 9)

Obs. ν	1297	1270	1190	950	874	760	693	630	588	514	434	336	278	132	70	cm^{-1}
Calc. ν	1285	1241	1174	948	892	760	693	631	583	528	432	330	286	131	69	cm^{-1}
1	103	125	46	50	5		12	6	5							
2	8		63	17			6				7					
3					91											
4	22	23	29				22	35	72	62	40	14				
5	11	12	16		7		13	25	8	8	35	53	75	11		
6	11				11		23				16	6	20	10		
7															95	
8	-14	-17	8	12												
9			-26	16												
10																
11																
12	-23	-26	-32				11	7	10							
13	-17	-21	11					6					- 5			
14																
15			9													
16			-27				7									
17																
18					-10											
19			9				7	- 6	-10	-11						
20																
21			- 8				- 6	5			- 8	- 5				
22													- 6			
23						95										
24					5	12		15	5	34		27				
25											6		10	75		
26						- 5										
27					- 8											
28						-13										

% Error = 1.19%

Table 14. Potential Energy Distribution for $CF_3OO^{35}Cl$ (Twist = 15.5°)

Force Constant Number (Table 9)

	Obs. ν	1281	1241	1213	903	828	697	665	613	583	478	424	290	259	72	50	cm^{-1}
	Calc. ν	1285	1240	1216	904	832	688	668	611	584	487	410	278	253	71.5	50	cm^{-1}
1		109	119	45	51			7	6	5							
2		7		59	21			11									
3						91											
4		23	25	26				23	66	75	32	30	7				
5		10	11	14		10		12	13	6	27	53	42	85			
6		8				13		19			7	15	7	27			
7															82	12	
8		-13	-14	6	12												
9				-15	11												
10																	
11																	
12		-25	-27	-30	6			7	10	9							
13		-16	-18	8					5					- 8			
14																	
15				8													
16				-24				9									
17																	
18						-12											
19				7				5	-10	- 8							
20																	
21				- 6					5		- 5	- 7					
22												- 7	- 6	-12			
23							68	9	7		10		7				
24							19	7			31		37		5		
25															10	84	
26							- 6										
27						- 6											
28							- 7										

% Error = 1.06%

Table 15a. Potential Energy Distribution For All CF_3OX and CF_3OOX Compounds For Each Normal Mode

a. $\nu_{CF_3}(A')$

	CF_3OF	CF_3OCl	CF_3OOH	CF_3OOD	CF_3OOF			CF_3OOCl
					a	b	c	
Calc. ν	1321	1309	1294.5	1295	1289	1288	1285	1285
Obs. ν	1294	1271	1269	1271	1297	1297	1297	1281
r	90	103	90	90	97	99	103	109
ℓ	12	5	18	18	13	11	8	7
α	21	23	22	22	22	22	22	23
β	13	12	13	13	11	11	11	10
γ	11	9	11	11	11	11	11	8
rr	-11	-13	-11	-11	-12	-13	-14	-13
$r\alpha'$	-22	-24	-23	-23	-23	-23	-23	-25
$r\beta$	-15	-16	-14	-14	-15	-16	-17	-16
$\ell\beta$			- 6	- 6				

Force constant symbols above from Tables 7 and 9.

Three columns for CF_3OOF labeled a, b, and c are for Tables 13a, 13b, and 13c, respectively.

Table 15b. Potential Energy Distribution For All CF_3OX and CF_3OOX Compounds For Each Normal Mode

a. ν_{CF_3} (A")

	CF_3OF	CF_3OCl	CF_3OOH	CF_3OOD	CF_3OOF			CF_3OOCl
					a	b	c	
Calc. ν	1256	1262	1232	1232	1241	1241	1241	1240
Obs. ν	1261	1230	1244	1246	1270	1270	1270	1241
r	120	119	126	126	125	125	125	119
α	24	24	25	25	23	23	23	25
β	13	13	14	14	12	12	12	11
rr	-16	-15	-17	-17	-17	-17	-17	-14
$r\alpha'$	-26	-26	-27	-27	-26	-26	-26	-27
$r\beta$	-21	-19	-22	-22	-21	-21	-21	-18

Force constant symbols above from Tables 7 and 9.

Three columns for CF_3OOF labeled a, b, and c are for Tables 13a, 13b, and 13c, respectively.

Table 15c. Potential Energy Distribution For All CF_3OX and CF_3OOX Compounds For Each Normal Mode

	s. ν_{CF_3}							
	CF_3OF	CF_3OCl	CF_3OOH	CF_3OOD	CF_3OOF			CF_3OOCl
					a	b	c	
Calc. ν	1214	1208	1202	1204	1195	1188	1174	1216
Obs. ν	1222	1213	1230	1235	1190	1190	1190	1213
r	49	38	53	53	48	47	46	45
ℓ	54	67	55	55	62	63	63	59
α	27	29	28	28	27	28	29	26
β	14	16	16	16	15	15	16	14
rr	5	8	5	5	6	7	8	6
rℓ	-20	-24	-19	-19	-23	-24	-26	-15
rα'	-30	-30	-30	-30	-30	-31	-32	-30
rβ	8	10	6	6	8	9	11	8
$\ell\alpha$	8	9	8	8	8	9	9	8
$\ell\beta$	-22	-27	-22	-22	-24	-25	-27	-24
$\alpha\alpha$	6	9	7	7	8	9	9	7
$\alpha\beta'$	- 6	- 8	- 6	- 6	- 7	- 7	- 8	- 6

Force constant symbols above from Tables 7 and 9.

Three columns for CF_3OOF labeled a, b, and c are for Tables 13a, 13b, and 13c, respectively.

Table 15d. Potential Energy Distribution For All CF_3OX and CF_3OOX Compounds For Each Normal Mode

			ν_{CO}					
	CF_3OF	CF_3OCl	CF_3OOH	CF_3OOD	CF_3OOF			CF_3OOCl
					a	b	c	
Calc. ν	941	935	938	937	951	950.5	948	904
Obs. ν	947	919	947	944	950	950	950	903
r	54	52	56	54	55	53	50	51
ℓ	8	16	14	14	14	15	17	21
d	7							
γ	8							
rr	12	13	14	13	14	13	12	12
rℓ	9	15	13	13	14	15	16	11
rα'								6

Force constant symbols above from Tables 7 and 9.

Three columns for CF_3OOF labeled a, b, and c are for Tables 13a, 13b, and 13c, respectively.

Table 15e. Potential Energy Distribution for All CF_3OX and CF_3OOX Compounds For Each Normal Mode

			ν_{OO}					
	CF_3OF	CF_3OCl	CF_3OOH	CF_3OOD	CF_3OOF			CF_3OOCl
					a	b	c	
Calc. ν	-	-	865	865	873	871	892	832
Obs. ν	-	-	865	863	874	874	874	828
r							5	
d			83	83	37	91	91	91
R					36			
β			10	10	5	8	7	10
γ			13	13	8	12	11	13
δ					13	6	5	
ℓd			- 5	- 5				
dγ			- 7	- 7		-10	-10	-12
Rd					21			
dδ			- 8	- 8	- 8	- 8	- 8	- 6
Rδ					- 8			

Force constant symbols above from Tables 7 and 9.

Three columns for CF_3OOF labeled a, b, and c are for Tables 13a, 13b, and 13c, respectively.

Table 15f. Potential Energy Distribution For All CF_3OX and CF_3OOX Compounds For Each Normal Mode

	ν_{OX}							
	CF_3OF	CF_3OCl	CF_3OOH	CF_3OOD	CF_3OOF			CF_3OOCl
					a	b	c	
Calc. ν	883	774	3579	2607	753	759	760	688
Obs. ν	882	780	3575	2642	760	760	760	697
r	5	10						
ℓ	18							
d	76	51			53			
R			100	100	69	96	95	68
β	9	15			7			
γ	5	22			8			
δ						12	12	19
ℓd	-17							
rβ		6						
$\ell\beta$	- 5							
dγ					- 7			
Rd					34	- 5	- 5	- 6
Rδ						-13	-13	- 7

Force constant symbols above from Tables 7 and 9.

Three columns for CF_3OOF labeled a, b, and c are for Tables 13a, 13b, and 13c, respectively.

Table 15g. Potential Energy Distribution For All CF_3OX and CF_3OOX Compounds For Each Normal Mode

a. δ_{CF_3}

	CF_3OF	CF_3OCl	CF_3OOH	CF_3OOD	CF_3OOF			CF_3OOCl
					a	b	c	
Calc. ν	674	658	687	687	692	693	698	668
Obs. ν	678	665	680	680	693	693	693	665
r	12	7	10	10	11	11	12	7
ℓ	11	15	9	9	7	6	6	11
d	12	9	10	10	11			
R								9
α	24	30	25	25	23	23	22	23
β	13	16	15	15	13	14	13	12
γ	17	8	17	17	18	22	23	19
δ								7
ℓd	- 5							
rα'	12	12	11	11	12	11	11	7
$\ell\beta$	10	13	9	9	8	7	7	9
dγ					5			
$\alpha\alpha$	6	9	8	8	8	7	7	5
$\alpha\beta'$	- 6	- 8	- 7	- 7	- 6	- 6	- 6	

Force constant symbols above from Tables 7 and 9.

Three columns for CF_3OOF labeled a, b, and c are for Tables 13a, 13b, and 13c, respectively.

Table 15h. Potential Energy Distribution For All CF_3OX and CF_3OOX Compounds For Each Normal Mode

a. δ_{CF_3} (A")

	CF_3OF	CF_3OCl	CF_3OOH	CF_3OOD	CF_3OOF			CF_3OOCl
					a	b	c	
Calc. ν	616	613	615	614	631	631	631	611
Obs. ν	607	609	615	614	630	630	630	613
r	9	9	8	8	6	6	6	6
R								7
α	65	69	65	66	35	35	35	66
β	16	14	20	19	24	25	25	13
δ					17	16	15	
rα'	12	12	11	11	7	7	7	10
rβ	6	6	6	6	6	6	6	5
αα	-10	-12	-11	-11	- 6	- 6	- 6	-10
αβ'	6	6	7	7	6	5	5	5

Force constant symbols above from Tables 7 and 9.

Three columns for CF_3OOF labeled a, b, and c are for Tables 13a, 13b, and 13c, respectivley.

Table 15i. Potential Energy Distribution For All CF_3OX and CF_3OOX Compounds For Each Normal Mode

		a.δ_{CF_3}(A')							
		CF_3OF	CF_3OCl	CF_3OOH	CF_3OOD	CF_3OOF			CF_3OOCl
						a	b	c	
Calc.	ν	589	571	584	583.5	582	583.5	583	584
Obs.	ν	585	557	587	585	588	588	588	583
r		6		5	5	5	5	5	5
d			8			6			
α		78	90	82	83	72	72	72	75
β		7		6	5	7	8	8	6
δ						5	5	5	
rα'		11	9	10	10	10	10	10	9
αα		- 9	-14	-11	-12	-10	-10	- 10	- 8

Force constant symbols above from Tables 7 and 9.

Three columns for CF_3OOF labeled a, b, and c are for Tables 13a, 13b, and 13c, respectively.

Table 15j. Potential Energy Distribution For All CF_3OX and CF_3OOX Compounds For Each Normal Mode

	ρ_{CF_3} (A")							
	CF_3OF	CF_3OCl	CF_3OOH	CF_3OOD	CF_3OOF			CF_3OOCl
					a	b	c	
Calc. ν	429	422	449	447	528	528	528	487
Obs. ν	431	430	-	-	514	514	514	478
R								10
α	37	36	39	38	62	62	62	32
β	83	85	71	70	7	8	8	27
γ								7
δ					36	34	34	31
rα'					5			
αα	- 6	- 6	- 6	- 6	-11	-11	-11	
αβ'	-11	-11	-10	-10				- 5
ββ	- 7	- 7	- 6	- 5				

Force constant symbols above from Tables 7 and 9.

Three columns for CF_3OOF labeled a, b, and c are for Tables 13a, 13b, and 13c, respectively.

Table 15k. Potential Energy Distribution For All CF_3OX and CF_3OOX Compounds For Each Normal Mode

	δ_{COO}							
	CF_3OF	CF_3OCl	CF_3OOH	CF_3OOD	CF_3OOF			CF_3OOCl
					a	b	c	
Calc. ν	-	-	431	427	433	433	432	410
Obs. ν	-	-	440	438	434	434	434	424
ℓ			6	5	6	7	7	
d			10	10				
α			33	32	40	40	40	30
β			36	39	33	34	35	53
γ			18	16	16	16	16	15
τ_2					6	6	6	
$\alpha\beta'$			- 7	- 7	- 8	- 8	- 8	- 7
$\beta\beta$								- 7

Force constant symbols above from Tables 7 and 9.

Three columns for CF_3OOF labeled a, b, and c are for Tables 13a, 13b, and 13c, respectively.

Table 151. Potential Energy Distribution For All CF_3OX and CF_3OOX Compounds For Each Normal Mode

		δ_{OOX} (or COX)							
		CF_3OF	CF_3OCl	CF_3OOH	CF_3OOD	CF_3OOF			CF_3OOCl
						a	b	c	
Calc.	ν	420	348	1353.5	1004	330	330	330	278
Obs.	ν	429	393	1383	1020	336	336	336	290
ℓ		5							
d		8	30						
R			.						7
α		35	18			14	14	14	7
β		35	44			53	53	53	42
γ		21	9			6	6	6	7
δ				100	98	27	27	27	37
$\alpha\beta'$		- 8	- 6			- 5	- 5	- 5	
$\beta\beta$									- 6

Force constant symbols above from Tables 7 and 9.

Three columns for CF_3OOF labeled a, b, and c are for Tables 13a, 13b, and 13c, respectively.

Table 15m. Potential Energy Distribution For All CF_3OX and CF_3OOX Compounds For Each Normal Mode

	ρ_{CF_3} (A')							
	CF_3OF	CF_3OCl	CF_3OOH	CF_3OOD	CF_3OOF			CF_3OOCl
					a	b	c	
Calc. ν	267	217	291	281	285	285.5	286	253
Obs. ν	278	233	290	290	278	278	278	259
ℓ	6							
β	64	48	47	62	75	75	75	85
γ	38	50	22	34	21	20	20	27
τ_2			34	8	10	10	10	
$r\beta$	- 5			- 6	- 5	- 5	- 5	- 8
$\beta\beta$	- 5			- 5	- 6	- 7	- 6	-12

Force constant symbols above from Tables 7 and 9.

Three columns for CF_3OOF labeled a, b, and c are for Tables 13a, 13b, and 13c, respectively.

Table 15n. Potential Energy Distribution For All CF_3OX and CF_3OOX Compounds For Each Normal Mode

		CF_3OF	CF_3OCl	CF_3OOH	CF_3OOD	CF_3OOF			CF_3OOCl
						a	b	c	
Calc.	ν	-	-	242	182	131	131	131	50
Obs.	ν	-	-	244	179	132	132	132	50
β				22	6	11	11	11	
γ				17	5	10	10	10	
τ_1									12
τ_2				62	86	75	75	75	84

τ_{OX}

Force constant symbols above from Tables 7 and 9.

Three columns for CF_3OOF labeled a, b, and c are for Tables 13a, 13b, and 13c, repsectively.

Table 15o. Potential Energy Distribution For All CF_3OX and CF_3OOX Compounds For Each Normal Mode

		CF_3OF	CF_3OCl	CF_3OOH	CF_3OOD	CF_3OOF			CF_3OOCl
				τ_{CF_3}		a	b	c	
Calc.	ν	128	108	143	138	69	69	69	71.5
Obs.	ν	127	108	142	142	70	70	70	72
β		5	5	5					
δ									5
τ_1		96	96	95	92	95	95	95	82
τ_2									10

Force constant symbols above from Tables 7 and 9.

Three columns for CF_3OOF labeled a, b, and c are for Tables 13a, 13b, 13c, respectively.

reasonably well, the CF_3OF, CF_3OOH, and CF_3OOD isoelectronic series might be expected to have similar Raman spectra below 1350 cm^{-1} with respect to frequencies, relative intensities and polarization properties. Similarities between the pair CF_3OCl and CF_3OOF would be expected to be less pronounced due to larger deviations from C_s symmetry properties for CF_3OOF. Also all fifteen normal modes of CF_3OOF would be in the frequency range below 1350 cm^{-1}. Once CF_3OOH and CF_3OOD were assigned by analogy with CF_3OF, CF_3OOH and CF_3OOD might be a more useful comparison for the CF_3OO fragment modes of CF_3OOF than CF_3OCl. Comparison between CF_3OOF and CF_3OOCl might be expected to be helpful as well.

In principle, the following are of potential utility in making the assignment: relative intensities and polarization properties of Raman bands, relative intensities and contours of infrared bands, and calculated frequencies and potential energy distribution from the normal coordinate analysis. In practice the isoelectronic series of CF_3OF, CF_3OOH and CF_3OOD could be assigned mainly on the basis of relative intensities and polarization of Raman bands in the liquid. However, the results of the preliminary normal coordinate analysis were also helpful. CF_3OOF was treated using CF_3OCl, CF_3OOH, CF_3OOD and CF_3OOCl for comparison but CF_3OOH comparisons and the results of the preliminary normal coordinate analysis were the most helpful items. CF_3OOCl was also treated using CF_3OCl, CF_3OOH and CF_3OOD for comparisons as well as CF_3OOF but CF_3OOF comparisons and the results of the preliminary normal coordinate analysis were the most helpful items. Since all CF_3OX and CF_3OOX structures are near prolate symmetric tops, infrared bands contours were of some use but were not exploited extensively.

2. CF_3OOH and CF_3OOD

a. OH and OD Vibrations

The OH and OD stretches are readily assigned to infrared bands at 3575 cm^{-1} and 2642 cm^{-1}, respectively, having PQR structure. The corresponding Raman bands in the liquid are broadened and shifted to lower frequencies by hydrogen bonding. The OOH and OOD bends are at 1383 cm^{-1} and 1020 cm^{-1}, respectively, in the infrared spectra, but only the OOH bend has a well defined PQR structure. The corresponding Raman bands in the liquid are shifted to higher frequencies by hydrogen bonding. The OH and OD torsions are assigned to surprisingly intense bands at 244 cm^{-1} and 179 cm^{-1}, respectively, with the latter frequency being the midpoint of an apparent doublet at 174 cm^{-1} and 183 cm^{-1}. Bands at 482 cm^{-1} and centered near 340 cm^{-1} are assigned to $\Delta v = 2$ transitiona in the OH and OD torsion, respectively. Small bands (not listed in Tables 1 and 2) equally displaced to the high and low frequency sidea of both the OH and OD stretches are readily assigned to the binary combination $\nu OH \pm \tau OH$ and $\nu OD \pm \tau OD$, respectively. The OH and OD torsions are broadened beyond definte recognition in the Raman spectrum of the liquid due to hydrogen bonding. The OH torsion is so intense in the infrared spectrum that the expected CF_3 rocking region from 300 cm^{-1} to 200 cm^{-1} is obscured even in the case of CF_3OOD containing an appreciable amount of CF_3OOH as an impurity. Thus, until the gas phase Raman spectrum of CF_3OOH shown in Figure 5 was obtained the only access to the CF_3 rocking frequency was the Raman spectrum of the liquid where the CF_3 rock is assigned to a weak band superimposed on the broad background of the OH torsion disturbed by hydrogen bonding.

The potential energy distributions discussed in Section H show that all these modes are very pure except for the OH torsion. Thus the OH and

OD stretching frequencies and the OH bending frequency are essentially 100 percent pure while the OD bending is 98 percent pure. The OD torsion is 86 percent pure with contributions from the other coordinates of less than 7 percent for any one coordinate. For the OH torsion the potential energy comes from about 62 percent from the OH torsion with secondary contributions of about 22 percent from changes in the β type angles and about 17 percent from changes in the γ type angle. These internal coordinates were illustrated in Figure 9 in Section D.

b. CF_3 and CO Stretching

The dominant feature of the infrared spectra of the CF_3OOX series members is a collection of very intense bands between 1350 cm^{-1} and 1150 cm^{-1}. However, these bands are very weak in the Raman spectra and polarization measurements are very uncertain. The contours of the infrared bands for the various compounds are sufficiently different to allow identification of each in the presence of the others. For CF_3OOF and CF_3OOCl there are three peaks readily assigned to three fundamentals but for CF_3OOH and CF_3OOD the choice is not unambiguous. The choices made are shown in Tables 1 and 2 where the symmetry coordinates from Table 6 numbered 1, 11 and 2 are assigned to the frequencies in the order highest to lowest. The three frequencies calculated in the normal coordinate analysis are sensitive to many force constants as can be seen in the potential energy distributions discussed in Section H. For CF_3OX under C_s symmetry normal coordinate calculations always give the highest and lowest frequency in the A' block and the intermediate frequency in A" block. Thus, our designations of ν_1, ν_{11}, and ν_2 in Tables 1 and 2 are by analogy with CF_3OX. For CF_3OOH and CF_3OOD under C_1 symmetry, the potential energy distribution for the

intermediate frequency is very similar to that for the intermediate frequency in CF_3OX when the symmetry is taken as C_1 rather than C_s. The potential energy distributions for CF_3OOH and CF_3OOD are consistent with the highest and intermediate frequencies having a major contribution from stretching the C-F bonds while the lowest frequency has major contributions from stretching the C-O bond as well as the C-F bond.

CF_3OOH and CF_3OOD have polarized bands in the Raman spectrum of the liquid at 948 cm^{-1} and 947 cm^{-1}, respectively. The corresponding bands in the infrared spectra of the gases at 947 cm^{-1} and 944 cm^{-1} have PQR structure. These bands are assigned to the CO stretching mode in analogy to CF_3OF. However, the potential energy distributions indicate that this mode has the stretching of the C-F bond as its major contributor rather than stretching of the C-O bond. Thus, the conventional designations in Tables 1 and 2 are misleading and four bands in the 1150-1350 cm^{-1} and 900-950 cm^{-1} regions appear to include both CF and CO stretching. The mixing of CF stretching modes of the CF_3 group with modes of the remainder of the molecule has been reported by Tuazon, Fateley and Bentley (27). For both the two CF_3OX and these two CF_3OOX series members it would seem more appropriate to specify that two predominantely CF stretching modes are in the 1150-1350 cm^{-1} region along with one mixed CF and CO stretching mode and one predominantly CF stretching mode is in the 900-950 cm^{-1} region rather than restricting the CF stretching modes to the 1150-1350 cm^{-1} region and the CO stretching modes to the 900-950 cm^{-1} region.

c. OO Stretching

The dominant features of the Raman spectra of liquid CF_3OOH and CF_3OOD are very intense and highly polarized bands at 872 cm^{-1} and 867 cm^{-1},

respectively. The gas phase Raman spectrum of CF_3OOH has its most intense band at 866 cm^{-1}. The corresponding bands in the gas phase infrared spectra of CF_3OOH and CF_3OOD at 865 cm^{-1} and 863 cm^{-1}, respectively, are weak and show no discernible PQR structure. These bands are assigned to the OO stretching mode by analogy to CF_3OF having the OF stretching mode as its most intense Raman band (15, 18) and to many alkyl peroxides and fluoro substituted alkyl peroxides having the OO stretching mode as the most intense Raman band (28). The potential energy distribution for CF_3OOH and CF_3OOD shows the OO stretching as the dominant contributor to these frequencies.

d. CF_3 Deformation

The three CF_3 deformations in CF_3OOH and CF_3OOD are easily assigned by analogy to CF_3OF to bands at 680, 615, and 587 cm^{-1} and 680, 614, and 585 cm^{-1}, respectively, in the infrared spectra of the gases. The two higher frequency bands have a discernible PQR structure while the lower frequency band does not. The intensity of the three bands decreases with decreasing frequency in both CF_3OOH and CF_3OOD; the same intensity pattern occures in CF_3OF and CF_3OCl. The corresponding bands in the Raman spectrum of liquid CF_3OOH and CF_3OOD alternate in both intensity and polarization properties from high to low frequency with the highest and lowest frequencies being of comparable intensity and definitely polarized while the intermediate frequency is much less intense and very weakly polarized. For CF_3OX under C_s symmetry one of these bands must be depolarized and CF_3OF has the same variation in intensity with the

intermediate frequency being depolarized and assigned to the A" symmetry block. Thus, the polarization properties of CF_3OF under C_s symmetry are quite well approximated by CF_3OOH and CF_3OOD under C_1 symmetry which fails to be C_s only due to H and D being the odd atoms off the plane of symmetry. The potential energy distribution show the highest frequency having contributions from many stretching and bending coordinates with none dominant. For both the intermediate frequency and the lowest frequency changing the α type angles (see Figure 9) is the major contribution in the potential energy distribution.

e. COO Bending and CF_3 Rocking

The COO Bending mode is assigned to bands at 488 cm^{-1} and 445 cm^{-1} in the Raman spectra of liquid CF_3OOH and CF_3OOD, respectively. These bands are definitely polarized and are the most intense Raman bands below 500 cm^{-1}. For CF_3OF and CF_3OCl the most intense Raman bands below 500 cm^{-1} are at 436 cm^{-1} and 397 cm^{-1}, respectively, and are assigned to the COX bending modes. It seems reasonable for the COO bending mode in CF_3OOH and CF_3OOD to be similar in frequency, relative intensity and polarization

properties to the COF bending mode in the iseolectronic CF_3OF molecule. The corresponding infrared bands in gaseous CF_3OOH and CF_3OOD at 440 cm^{-1} and 438 cm^{-1}, respectively, show suggestions of PQR structure.

One CF_3 rocking mode would be expected in the 200-300 cm^{-1} region by analogy with CF_3OF and CF_3OCl as reassigned following Dr. Marsden's preliminary normal coordinate analysis (see Section E). By analogy to CF_3OF, gas pressures for CF_3OOH and CF_3OOD of 150-400 torr in a 10 cm length gas cell would be necessary for observation of the band in the infrared spectrum. However, the OH torsion is so intense in the infrared that at a CF_3OOH pressure of 20 torr or even at a combined pressure of 20 torr for CF_3OOD with some CF_3OOH impurity the 200-300 cm^{-1} region is completely obscured. In the Raman spectra of liquid CF_3OOH and CF_3OOD where the OH or OD torsion is broadened beyond recognition a weak but definitely polarized Raman band is observed near 275 cm^{-1}. This band is assigned to the CF_3 rocking mode which would be in the A' block under C_s symmetry. In the gas phase Raman spectrum of CF_3OOH in Figure 5, this band has shifted to 290 cm^{-1} and is on the side of the OH torsion so 290 cm^{-1} was used for one CF_3 rocking mode in both CF_3OOH and CF_3OOD in the normal coordinate analysis.

According to the normal coordinate analysis the second CF_3 rocking mode would be above 400 cm^{-1} in all CF_3OX and CF_3OOX series members. In both CF_3OX compounds weak bands near 430 cm^{-1} were assigned to this second CF_3 rocking mode which is in the A" block under C_s symmetry (see Section E). For CF_3OOH and for CF_3OOD with some CF_3OOH impurity, the 400-500 cm^{-1} region of the infrared spectrum was obscured by the COO bending mode at 440 cm^{-1} and the first overtone of the OH torsion at 482 cm^{-1}. Since the preliminary normal coordinate analysis predicted that the second CF_3 rocking mode will be within 20 cm^{-1} of the COO bending mode near 440 cm^{-1} in CF_3OOH

and CF_3OOD, the region 400-500 cm^{-1} in both the infrared and Raman spectra was carefully studied for traces of weak bands. The infrared bands at 482 cm^{-1} and 440 cm^{-1} for gaseous CF_3OOH suggest PQR structure but the band shapes are distorted so that the R branch of the 482 cm^{-1} and the P branch of the 440 cm^{-1} are only shoulders for CF_3OOH. It is possible that these band shapes are due only to the modes assigned or there might be a second band reasonably assigned to the CF_3 rock overlapping either the 482 cm^{-1} or the 440 cm^{-1} band. The shape of the 438 cm^{-1} infrared band in CF_3OOD is somewhat different from the 440 cm^{-1} band in CF_3OOH but the situation is complicated by the fact that the CF_3OOD gas sample always has appreciable CF_3OOH impurity present. The bands at 448 cm^{-1} and 445 cm^{-1} in the Raman spectra of liquid CF_3OOH and CF_3OOD, respectively, are asymmetric to low frequencies consistent with the presence of second weak band. However, this asymmetry may be due to hydrogen bonding in the liquids rather than the presence of a second weak band. Although the infrared spectra of the four CF_3OOX gases were not recorded with quantitative analysis in mind apparent absorption coefficient for the modes assigned as COO bending can be computed as follows in units of $10^4 cm^{-1}$ $torr^{-1}$: CF_3OOH 440 cm^{-1} band 3.1, CF_3OOD 438 cm^{-1} band 1.8, CF_3OOF 434 cm^{-1} band 0.44, and CF_3OOCl 424 cm^{-1} 0.36. The value for CF_3OOD is too small due to the use in its calculation of the total gas pressure of CF_3OOD with some CF_3OOH impurity present. For CF_3OOF and CF_3OOCl bands at 514 cm^{-1} and 478 cm^{-1}, respectively, can be assigned to the CF_3 rocking mode so the bands at 434 cm^{-1} and 424 cm^{-1} are due to the COO bending mode only. While the apparent absorption coefficients for the COO bending mode need not be constant over the CF_3OOX series, the large difference between the pair CF_3OOF and CF_3OOCl and the pair CF_3OOH and CF_3OOD is consistent with the presence of a second

band under the bands assigned to the COO bending mode in CF_3OOH and CF_3OOD.

The infrared spectra of gaseous CF_3OOH and CF_3OOD contain bands centered at 374 cm^{-1} and 340 cm^{-1}, respectively, which are of roughly half the intensity of those at 440 cm^{-1} and 438 cm^{-1}, respectively. No counterparts to these band appear in the Raman spectra of liquid CF_3OOH and CF_3OOD. Assignement of these bands to the second CF_3 rocking seems to be precluded by the deuterium isotope shift of 34 cm^{-1} or ratio 1.1 which is too large for any modes other than OH stretching or bending or torsion and too small for these latter three. Four transitions which are not fundamentals would give frequencies to account for bands centered near 374 cm^{-1} and 340 cm^{-1} as follows using gas phase infrared or Raman frequencies in cm^{-1}.

Mode	CF_3OOH	CF_3OOD
$\tau_{OH,D} + \tau_{CF_3}$	244 + 142 = 386	179 + 142 = 321
$2\tau_{OH,D}$	2 x 244 + 488	2 x 179 = 358
$\delta_{CF_3} - \tau_{OH,D}$	615 - 244 = 371	614 - 179 = 435
$\delta_{CF_3} - \rho_{CF_3}$	615 - 290 = 325	614 - 290 = 324

The latter two transitions probably would make minor contributions as they do not originate in the ground vibrational state. All observed transition frequencies would be expected to be lower than the values calculated due to anharmonicity. The 488 cm^{-1} band actually comes at 482 cm^{-1} in CF_3OOH and is somewhat more intense than the 374 cm^{-1} band. Since both τ_{OH} and τ_{OD} are very intense and $2\tau_{OH}$ is of almost equal intensity with the COO bend, it is reasonable for $\tau_{OH} + \tau_{CF_3}$ and the overlap of $\tau_{OD} + \tau_{CF_3}$ and $2\tau_{OD}$ to both have intensity comparable to the COO bend. Thus, we assign the band centered at 374 cm^{-1} in CF_3OOH gas to $\tau_{OH} + \tau_{CF_3}$ and the band centered at 340 cm^{-1} in CF_3OOD gas to the overlap of $2\tau_{OD}$ and $\tau_{OD} + \tau_{CF_3}$.

We now assume that the second CF_3 rock is near the COO bend but is either too close in frequency or too weak in intensity to be definitely

identified. In the normal coordinate analysis we list the second CF_3 rock ss not observed. The calculated value of the second CF_3 rock is always sbout 20 cm^{-1} higher than the calculated value of the COO bend. If the CF_3 rock really is within 20 cm^{-1} on the high frequency side of the COO bend, then either it is too weak to observe or the suggested R branch is really the CF_3 rock and the COO bend has a prominant Q branch with the R and P branches only showing as weak shoulders. CF_3OF does have such a band shape for its COF bend at 429 cm^{-1}. If one assumes that the COO bend in CF_3OOH and the COF bend in CF_3OF have similar shapes, then the supposed R branch at 451 cm^{-1} can be assigned to the second CF_3 rock. However, in view of all these uncertainties, it seems preferable to list the second CF_3 rock as not observed with its frequency definitely expected between 400-500 cm^{-1}, most probably near 450 cm^{-1}.

The potential energy distributions for CF_3OOH and CF_3OOD show that the frequencies assigned as COO bending modes have minor contributions from CO and OO stretching coordinates as well as larger contributions from changes of α, β, γ type angles with none dominant. For a true COO bend the major contribution to the potential energy distribution would be the γ type angle change. For the higher frequency CF_3 rock in CF_3OOH and CF_3OOD, the potential energy distribution has changes in the β type angles ss the primary contributor with changes in the α type angles as a secondary contributor. For the lower frequency CF_3 rock in both CF_3OOH and CF_3OOD, a change in the β type angles in the primary contributor with changes in the γ type angles as a secondary contributor. For CF_3OOH but not for CF_3OOD the potential energy distribution for the lower frequency CF_3 rock also has a secondary contribution from the OH torsion coordinate that is somewhat larger than the contribution from the change in the γ type angle.

As might be expected from the result and already noted, the potential energy distribution for the OH torsion but not for the OD torsion has a secondary contribution from the change in both the β type angles and the γ type angle.

f. CF_3 Torsion

The lowest frequency band in the Raman spectrum of both liquid CF_3OOH and CF_3OOD is at 155 cm^{-1}. The band occurs at 142 cm^{-1} in the Raman spectrum of gaseous CF_3OOH. The corresponding infrared spectrum is below the range of our infrared spectrophotometer (Perkin-Elmer Model 180). By analogy with CF_3OF we assign this band as the 0→1 transition in the CF_3 torsion rather than the 0→2 transition (see Section E). The potential energy distribution shows the CF_3 torsion frequencies to be greater than 90 percent pure with contributions from the other coordinates of less than 6 percent from any one coordinate.

3. CF_3OOF and CF_3OOCl

a. CF_3 and CO Stretching

As in all CF_3OX and CF_3OOX series members the dominant feature of the infrared spectra of both CF_3OOF and CF_3OOCl are very intense bands between 1350 cm^{-1} and 1150 cm^{-1}. The corresponding bands in the Raman spectra are very weak and polarization measurements are very uncertain. The three most prominent peaks are assigned to the three fundamentals expected in this region. By analogy to CF_3OCl as well as the CF_3OF, CF_3OOH and CF_3OOD isoelectronic series, the symmetry coordinates from Table 6 numbered 1, 11 and 2 are assigned to the frequencies in the order highest to lowest as shown in Tables 3 and 4. The potential energy distribution for the intermediate frequency in both CF_3OOF and CF_3OOCl is very similar to that

of the intermediate frequency in CF_3OX which is in the A" block under C_s symmetry. For both CF_3OOF and CF_3OOCl the potential energy distributions are consistent with the highest and intermediate frequencies having a major contribution from stretching the C-F bonds while the lowest frequency has major contributions from stretching the C-O bonds as well as the C-F bond.

CF_3OOF and CF_3OOCl have polarized bands in the Raman spectrum of the liquid at 949 cm^{-1} and 905 cm^{-1}, respectively. The corresponding bands in the infrared spectra of the gases at 950 cm^{-1} and 903 cm^{-1} have PQR structure. These bands are assigned to the CO stretching mode in analogy to CF_3OCl as well as the CF_3OF, CF_3OOH and CF_3OOD isoelectronic series. However, as was the case for CF_3OOH and CF_3OOD, the potential energy distributions for both CF_3OOF and CF_3OOCl indicate that this mode has stretching of the C-F bond as its major contributor rather than stretching of the C-O bond. Thus, the conventional designations in Tables 1, 2, 3 and 4 are misleading and for all four CF_3OOX series members the four bands in the 1150-1350 cm^{-1} and 900-950 cm^{-1} regions appear to include both CF and CO stretching. Consistent with the mixing of CF and other stretching modes reported by Tuazon, Fateley and Bentley (27), for all members of both the CF_3OX and CF_3OOX series, it now seems more appropriate to specify that two predominantly CF stretching modes are in the 1150-1350 cm^{-1} region along with one mixed CF and CO stretching mode and that one predominantly CF stretching mode is in the 900-950 cm^{-1} region rather than restricing the CF stretching modes to the 1150-1350 cm^{-1} region and the CO stretching mode to the 900-950 cm^{-1} region.

b. OO and OX Stretching

The dominant features of the Raman spectra of liquid CF_3OOF and CF_3OOCl are very intense and highly polarized bands at 876 cm^{-1} and 830 cm^{-1},

respectively. The gas phase Raman spectrum of CF_3OOF has its most intense band at 875 cm^{-1}. The corresponding bands in the gas phase infrared spectra of CF_3OOF and CF_3OOCl are at 874 cm^{-1} with possible PQR structure and 828 cm^{-1} with definite PQR structure, respectively. The 874 cm^{-1} band of CF_3OOF is weak compared to the 950 cm^{-1} band (conventionally assigned to CO stretching but really CF stretching according to the potential energy distribution) while the 828 cm^{-1} band of CF_3OOCl is almost as intense as the 903 cm^{-1} band (conventionally assigned to CO stretching but really CF stretching according to the potential energy distribution). The bands near 875 cm^{-1} and 828 cm^{-1} for CF_3OOF and CF_3OOCl, respectively, are assigned to the OO stretching mode by analogy to CF_3OOH and CF_3OOD having their OO stretching modes as their most intense Raman bands and to many alkyl peroxides and fluoro substituted alkyl peroxides having the OO stretching mode as the most intense Raman band (28).

The most intense band in the gas phase infrared spectrum of CF_3OOF below 1000 cm^{-1} is at 760 cm^{-1} with definite PQR structure. The second most intense band above 500 cm^{-1} in the Raman spectra of both gaseous and liquid CF_3OOF is at 752 cm^{-1} and 751 cm^{-1}, respectively. With the exception of CF_3OCl, which has the OCl stretch assigned to the most intense band in the Raman spectrum of the liquid at 781 cm^{-1} and a corresponding weak band at 780 cm^{-1} in the infrared spectrum of the gas, none of the other CF_3OX and CF_3OOX series members have Raman or infrared bands between 700 cm^{-1} and 800 cm^{-1}. Consequently, the OF stretch of CF_3OOF is assigned to this band consistent with the fact that the OF stretch is intense in both the Raman and infrared spectra of CF_3OF (15, 18).

Both the infrared spectrum of gaseous CF_3OOCl and the Raman spectrum of liquid CF_3OOCl have four bands in the 580-700 cm^{-1} region where three

CF_3 deformation modes are expected. Going from CF_3OF to CF_3OOF the OF stretching frequency decreased from 882 cm^{-1} to 760 cm^{-1} using infrared frequencies of the gas. A similar decrease in frequency from the OCl stretch at 780 cm^{-1} in CF_3OCl would place the OCl stretch in CF_3OOCl near 660 cm^{-1}. Thus, it seems reasonable to account for the four bands between 580 cm^{-1} and 700 cm^{-1} by adding the OCl stretch to the expected three CF_3 deformations. The four infrared bands of gaseous CF_3OOCl are at 697 cm^{-1}, 665 cm^{-1}, 613 cm^{-1} and 583 cm^{-1} with all four bands showing some suggestions of PQR structure. The 665 cm^{-1} band is most intense and the 697 cm^{-1} band is least intense with the two lower frequency bands being of comparable intensity and about half that of the 665 cm^{-1} band. The two lower frequency bands would both be reasonably assigned as CF_3 deformations by comparison with CF_3OF, CF_3OCl, CF_3OOH and CF_3OOD. For gaseous CF_3OF, CF_3OCl, CF_3OOH and CF_3OOD the highest frequency CF_3 deformation mode is the most intense or second most intense infrared band in the 500-1000 cm^{-1} region. On this basis the 665 cm^{-1} infrared band of gaseous CF_3OOCl would be a CF_3 deformation and the lower intensity 697 cm^{-1} band would be the OCl stretch, consistent with the low intensity of the 780 cm^{-1} band in CF_3OCl assigned as the OCl stretch. The Raman spectrum of liquid CF_3OOCl suggests the reverse assignment since the band at 667 cm^{-1} is the second most intense Raman band above 500 cm^{-1} and is definitely polarized while the 696 cm^{-1} band is much less intense and weakly polarized. For liquid CF_3OCl the OCl stretch is the most intense Raman band above 500 cm^{-1} and is strongly polarized. For liquid CF_3OOF the OF stretch is the second most intense Raman band above 500 cm^{-1} and is strongly polarized. The Raman spectrum of liquid CF_3OOCl is somewhat surprising since both the OCl stretch and the highest frequency CF_3 deformation would be expected to have appreciable

intensity and be definitely polarized by analogy to CF_3OF, CF_3OCl, CF_3OOH, and CF_3OOD. Thus, assigning the 665 cm^{-1} band to the OCl stretch would create the new difficulty of having the CF_3 deformation weakly polarized and of low intensity in addition to contradicting the assignement based on infrared intensities.

The potential energy distribution for the 665 cm^{-1} band of CF_3OOCl is very similar to that for the highest frequency CF_3 deformation of CF_3OF, CF_3OCl, CF_3OOH and CF_3OOD and has contributions from many stretching and bending coordinates with none dominant. For the 697 cm^{-1} band of CF_3OOCl the major contributor is the OCl stretching coordinate. Since the infrared and Raman data lead to contradictory assignements for CF_3OOCl we have chosen to use the potential energy distribution to make the assignment in Table 4 where 665 cm^{-1} is listed as a CF_3 deformation and 697 cm^{-1} is listed as the OCl stretch for gas phase infrared frequencies. The potential energy distribution for the 828 cm^{-1} band (gas phase infrared frequency) of CF_3OOCl has stretching the O-O bond as its dominant contributor. For CF_3OOF the potential energy distribution for force constant values nearly identical to Dr. Marsden's results shows that both the 874 cm^{-1} band and the 760 cm^{-1} band, using gas phase infrared frequencies, have important contributions both from stretching the O-O bond and from stretching the O-F bond. For CF_3OOF, it is possible to get a reasonable but definitely poorer overall fit by raising the force constant for OO stretching and lowering the force constants for OF stretching and for interaction between OO and OF stretching from Dr. Marsden's values. The latter force field is more consistent with the decomposition reaction and structure of CF_3OOF and has a potential energy distribution where stretching the O-O bond is the major contributor to the 874 cm^{-1} band and stretching the O-F bond is the major

contributor to the 760 cm^{-1} band.

c. CF_3 Deformation

The three CF_3 deformations in CF_3OOF are reasonably assigned by frequency analogy with isoelectronic CF_3OCl and the other isoelectronic series of CF_3OF, CF_3OOH and CF_3OOD to bands at 693 cm^{-1}, 630 cm^{-1} and 588 cm^{-1} in the infrared spectrum of the gas. For CF_3OOCl, the decision to assign the band at 697 cm^{-1} in the infrared spectrum of the gas to the OCl stretch, leaves the frequencies 665 cm^{-1}, 613 cm^{-1} and 583 cm^{-1} available for assignment to the three CF_3 deformations. For gaseous CF_3OOF the intensity of the three infrared bands increases with decreasing frequency, a reversal from the behavior of CF_3OOH, CF_3OOD, CF_3OF and CF_3OCl. The highest frequency infrared band of gaseous CF_3OOF has about half the intensity of the intermediate frequency band which is almost as intense as the lowest frequency band. All three infrared bands of gaseous CF_3OOF show possible PQR structure but the lowest frequency band has the most easily discernible PQR structure in contrast to gaseous CF_3OOH, CF_3OOD, CF_3OF and CF_3OCl where the highest frequency band has easily discernible PQR structure and the lowest frequency band does not. For gaseous CF_3OOCl, the highest frequency infrared band at 665 cm^{-1} is the most intense while the other two bands at 613 cm^{-1} and 583 cm^{-1} are about half as intense with the 583 cm^{-1} band being slightly more intense than the 613 cm^{-1} band. This intensity pattern agrees with that of CF_3OF, CF_3OCl, CF_3OOH, and CF_3OOD in the highest frequency CF_3 deformation being the most intense but disagrees in the lowest frequency band being slightly more intense rather than definitely less intense than the intermediate frequency band. The band shapes for the CF_3OOCl gas phase infrared bands agree with those of CF_3OF, CF_3OCl, CF_3OOH and CF_3OOD

in having possible PQR structure for the highest and intermediate frequency but disagree in the lowest frequency for CF_3OOCl having possible PQR structure rather than no readily discernible PQR structure. If the OCl stretch and the highest frequency CF_3 deformation assignments were reversed so that the 697 cm^{-1} infrared band for gaseous CF_3OOCl were the highest frequency CF_3 deformation, then the intensity variation with frequency for CF_3OOCl would be similar to that for CF_3OOF. However, this assignment reversal for CF_3OOCl would be in conflict with the potential energy distribution.

For the three frequencies logically assigned to the CF_3 deformation, the difference between CF_3OOF and the four other compounds CF_3OF, CF_3OCl, CF_3OOH and CF_3OOD is even more striking in the Raman spectrum of the liquids. For liquid CF_3OOF the bands at 695 cm^{-1}, 628 cm^{-1}, and 587 cm^{-1} alternate in intensity with the highest and lowest being of lower and comparable intensity and weakly polarized while the intermediate frequency has higher intensity and is definitely polarized. This pattern is the opposite to that found in the CF_3OX series and in CF_3OOH and CF_3OOD where the highest and lowest frequencies are of comparable intensity and definitely polarized while the intermediate frequency is much less intense and weakly polarized. If CF_3OOF had C_s symmetry then the present assignment would be modified by assuming that the 695 cm^{-1} in the Raman spectrum of the liquids CF_3OOF was not a CF_3 deformation and moving the whole pattern of CF_3 deformation downward in frequency. If one assumes that a band in the Raman spectrum of liquid CF_3OOF at 516 cm^{-1} is the lowest frequency CF_3 deformation, then the three bands at 628 cm^{-1}, 587 cm^{-1}, and 514 cm^{-1} would show a similar pattern of relative intensities and polarization properties to the 679 cm^{-1}, 612 cm^{-1}, and 582 cm^{-1} Raman bands of liquid CF_3OOH. Initially we had

adopted such an assignement which then required the 695 cm^{-1} band in the Raman spectrum of liquid CF_3OOF to be assigned as the first overtone of the OOF bend to be assigned at 342 cm^{-1}. Anharmonicity would be expected to place this first overtone below 684 cm^{-1} (from 2x342 cm^{-1}) and the band would also be expected to be definitely polarized since the 342 cm^{-1} band is definitely polarized. Then the higher than expected frequency of the 695 cm^{-1} band would have to be explained by Fermi resonance with a lower frequency band of appreciable intensity. The 628 cm^{-1} band is the nearest in frequency below a band near 684 cm^{-1} (from 2x342 cm^{-1}) but the frequency increases of a 684 cm^{-1} band due to Fermi resonance with the 628 cm^{-1} band would probably be balanced or exceeded by the frequency decrease of a 684 cm^{-1} band due to Fermi resonance with the intense band at 751 cm^{-1} assigned to the OF stretch. Thus, the 695 cm^{-1} band is still anomalously high in frequency for the first overtone of a band at 342 cm^{-1}. The preliminary normal coordinate analysis by Dr. Marsden always gave a CF_3 rocking mode above 400 cm^{-1} for all CF_3OX and CF_3OOX cases and for CF_3OOF the suggested frequency was about 530 cm^{-1}. Thus, the 516 cm^{-1} band in the Raman spectrum of liquid CF_3OOF could be assigned to the higher frequency CF_3 rock. Then the three CF_3 deformations move back up to 695 cm^{-1}, 628 cm^{-1}, and 587 cm^{-1} and are in the same frequency range as CF_3OF, CF_3OCl, CF_3OOH and CF_3OOD. Now it is no longer necessary to assign the 695 cm^{-1} band in the Raman spectrum of liquid CF_3OOF to a first overtone, but the difference in infrared intensity distribution, Raman intensity distribution, and polarization properties between CF_3OOF and the four other compounds CF_3OF, CF_3OCl, CF_3OOH and CF_3OOD is difficult to understand.

Polarization properties for C_s symmetry would require two polarized and one depolarized CF_3 deformations. Under C_1 symmetry all bands are

polarized but bands too weakly polarized to be distinguished from being depolarized are possible. Since CF_3OOF is expected to show large deviations from C_s symmetry due to having F rather than H or D as the odd atom off the plane of symmetry, differences between polarization property between CF_3OOH and CF_3OOF may be expected. However, one might have expected CF_3OOF to show all three band more strongly polarized than in CF_3OOH rather than going from two definitely polarized bands and one weakly polarized band in CF_3OOH to one definitely polarized band and two weakly polarized bands in CF_3OOF. Changing the CF_3 deformation frequencies downward from 693 cm^{-1}, 630 cm^{-1}, and 588 cm^{-1} in the gas phase infrared spectrum of CF_3OOF to 630 cm^{-1}, 588 cm^{-1} and 514 cm^{-1} does not bring the infrared intensity distribution into agreement with gaseous CF_3OOH. The bands at 630 cm^{-1} and 514 cm^{-1} are of comparable intensity and less intense respectively, than the 588 cm^{-1} band which has the most easily discernible PQR structure in the infrared spectrum of gaseous CF_3OOF. The band at 680 cm^{-1} in the infrared spectrum of gaseous CF_3OOH has the most easily discernible PQR structure and is more intense than the band at 615 cm^{-1} with possible PQR structure which is more intense than the band at 587 cm^{-1} which does not have PQR structure. Thus the higher frequency assignement for the CF_3 deformation in CF_3OOF makes a reasonable match with CF_3OF, CF_3OCl, CF_3OOH and CF_3OOD in frequency range but a poor match in intensity distribution in the infrared spectrum, intensity distribution in the Raman spectrum and polarization properties in the Raman spectrum. The lower frequency assignment for the CF_3 deformation in CF_3OOF makes a reasonable match with CF_3OF, CF_3OCl, CF_3OOH and CF_3OOD in intensity distribution and polarization properties in the Raman spectrum but a poor match in frequency range and intensity distribution in the infrared spectrum as well as having the

difficulty of the 695 cm^{-1} in the Raman spectrum of liquid CF_3OOF being anomalously high for a first overtone of the OOF bend.

Since the infrared and Raman data lead to contradictory assignements for CF_3OOF, we turn to the potential energy distribution to choose the more desirable assignment. The potential energy distribution for CF_3OOF shows the 693 cm^{-1} band (gas phase infrared frequency) to have contributions from many stretching and bending coordinates with none dominant as is the case for the highest frequency CF_3 deformation in CF_3OF, CF_3OCl, CF_3OOH, and CF_3OOD. For the 588 cm^{-1} band (gas phase infrared frequency) of CF_3OOF changing the α type angles is the major contributor to the potential energy distribution as is the case for the lowest frequency CF_3 deformation in CF_3OF, CF_3OCl, CF_3OOH, and CF_3OOD. The potential energy distribution for the 630 cm^{-1} band (gas phase infrared frequency) of CF_3OOF has its three major contributions from changing the α type angles, changing the β type angles, and changing the δ type angle with none of these dominant. The potential energy distribution for the 514 cm^{-1} band (gas phase infrared frequency) of CF_3OOF has the changes in the α type angles as its primary contributor and the changes in the δ type angle as a secondary contributor. For these latter two bands, 630 cm^{-1} and 514 cm^{-1}, the potential energy distribution does not match well with any modes of CF_3OF, CF_3OCl, CF_3OOH, and CF_3OOD. A comparison of the higher and lower frequency assignments for the CF_3 deformations in CF_3OOF favors the higher frequency assignment. In the higher frequency assignement, the 693 cm^{-1} and 588 cm^{-1} bands for CF_3OOF match the potential energy distribution of CF_3OF, CF_3OCl, CF_3OOH, and CF_3OOD while 630 cm^{-1} band does not. In the lower frequency assignment the 630 cm^{-1} and 514 cm^{-1} bands do not match the potential energy distribution of CF_3OF, CF_3OCl, CF_3OOH, and CF_3OOD while 588 cm^{-1} band will as both

the intermediate frequency and the lowest frequency bands in CF_3OF, CF_3OCl, CF_3OOH, and CF_3OOD have changes of the α type angles as the major contributor to the potential energy distribution. However, the potential energy distribution for the 588 cm^{-1} band (gas phase infrared frequency) of CF_3OOF does match CF_3OF, CF_3OCl, CF_3OOH and CF_3OOD better as the lowest frequency CF_3 deformation rather than the intermediate frequency one. Thus, the higher frequency assignment for the CF_3 deformations as shown in Table 3 is chosen on the basis of the potential energy distribution.

The Raman spectrum of liquid CF_3OOCl has bands at 696 cm^{-1}, 617 cm^{-1}, 588 cm^{-1}, and 483 cm^{-1} which show a pattern of relative intensities and polarization properties similar to the 695 cm^{-1}, 628 cm^{-1}, 587 cm^{-1}, and 516 cm^{-1} bands of liquid CF_3OOF. Liquid CF_3OOCl also has a definitely polarized Raman band at 667 cm^{-1} which is more intense than any of the other bands between 700 Cm^{-1} and 450 cm^{-1}. Extension to CF_3OOCl of the assignment just made for the CF_3 deformations of CF_3OOF on the basis of the potential energy distribution would place the three CF_3 deformations at 696 cm^{-1}, 617 cm^{-1} and 588 cm^{-1} in the Raman spectrum of liquid CF_3OOCl. Then the bands at 667 cm^{-1} and 483 cm^{-1} in the Raman spectrum of liquid CF_3OOCl would be assigned to the OCl stretch and the higher frequency CF_3 rock, respectively. However, as already discussed earlier, the potential energy distribution for CF_3OOCl makes the 696 cm^{-1} band and the 667 cm^{-1} bands in the Raman spectrum of liquid CF_3OOCl the OCl stretch and the highest frequency CF_3 deformation, respectively. With the highest frequency CF_3 deformation assigned to the 667 cm^{-1} band in the Raman spectrum of liquid CF_3OOCl the bands at 617 cm^{-1} and 588 cm^{-1} are assigned to the other two CF_3 deformations. Now the frequency range for the three CF_3 deformations in CF_3OOCl agrees with that for all other CF_3OX and CF_3OOX compounds. For the 667 cm^{-1}, 617 cm^{-1} and 588 cm^{-1} bands in the Raman spectrum of liquid

CF_3OOCl, the intensity decreases by a factor of about 2 from the 667 cm^{-1} band to the 617 cm^{-1} band and by a factor of about 5 from the 617 cm^{-1} band to the 588 cm^{-1} band with the 667 cm^{-1} and 617 cm^{-1} bands being definitely polarized and the 588 cm^{-1} band being weakly polarized. Thia intensity pattern agrees with that of CF_3OF, CF_3OCl, CF_3OOH and CF_3OOD in the highest frequency band being the most intense and definitely polarized but disagrees in the relative intensity and polarization properties of the intermediate and lowest frequency bands being reversed from that of CF_3OF, CF_3OCl, CF_3OOH and CF_3OOD. Since CF_3OOCl is expected to show large deviationa from C_s symmetry due to having Cl rather than H or D as the odd atom off the plane of symmetry, even if there were not non-zero angles of twist, one might have expected all three CF_3 deformations to be definitely polarized. However, the result that CF_3OOCl has two definitely polarized bands and one weakly polarized band is less surprising than CF_3OOF having one definitely polarized band and two weakly polarized bands for the CF_3 deformations.

The lower frequency CF_3 deformation assignment suggested for CF_3OOF and finally replaced by the higher frequency one could be applied to CF_3OOCl by taking the bands at 617 cm^{-1}, 588 cm^{-1} and 483 cm^{-1} in Raman spectrum of liquid. This assignment would bring the relative intensity pattern and polarization properties in the Raman spectrum of liquid CF_3OOCl into agreement with those of CF_3OF, CF_3OCl, CF_3OOH and CF_3OOD at the expense of frequency range agreement and intensity distribution in the infrared spectrum. Then, the 667 cm^{-1} band in the Raman spectrum of liquid CF_3OOCl could be assigned to the ClO stretch, but that would require assigument of the 696 cm^{-1} bands as an overtone or combination band of a lower frequency fundamental of appreciable intensity in Fermi resonance with another intense fundamental. The combination band 431 cm^{-1} + 266 cm^{-1} = 697

cm^{-1} for the Raman spectrum of liquid CF_3OOCl is reasonable on a frequency basis. Application of the equation of Dixon (29) as modified by Saier, Cousins, and Basila (30) assuming zero intensity for the combination band unperturbed by Fermi resonance gave the unperturbed frequencies for the 696 cm^{-1} and 667 cm^{-1} Raman bands of liquid CF_3OOCl as 693 cm^{-1} and 670 cm^{-1}, respectively. The combination band 431 cm^{-1} + 266 cm^{-1} = 697 cm^{-1} could easily have its unperturbed frequency at 693 cm^{-1} due to anharmonicity. However, the fact that both the 431 cm^{-1} and 266 cm^{-1} bands are of modest intensity and the 667 cm^{-1} band is only the third most intense Raman band in liquid CF_3OOCl makes it seem unlikely that this combination band would be observed. For the four compounds CF_3OF, CF_3OCl, CF_3OOH and CF_3OOD, the only non-fundamental observed is the first overtone of the COF bend in Fermi resonance with the O-F stretch of CF_3OF. However, in the CF_3OF case, an overtone of the third most intense band in Fermi resonance with the most intense band is involved rather than a combination of two modest intensity bands in Fermi resonance with the third most intense band. Consequently, we reject the assignment of the 696 cm^{-1} band as a non-fundamental. Also, the 483 cm^{-1} Raman frequency of liquid CF_3OOCl seems anomalously low for a CF_3 deformation. The lower frequency CF_3 deformation assignment is then rejected in favor of the higher frequency CF_3 deformation assignment due to the difficulty of accounting for the 696 cm^{-1} band and the need to assign the lowest frequency CF_3 deformation below 500 cm^{-1}.

All assignments considered for the five bands between 700 cm^{-1} and 450 cm^{-1} in the Raman and infrared spectra of CF_3OOCl lead to some unexpected results and apparent anomalies. As already noted, such is also the case for CF_3OOF where the potential energy distribution is used to choose the best compromise for assigning the four infrared and Raman bands between 700 cm^{-1} and 500 cm^{-1}. The potential energy distribution for the 697 cm^{-1} band (gas phase infrared frequency) of CF_3OOCl has the OCl stretching

coordinate as its major contributor. For the 665 cm^{-1} band (gas phase infrared frequency) of CF_3OOCl the potential energy distribution is very similar to that for the highest frequency CF_3 deformation of all the other CF_3OX and CF_3OOX molecules and has contributions from many stretching and bending coordinates with none dominant. The potential energy distribution for the 613 cm^{-1} band (gas phased infrared frequency) of CF_3OOCl is similar to that of the intermediate frequency CF_3 deformations for CF_3OF, CF_3OCl, CF_3OOH and CF_3OOD in having changing the α type angles as the major contributor but differs in having a small contritution from stretching the O-Cl bonds. For the 583 cm^{-1} band (gas phase infrared frequency) the major contributor to the potential energy distribution is the change in the α type angles as is the case for the lowest frequency CF_3 deformation of the other CF_3OX and CF_3OOX molecules. The potential energy distributions for the highest and lowest frequency CF_3 deformations are very similar for all six CF_3OX and CF_3OOX compounds if the higher frequency CF_3 deformation assignments for both CF_3OOF and CF_3OOCl are taken. For the intermediate frequency CF_3 deformation, the five compounds CF_3OF, CF_3OCl, CF_3OOH, CF_3OOD and CF_3OOCl are similar in having changes in the α type angles as the major contributor with a small contribution from changes in the β type angles (also a small contribution from stretching the O-Cl bond for CF_3OOCl). For CF_3OOF the intermediate frequency CF_3 deformation still has changes in the α type angles and β type angles as the largest (35 percent) but no longer dominant and second largest (25 percent) contributions respectively, but there is a third important contribution (15 percent) from the δ type angle which does not occur for the other five compounds. Thus, the potential energy distributions are consistent over all six compounds for two of the CF_3 deformations and over five of the six compounds for the other CF_3

deformation.

d. COO Bending and CF_3 Rocking

The COO bending mode is assigned to bands at 441 cm^{-1} and 431 cm^{-1} in the Raman spectra of liquid CF_3OOF and CF_3OOCl, respectively, by analogy to CF_3OOH and CF_3OOD. These bands are definitely polarized and are of modest intensity being the second strongest bands below 500 cm^{-1} but far less intense than the bands assigned to the OOX stretch. The corresponding infrared bands in gaseous CF_3OOF and CF_3OOCl at 434 cm^{-1} and 424 cm^{-1}, respectively, are weak and show possible PQR structure. The potential energy distributions for CF_3OOF and CF_3OOCl are similar to those for CF_3OOH and CF_3OOD in having their largest contributions from the changes in the α, β, and γ type angles. CF_3OOCl agrees with CF_3OOH and CF_3OOD in having the order of contribution to the potential energy $\beta>\alpha>\gamma$ while for CF_3OOF the order is $\alpha>\beta>\gamma$. For a true COO bend the change in the γ type angle would be the major contributor to the potential energy.

The CF_3 rocking mode expected in the 200-300 cm^{-1} region is assigned to weak but definitely polarized bands at 283 cm^{-1} and 266 cm^{-1} in the Raman spectra of liquid CF_3OOF and CF_3OOCl, respectively, by analogy with CF_3OF, CF_3OCl, CF_3OOH, and CF_3OOD. The corresponding infrared bands in gaseous CF_3OOF and CF_3OOCl at 278 cm^{-1} and 259 cm^{-1} are weak with no discernible PQR structure. The potential energy distributions for the lower frequency CF_3 rock in both CF_3OOF and CF_3OOCl are similar to those of CF_3OOH and CF_3OOD in having a change in the β type angles as the primary contributor with changes in the γ type angle as a secondary contributor. CF_3OOH also has a secondary contribution to the potential energy distribution from the OH torsion coordinate which is somewhat larger than the contribution from the changes in the γ type angle. Although, as noted, the

changes in the β type angles is the primary contributor to the potential energy distribution in all cases, this contribution rises from 47 percent to 85 percent on going from CF_3OOH to CF_3OOCl.

The CF_3 rocking mode expected above 400 cm^{-1} has already been discussed in part in the course of considering the CF_3 deformation for CF_3OOF and CF_3OOCl. Bands in the Raman spectra of liquid CF_3OOF and CF_3OOCl at 516 cm^{-1} and 483 cm^{-1}, respectively, are assigned to the higher frequency CF_3 rock. These Raman bands are of modest intensity and definitely polarized; a definitely polarized Raman band for this mode would be forbidden under C_s symmetry but is compatible with C_1 symmetry and the expectation that both CF_3OOF and CF_3OOCl would deviate significantly from C_s polarization properties due to F or Cl rsther H or D being the odd atom off the plane of symmetry. The corresponding infrared bands in gaseous CF_3OOF and CF_3OOCl at 514 cm^{-1} and 487 cm^{-1}, respectively, are of medium intensity with discernible PQR structure and of low intensity with no discernible PQR structure, respectively.

The pattern of intensity for the higher frequency CF_3 rock over both the Raman and infrared spectra of the six CF_3OX and CF_3OOX compounds requires comment. For CF_3OF only a shoulder at 431 cm^{-1} in the infrared spectrum of the gas is observed. For CF_3OCl only a very weak band at 430 cm^{-1} in the Raman spectrum of the liquid is observed. For both Raman and infrared spectra of both CF_3OOH and CF_3OOD the higher frequency CF_3 rock is either too weak to be observed or overlapped by the COO bend. Thus, it is only CF_3OOF and CF_3OOCl which have readily observed bands in both the Raman and infrared spectra. The following sequence of frequencies using gas phase infrared data for all but CF_3OCl with only a Raman frequency of the liquid available is somewhat surprising: CF_3OF, 431 cm^{-1}, CF_3OCl, 430 cm^{-1},

CF_3OOH and CF_3OOD ~450 cm^{-1}??, CF_3OOF 514 cm^{-1}, and CF_3OOCl 478 cm^{-1}. However, this sequence is predicted by the force field adopted by Dr. Marsden at the University of Michigan with the force constant values as modified in the calculations done at Kansas State University. The potential energy distributions for the highest frequency CF_3 rock are quite different for CF_3OOF and CF_3OOCl and both are quite different from these of CF_3OF, CF_3OCl, CF_3OOH, and CF_3OOD which are similar in having changes in the β type angles as the major contributor with changes in the α type angles as secondary contributors. For CF_3OOF the major contributor is changing the α type angles and the secondary contributor is changing the δ type angle. The potential energy distribution for CF_3OOCl has not dominant term; the three largest and almost equal contributors are changing the α type angles, changing the δ type angle and changing the β type angles, and another smaller contribution comes from the OCl stretch. In view of these differences in potential energy distribution, differences in Raman and infrared intensities between CF_3OOF and CF_3OOCl and between both CF_3OOF and CF_3OOCl and the other four compounds are not surprising.

e. OOX Bending

The OOX bending mode for both CF_3OOF and CF_3OOCl is assigned to the most intense band in the Raman spectrum of the liquid below 500 cm^{-1} by analogy to CF_3OF and CF_3OCl. These bands which are definitely polarized, are at 342 cm^{-1} and 295 cm^{-1} in CF_3OOF and CF_3OOCl, respectively. The corresponding band in the infrared spectrum of gaseous CF_3OOF is at 336 cm^{-1} with definite PQR structure. For CF_3OOCl the infrared spectrum of the gas shows only a shoulder near 290 cm^{-1} on the weak band at 259 cm^{-1} assigned to the lower frequency CF_3 rock. CF_3OOCl is then the only one among the six CF_3OX and CF_3OOX compounds to fail to shown an easily indentified

infrared band that may be assigned to the COX bend, a surprising result. However, the high intensity and definite polarization of the Raman band at 295 cm^{-1} in liquid CF_3OOCl leaves little doubt that it should be assigned to the OOCl bend. For both CF_3OOF and CF_3OOCl the largest contributor to the potential energy distribution is a change in the β type angles with the second largest contributor being changes in the δ type angles. This mode does not lend itself well to comparison with CF_3OOH and CF_3OOD due to the small H and D atom masses nor to comparison with CF_3OX compounds due to differences in number of angle changes that may be involved (α, β, γ in CF_3OX and α, β, γ, and δ in CF_3OOX). CF_3OOF and CF_3OOCl do differ in relative values of the contributions of the β and δ type angle changes with CF_3OOCl having the δ contribution almost as large as the β contribution while CF_3OOF has the δ contribution only half as large as the β contribution.

f. CF_3 and OX Torsions

For CF_3OOF bands in the Raman spectrum of the liquid at 78 cm^{-1} and 147 cm^{-1} are assigned to the CF_3 torsion and the OF torsion, respectively. The Raman spectrum of CF_3OOF gas is badly obscured by the pure rotational Raman spectrum of oxygen from the decomposition of CF_3OOF to CF_4 and O_2. By comparison of the observed spectrum in Figure 6 with the O_2 pure rotational transition frequencies calculated from literature data (31) and the assumption that the O_2 has a Boltzmann distribution, one may conclude that a band at 132 cm^{-1} corresponds to the 147 cm^{-1} band in the Raman spectrum of the liquid. It is not possible to get close enough to the Rayleigh line in this sample to search for the gas phase Raman band corresponding to the Raman band at 78 cm^{-1} in the liquid. By analogy to

CF_3OF and CF_3OOH we would expect the CF_3 torsion frequency to decrease by about 10 percent from the liquid to gas phase (CF_3OF 144 cm^{-1} to 127 cm^{-1} or 12 percent, CF_3OOH 155 cm^{-1} to 142 cm^{-1} or 8 percent). Consequently, we reduce the 78 cm^{-1} in the liquid state to 70 cm^{-1} in the vapor for the CF_3 torsion for use in the normal coordinate calculations. For the OF torsion we use 132 cm^{-1} deduced from the Raman spectrum of gaseous CF_3OOF. The potential energy distribution for the CF_3 torsion of CF_3OOF shows the mode to be 95 percent pure. The potential energy distribution for the OF torsion shows the mode to be about 75 percent pure with about 10 percent contributions from changes in the β and γ type angles.

Liquid CF_3OOCl does not have any Raman bands below 200 cm^{-1} that are as prominant as those at 147 cm^{-1} and 78 cm^{-1} in the Raman spectrum of liquid CF_3OOF. However, these are weak bands at 80 cm^{-1}, 150 cm^{-1}, and 204 cm^{-1} in the Raman spectrum of liquid CF_3OOCl which may be interpreted in terms of CF_3 and OCl torsions. Polarization results are uncertain for these weak bands but the 80 cm^{-1} and 204 cm^{-1} bands do appear to be polarized. We suggest the following assignments: 80 cm^{-1} as τ_{CF_3}, 150 cm^{-1} as $2\tau_{CF_3}$, and 204 cm^{-1} as $2\tau_{CF_3} + \tau_{OCl}$.

Since the Raman spectra of the liquid CF_3OOCl are recorded with liquid N_2 as the coolant in the low temperature cell, the low sample temperature would be expected to allow only non-fundamental transitions from the vibrational ground state of the molecule to be observed. Consequently, the three Raman bands may be τ_{CF_3}, τ_{OCl} and one non-fundamental or two non-fundamentals and either τ_{CF_3} or τ_{OCl}. Since CF_3OOH and CF_3OOCl have the same $C\text{-}O_1$, and $O_1\text{-}O_2$ bond length (Figure 7 and Table 5) we assume they have similar force constants for CF_3 torsions. Since CF_3OOF has a shorter $O_1\text{-}O_2$ bond and a longer $C\text{-}O_1$ bond than CF_3OOH and CF_3OOCl we use the values

of the force constants for CF_3 torsion in CF_3OOH and CF_3OOF to establish a probable limiting range of force constant values for CF_3 torsion in CF_3OOCl. Using this range of 0.02 to 0.01 m dyne Å rad.$^{-2}$ and the treatment developed by Fsteley and Miller (32), the range of τ_{CF_3} in the gas phase is 60-87 cm^{-1}. Reducing the liquid phase frequency by 10 percent to estimate the gas phase frequency for the CF_3 torsion by analogy to CF_3OF and CF_3OOH, gives 72 cm^{-1} from the 80 cm^{-1} band of liquid CF_3OOCl.

Again since CF_3OOF has a shorter O_1-O_2 bond than CF_3OOCl and CF_3OOH, we assume the force constant for OCl torsion in CF_3OOCl is much smaller than the force constant for OF torsion in CF_3OOF in analogy to the force constant for OH torsion in CF_3OOH being much smaller than the force constant for OF torsion in CF_3OOF. Thus with a much smaller force constant for OX torsion and a much larger X mass, CF_3OOCl would be expected to have τ_{OCl} in the gas phase much lower in frequency than the 132 cm^{-1} for τ_{OF} in gaseous CF_3OOF. Then, the bands at 204 cm^{-1} and 150 cm^{-1} in the Raman spectrum of liquid CF_3OOCl are not fundamentsls and the band at 80 cm^{-1} in the Raman spectrum of liquid CF_3OOCl, estimated to be 72 cm^{-1} in the gaseous state, is either τ_{CF_3} or τ_{OCl}. The choice is τ_{CF_3} in order to keep the force constant for CF_3 torsion in the probable limiting range of 0.02 to 0.01 mdyne Å rad.$^{-2}$. Then the 150 cm^{-1} band must be assigned to $2\tau_{CF_3}$ although the anhsrmonicity effect of 10 cm^{-1} (i.e. 2x80 cm^{-1} -150 cm^{-1} = 10 cm^{-1}) seems on the high side. Now the 204 cm^{-1} band can be assigned ss $2\tau_{CF_3} + \tau_{OCl}$ to give τ_{OCl} as 54 cm^{-1} (i.e. 204 cm^{-1}-150 cm^{-1}) for liquid CF_3OOCl. Again reducing the liquid phase torsion frequency by 10 percent to estimate the gas frequency gives 49 cm^{-1} which is surely too low due to some anharmoncity in the τ_{OCl} mode having made 204 cm^{-1} less than 150 cm^{-1} + τ_{OCl}. Thus, we choose 50 cm^{-1} as a reasonable estimate for the frequncy for τ_{OCl} in gaseous CF_3OOCl.

The polarization data are somewhat surprising for our assignement. Under C_s symmetry τ_{CF_3} and $2\tau_{CF_3} + \tau_{OCl}$ would be depolarized and $2\tau_{CF_3}$ would be polarized. Our uncertain polarization data make τ_{CF_3} and $2\tau_{CF_3} + \tau_{OCl}$ appear to be polarized while $2\tau_{CF_3}$ is only weakly polarized. Such a result is possible under the C_1 symmetry that CF_3OOCl possess: however, in CF_3OOF the reduction from C_s to C_1 symmetry still left both τ_{CF_3} and τ_{OF} so weakly polarized as to be indistinguishable from being depolarized. We would have expected similar behavior in CF_3OOCl; perhaps the larger angles of twist in the two CF_3OOCl conformers could be the cause of this unexpected result. In any case, we have another example of unexpected polarization behavior to add to those already noted in the CF_3 deformations and OCl stretch of CF_3OOCl and CF_3 deformations of CF_3OOF. For the assignements finally choosen, the potential energy distribution for the CF_3 torsion of CF_3OOCl shows the mode to be 82 percent pure with a 10 percent contribution from the OCl torsion and a 5 percent contribution from the OOCl bend. For the OCl torsion of CF_3OOCl, the potential energy distribution shows the mode to be 84 percent pure with a 12 percent contribution from the CF_3 torsion.

H. Discussion of Normal Coordinate Analysis

1. General Considerations

Our general philosphy of normal coordinate analysis is a chemical one rather than a mathematical one. We reject the view that vibrational analysis is a problem in applied mathematics with no necessary relationship between force constant values and the chemistry of the molecule and with the only objective being to fit the frequencies as closely as possible. Thus, we believe that the force constant values must be consistent with the chemistry of the molecule and that within a related series of molecules it should be a good approximation to transfer force constants for similar

groups.

In the work done at the University of Michigan, Dr. Marsden has used results from simple molecules Cl_2O (33), F_2O (34), F_2O_2 (35), H_2O_2 (36), CF_3H (37), and CF_4 (38) where extensive data are available to choose ranges of values for force constants that should be transferrable to the CF_3OX and CF_3OOX series. He then selected values within these ranges of values that do a reasonably good job of fitting the frequencies of all members of the series. The bond strengths implied by the chemical reactions of the series members were also taken into account. In our opinion the normal coordinate analysis should never be said to confirm an assignment. However, the results of the normal coordinate analysis can be extremely helpful in two ways. First, the result may suggest reasonable alternatives to the current assignments which merit further consideration. Second, the results may assist in reaching a reasonable conclusion when the observed data are somewhat contradictory. The decision made in Section G to assign one CF_3 rocking mode above 400 cm^{-1} is an example of the first. A number of examples of the second occurred in the discussion of CF_3 deformations in both CF_3OOF and CF_3OOCl and OCl stretching in CF_3OOCl in Section G.

Aside from the calculated frequencies, the most useful result from the normal coordinate analysis was the potential energy distribution. For a given choice of force constant values, each calculated frequency has a contribution from each type of force constant. For the CF_3OOX series members which have only C_1 symmetry, force constants for internal coordinates must be used. For higher symmetry than C_1 either internal coordinates or symmetry coordinates may be used. Although the CF_3OX series can be treated using symmetry coordinates under C_s symmetry, we used internal coordinates to facilitate comparison with the CF_3OOX series. A given type of force constant may correspond to only one internal coor-

dinate (such as OX stretching or OOX bending for example) or more than one internal coordinate (such as three CF stretchings or three α type FCF bendings for example). As can be seen in the F matrix in Table 7, in Section F there are diagonal force constants which appear in the diagonal or squared terms in the potential energy and off diagonal or interaction force constants which appear in off diagonal or cross terms in the potential energy. For each normal mode of vibration with its characteristic frequency, the potential energy has contributions from the diagonal force constants and the off diagonal or interaction force constants. The potential energy distribution for the calculated frequency for each normal mode of vibration is expressed by giving the fraction that the terms for each type of force constant contributes to the calculated frequency (39, 40). For diagonal force constants the fractions are all positive. For off diagonal or interaction force constants both positive and negative fractions occur. The sum of all the diagonal force constant fractions and all the off diagonal or interaction force constant fractions for each normal mode must be unity.

In making Tables 11 through 15, the fractions calculated in the VSEC and/or FPERT programs of Schachtschneider (19) have been multiplied by 100 to give percentages. For each calculated frequency in Tables 11 through 15, the sum of the entries shown plus other entries not shown (those of absolute values less than 5 percent) would be 100. The potential energy distributions in Tables 11 through 15 show whether a given frequency corresponds to localized motion of a small part of the molecule or a more delocalized motion involving many parts of the molecule. The reorganization of the information from Tables 11 through 14 into Table 15 shows for a given calculated frequency assigned to a given type of mode how similar or different the nature of the motion is across the CF_3OX and CF_3OOX series members. It is wise to remember that these potential energy dis-

tributions are determined by the numerical values used for the force constant and could be altered significantly by changing the force constant values.

2. Force Constant Values

Inspection of Table 9 in Section F shows that the pattern of force constants over the series is generally consistent with the idea of transferability of force constants for related groups and with the structures and chemical behavior of the compounds. The force constants expected to change over the CF_3OX and CF_3OOX series members are d, γ, τ_1, ld, lγ, dγ, R, δ, τ_2, Rd, dδ, and Rδ. All the other force constants have identical or nearly identical values for all series members. Among the off diagonal or interaction force constants expected to change, the results are generally reasonable. Thus, ld changes significantly in the CF_3OX series but not in the CF_3OOX series, lγ is non-zero only for CF_3OCl and CF_3OOCl, dγ is the same value for CF_3OF and CF_3OOH, D and a different equal value for CF_3OOF and CF_3OOCl. For Rd and Rδ, zero values for CF_3OOH, D and non zero values for CF_3OOF and CF_3OOCl are reasonable considering how far removed in frequency the OH stretching mode is from other modes. That dδ is the same in all CF_3OOX series members would not necessarily be expected but does not seem unreasonable. Our modification of Dr. Marsden's values for d and R in CF_3OOF leads to an Rd value similar to that in CF_3OOCl, a reasonable situation.

The values for the diagonal stretching force constants expected to change are of particular interest. For CF_3OF and CF_3OCl the decrease in d adopted by analogy to F_2O (34) and Cl_2O (33) is consistent with the greater stability of CF_3OF and consequent implication that the O-F bond in CF_3OF is stronger than the O-Cl bond in CF_3OCl (18). The frequency fit (Table 10 in Section F) is poorer for CF_3OCl and can only be greatly

improved by raising d to a higher and chemically unreasonable value (18). We reject such a change as contrary to our philosophy of normal coordinate analysis. For CF_3OOF, the values of d and R (and consequently of Rd) used by Dr. Marsden to get a reasonable fit were in apparent disagreement with his electron diffraction analysis and the chemistry of CF_3OOF. The bond lengths in Table 5 in Section D show that CF_3OOF has a shorter O_1-O_2 bond and a longer C-O_1 bond (Figure 7 in Section D) than CF_3OOH and CF_3OOCl. In addition CF_3OOF decomposes to CF_4 and O_2 at room temperature implying that the C-O_1 and C_2-F bonds are easily broken. Thus, one might expect l and d for CF_3OOF to be smaller and larger, respectively, than for CF_3OOH and CF_3OOCl. Also one might expect R in CF_3OOF to be significantly smaller than d in CF_3OF consistent with an easily broken OF bond in CF_3OOF and a less easily broken OF bond in CF_3OF. In using the FPERT program to search in l, d, R and Rd it became clear that d and R were strongly correlated and that to explore various combinations l, d, and R it would be necessary to fix Rd over a range of possible values and do a calculation at each fixed Rd value chosen. The Rd value 0.5 m dyne Å^{-1} was chosen as the best value from such calculations. For Rd and R at 0.5 and 3.0 m dyne Å^{-1} respectively, two combinations of l and d are included in Table 9 in addition to Dr. Marsden's values. The larger d value leads to a poorer fit with the frequency calculated for the OO stretching becoming too large. Since Dr. Marsden needed only approximate values of l, d, and R in CF_3OOF for use in analysis of his electron diffraction data, he probably did not want to take the time to look for other possible sets of force constants. The values of R for CF_3OOH and CF_3OOCl seem reasonable in comparison with OH groups in general and the OCl bond in CF_3OCl (Table 9 and reference (18)), Cl_2O (33) and Cl_2O_7 (22). Although Dr. Marsden's value of R=3.5

mdyne Å^{-1} for CF_3OOF is below 3.85 mdyne Å^{-1} for the OF bond in CF_3OF, as it should be, the new value of 3.0 mdyne Å^{-1} seems even more reasonable as it nearer to the OCl bond values in CF_3OCl and CF_3OOCl where the OCl bond is easily broken.

The diagonal force constants for bending are also of some interest. The γ values might be expected to change from CF_3OF to CF_3OCl and the small change seems reasonable. For the CF_3OOX series γ might be expected to change or remain about the same so equal values for CF_3OOH and CF_3OOF and a little smaller value for CF_3OOCl seems reasonable. For the CF_3OOX series δ might be expected to change and CF_3OOH having a different value from CF_3OOF and CF_3OOCl seems reasonable. The fact that δ for CF_3OOCl is only a little smaller than for CF_3OOF is not surprising and seems analogous to γ for CF_3OCl being somewhat smaller than for CF_3OF.

The diagonal force constants for torsion are of great interest. For the CF_3 torsion in CF_3OF and CF_3OCl the nearly equal values seem reasonable. In fact the two values could be equal since we have no data for the gas phase frequency for CF_3OCl and have estimated it from the liquid Raman frequency by assuming the same percentage change of frequency with phase as found for CF_3OF (18). In the CF_3OOX series, the pattern of $C\text{-}O_1$, and $O_1\text{-}O_2$ bond lengths (Table 5 and Figure 7 in Section D) are assumed to be related to the CF_3 (or $C\text{-}O_1$) and OX (or $O_1\text{-}O_2$) torsional barriers and frequencies. For CF_3OOH the torsions are measured directly in the gas phase. For CF_3OOF the OF torsion can be located approximately in the gas phase Raman spectrum in spite of interference from the rotational Raman spectrum of O_2 from the decomposition of CF_3OOF; however, the CF_3 torsion must be estimated from the liquid Raman frequency. For CF_3OOCl no gas phase spectra could be obtained and only one liquid Raman band reasonably

assigned to a torsional fundamental was found. The assignment of the band extrapolated to 72 cm^{-1} in the gas from 80 cm^{-1} in the liquid as a CF_3 torsion rather than an OCl torsion, as described in Section G, was based on using the τ_1 values of CF_3OOH and CF_3OOF as the limits for the τ_1 range expected for CF_3OOCl. Then, as described in Section G, a proposed combination band was used to estimate the liquid Raman frequency for the OCl torsion and then extrapolation to the gas phase gave ~50 cm^{-1}.

Table 16 contains a summary of some bond lengths, force constants, and torsional frequencies and barriers. The length of the C-O bond seems to correlate with the τ_1 value for CF_3OF, CF_3OOH, and CF_3OOF; however, the τ_1 value for CF_3OOCl is then unexpectedly small, but does at least fall between the values for CF_3OOH and CF_3OOF. The assignment discussed in Section G, of the liquid phase Raman bond at 80 cm^{-1} that lead to the estimate of 72 cm^{-1} for τ_{CF_3} and τ_1 = 0.013 mdyne Å $rad.^{-2}$ in the gas phase relied on the assumption that τ_1 for CF_3OOCl would be between the τ_1 values for CF_3OOH and CF_3OOF. For CF_3OCl where the assignment of the CF_3 torsion at 122 cm^{-1} in the liquid Raman spectrum seems certain (18), extrapolation to 108 cm^{-1} in the gas gives τ_1 = 0.016 mdyne Å $rad.^{-2}$ in better agreement with τ_1 = 0.013 mdyne Å $rad.^{-2}$ for CF_3OOCl. Since the τ_{CF_3} frequencies and τ_1 value for CF_3OOCl are based on the least satisfactory experimental data in the CF_3OOX series, it is not possible to be sure whether the C-O bond length correlates roughly with τ_1 in the CF_3OOX series or not. The length of the O_1-O_2 bond does seem to show a rough correlation with the τ_2 values over the CF_3OOX series with the much shorter bond in CF_3OOF corresponding to a much larger τ_2 value. As was the case in the comparison of τ_1 with the C-O_1 bond length, CF_3OOH and CF_3OOCl have identical O_1-O_2 bond lengths but somewhat different τ_2 values. It is

Table 16: Some Bond Lengths, Force Constants, Torsional Frequencies[a] and Barriers[b]

	CF_3OF	CF_3OCl	CF_3OOH	CF_3OOF	CF_3OOCl
$r(C-O_1)$	1.395	-	1.376	1.419	1.372
1	5.2	5.2	5.3	5.2, 5.0	5.3
τ_1	0.017	0.016	0.021	0.010	0.013
τ_{CF_3}	127.	(108)	142.	(70)	(72)
V_3	4.8	4.6	6.0	2.9	3.7
$r(O_1-O_2)$	-	-	1.447	1.366	1.447
d	-	-	3.35	3.6, 3.8	3.35
τ_2	-	-	0.035	0.23	0.05
τ_{OX}	-	-	244.	132.	(50)
V_2	-	-	2.5	17.	3.6
$r(O_2-X)$	1.421	-	0.974	1.449	1.699
R(d)	3.85	2.80	7.15	3.0	2.77
Rd(ld)	1.00	0.30	0.0	0.5	0.6

Units: $r(C-O_1)$, $r(O_1-O_2)$ Å; 1,d,R,md/Å; τ_1 and τ_2, mdÅ/rad^2; Rd, ld,md/rad; τ_{CF_3} and τ_{OX}, cm^{-1}; V_3 and V_2 kcal/mole rad^2

a. Frequencies in parentheses are estimated from Raman spectra of liquids and other frequencies are from I.R. or Raman spectra of gases.

b. The calculation of torsional barriers from torsional force constants is discussed in Appendix B. The derivation given there assumes that the torsional mode is 100 percent pure. Consequently, the values for V_3 and V_2 in this table which are obtained from the equations in Appendix B are only an approximation.

interesting to note that CF_3OOCl has a τ_1 value that is about 40 percent lower than τ_1 for CF_3OOH and a τ_2 value that is about 40 percent higher than τ_2 for CF_3OOH. The results in Table 16 do tend to suggest a rough correlation of torsional force constant with the length of the bond about which torsion takes place. However, the lack of really satisfactory Raman data for CF_3OOCl does not allow this correlation of bond length and torsional force constant to be confirmed or denied. The values of the three fold barrier for CF_3 torsion are all in the reasonable range of about 3.0 to 6.0 kcal $mole^{-1}$ rad^{-2}. Durig and Wertz (41) report 5.4 kcal $mole^{-1}$ rad^{-2} as the upper limit to V_3 for the CF_3 torsion in bis (trifluoromethyl) peroxide, CF_3OOCF_3. The values of the assumed two fold barrier for OX torsion are also reasonable. Thus, CF_3OOH and CF_3OOCl should have equal τ_2 values and consequently equal V_2 values if these quantities are correlated with the O_1-O_2 bond length; however, the values 2.5 and 3.6 kcal $mole^{-1}$ rad^{-2}, respectively, are not too different in absolute value. The large value of 17 kcal $mole^{-1}$ rad^{-2} for V_2 in CF_3OOF is consistent with the short O_1-O_2 bond in CF_3OOF and the view that while CF_3OOF had some of the character of O_2F_2 it is more like H_2O_2 or CF_3OOH than like O_2F_2 (14).

3. Potential Energy Distribution

The potential energy distribution reported in Tables 11 through 14 and resummarized in Table 15 in Section F have been referenced extensively in the discussion of assignments in Section G. Careful inspection of either Table 15 alone or Tables 11 through 14 together leads to a number of generalizations. For the two CF_3OX compounds four modes differ significantly in potential energy distribution: the lowest frequency CF stretch (which is really a mixture of CO and OF stretching), the OX stretch, the COX bend, and the lower frequency CF_3 rock. As might be expected due to

the increased complexity and lowered symmetry of their structures, the CF_3OOX series presents a more complex picture. Thus, for the CF_3OOX compounds the six modes that differ significantly in potential energy distribution over the series are: the OX stretch, the intermediate frequency CF_3 deformation, the higher frequency CF_3 rock, the OOX bend, the lower frequency CF_3 rock and OX torsion (and the O-O stretch for CF_3OOF if Dr. Marsden's force constant values are used).

One reason for these potential energy distribution differences is the low masses of the H and D atoms. The OOX bend in CF_3OOH and CF_3OOD is a pure mode while in CF_3OOF and CF_3OOCl both the β type angles (FCO) and the δ type angle (OOX) are major contributors. The OH torsion in CF_3OOH is at sufficiently high frequency to mix with the lower frequency CF_3 rock causing significant differences in the potential energy distributions across the CF_3OOX series for both the lower frequency CF_3 rock and the OX torsion. For the OX stretch CF_3OOCl has only a 68 percent contribution from stretching the O-Cl bond while CF_3OOH, CF_3OOD, and CF_3OOF (with our revised force constant values) have 95 to 100 percent contributions from stretching the O-X bond. This behavior is consistent with (but not necessarily the explanation of) the unexpectedly low Raman intensity and high depolarization ratio for the band assigned to the OX stretch at 696 cm^{-1} in the Raman spectrum of liquid CF_3OOCl. The intermediate frequency CF_3 deformation for CF_3OOF differes greatly in potential energy distribution from those of CF_3OOH, CF_3OOD and CF_3OOCl which are very similar. This behavior is consistent with (but not necessarily the explanation of) the unexpectedly high Raman intensity and low depolarization ratio for the band at 628 cm^{-1} in the Raman spectrum of liquid CF_3OOF. The higher frequency CF_3 rock for CF_3OOF and CF_3OOCl have very

different potential energy distributions both of which are quite different from the similar ones of CF_3OOH and CF_3OOD (and CF_3OF and CF_3OCl as well). This behavior is consistent with (but not necessarily the explanation for) the bands at 514 cm^{-1} and 478 cm^{-1} (gas phase infrared frequencies) for CF_3OOF and CF_3OOCl, respectively, having unexpectedly high infrared and Raman intensities and low depolarization ratios.

Inspection of the potential energy distributions in Table 15 alone or in Tables 11 through 14 together allows comparison among pairs of molecules. As expected CF_3OOH and CF_3OOD have almost identical potential energy distributions for all modes except the lower frequency CF_3 rock and the OX torsion where the coupling is much larger for H than for D due to the mass induced frequency difference in the OX torsion. For the ten CF_3O modes common to both CF_3OX and CF_3OOX, the isoelectronic and nearly constant mass series CF_3OF, CF_3OOH, and CF_3OOD has very similar potential energy distributions except for the lower frequency CF_3 rock where CF_3OOH differs from the other two due to extensive coupling with the OH torsion. For the ten CF_3O modes common to both CF_3OX and CF_3OOX, the isoelectronic and constant mass CF_3OCl and CF_3OOF pair have somewhat similar potential energy distributions with the exception of the following: the intermediate frequency CF_3 deformation, the higher frequency CF_3 rock, and the lower frequency CF_3 rock. These comparisons are consistent with CF_3OF having been of greater assistance in assigning CF_3OOH and CF_3OOD than was CF_3OCl in assigning CF_3OOF.

For twelve CF_3OO modes common to all CF_3OOX series members, the following results occur for various pairs. For the CF_3OOD and CF_3OOF pair the modes which fail to have somewhat similar potential energy distributions are: the intermediate frequency CF_3 deformation and the higher frequency

CF_3 rock. For the CF_3OOD and CF_3OOCl pair only the higher frequency CF_3 rock fails to have a somewhat similar potential energy distribution. For the CF_3OOF and CF_3OOCl pair the modes which fail to have somewhat similar potential energy distributions are: the intermediate frequency CF_3 deformation and the higher frequency CF_3 rock. In this paragraph CF_3OOD was used rather than CF_3OOH to eliminate the complication of coupling of the lower frequency CF_3 rock with the OH torsion. If CF_3OOH had been used then the lower frequency CF_3 rock would be added to the failures to have similar potential energy distributions. Also comparisons with CF_3OOF were for the potential energy distributions for our two sets of force constant values. Inclusion of Dr. Mardsen's values would add the OO stretch to the list of failures to have similar potential energy distributions. The considerations in this paragraph are restricted to the twelve CF_3OO modes common to the CF_3OOX series and do not include the OX stretch, OOX bend, and OX torsion. The cases of failure to have similar potential energy distributions in the comparison of pairs in this paragraph are all cases where unexpected Raman intensities and depolarization ratios occured: the intermediate frequency CF_3 deformation in CF_3OOF and the higher frequency CF_3 rock in both CF_3OOF and CF_3OOCl. To balance the record and to avoid concluding that all the usual intensity results have their explanation in the potential energy distribution it should be remembered that there are cases of unexpected intensity behavior where the potential energy distributions are similar to those in cases of normal intensity. Examples of this are the highest and lowest frequency CF_3 deformations in CF_3OOF and the lowest frequency CF_3 deformation in CF_3OOCl.

A very useful method of classifying fundamental modes by their potential energy distributions has been suggested by Fuhrer, Kartha, Kidd, Krueger

and Mantsch (40). Groups frequencies have a 66 percent or more contribution to the calculated frequency in one diagonal force constant. Zone frequencies have a 66 percent or more contribution to the calculated frequency in the sum of two diagonal force constants. Delocalized frequencies have a 33 percent or less contribution to the calculated frequency in any one diagonal force constant. Table 17 contains an assignment of the fundamentals of CF_3OX and CF_3OOX to the three types of group, zone, and delocalized frequencies. The fundamentals modes are listed in Table 17 in order of decreasing frequency with the exception of the OX stretch and OOX bend for CF_3OOH and CF_3OOD and the CF_3 torsion for CF_3OOCl. Table 17 is a very compact and convenient summary of the general nature of the potential energy distribution at the expense of the quantitative detail shown in Table 15.

Five of the fundamental modes are group frequencies in all compounds as follows: the higher and intermediate CF stretches, the OO stretch, the lowest frequency CF_3 deformation, and the CF_3 torsion. In these cases the name used to describe the mode is satisfactory in the sense that the large contributor is the diagonal force constant for the internal coordinate used to define the symmetry coordinate corresponding to the name (see Table 6, Section D). For the OX stretch and the OX torsion, the mode is a group frequency in all cases but one to two. The OCl stretch in CF_3OCl is a zone frequency due to mixing with the COCl bend and the OH torsion in CF_3OOH is a zone frequency due to mixing with the lower frequency CF_3 rock. For all compounds, OX stretch and OX torsion are satisfactory names in the sense that the large contributor is the diagonal force constant for the internal coordinate used to define the symmetry coordinate corresponding to the name (see Table 6, Section D). The higher frequency CF_3 rock is a

Table 17. Assignement of Fundamentals of CF_3OX and CF_3OOX Molecules to Frequency Types of Reference (40): G, Group Frequency, Z Zone Frequency, D, Delocalized Frequency[a]

Numbers[b]		Symbol[c]	CF_3OF	CF_3OCl	CF_3OOH	CF_3OOD	CF_3OOF	CF_3OOCl
1	1	$a.\nu_{CF_3}$	G	G	G	G	G	G
9	11	$a.\nu_{CF_3}$	G	G	G	G	G	G
2	2	$s.\nu_{CF_3}$	Z	G	Z	Z	Z	Z
3	3	ν_{CO}	Z[d]	Z	Z	Z	Z	Z
	4	ν_{OO}	-	-	G	G	G[e]	G
4	5	ν_{OX}	G	Z	G	G	G	G
5	6	$s.\delta_{CF_3}$	D	D	D	D	D	D
10	12	$a.\delta_{CF_3}$	Z	G	Z	G	Z[f]	G
6	7	$a.\delta_{CF_3}$	G	G	G	G	G	G
11	13	ρ_{CF_3}	G	G	G	G	Z	D
	9	δ_{COO}	-	-	Z	Z	Z	Z
8	10	δ_{OOX}	Z	Z	G	G	Z	Z
7	8	ρ_{CF_3}	Z	Z	Z	Z	G	G
	14	τ_{OX}	-	-	Z	G	G	G
12	15	τ_{CF_3}	G	G	G	G	G	G

a. The fundamental modes of vibration are classified according to the form of the potential energy distribution as follows. Group frequencies, G, have $\geq$ 66 percent in one diagonal foce constant. Zone frequencies, Z, have $\geq$ 66 percent in the sum of two diagonal force constants. Delocalized frequencies, D, have $\leq$ 33 percent in any one diagonal force constant.

b. These numbers are from Table 6 in Section D. The numbers on the left refer to the CF_3OX series and the numbers on the right refer to the CF_3OOX series. The fundamentals are listed in this table in the same order as in Table 15 which is the order of decreasing frequency for all but the OX stretch and OOX bend for CF_3OOH and CF_3OOD and the CF_3 torsion for CF_3OOCl.

Table 17 continued:

c. These symbols are a combination of the symbols and descriptions from Table 6 in Section D. For the CF_3OX series δ_{OOX} becomes δ_{COX}.

d. For CF_3OF the mode observed at 947 cm^{-1} and calculated to be at 941 cm^{-1} is not really a zone frequency since the sum of two diagonal force constants is only 62 percent. However, it is not a delocalized frequency either since the r diagonal force constant is 54 percent. We have chosen to list it as a zone frequency.

e. For Dr. Marsden's force constant values the mode observed at 874 cm^{-1} for CF_3OOF is a zone frequency but for our two sets of force constants this mode is a group frequency and is so listed in this table.

f. For CF_3OOF the mode observed at 630 cm^{-1} and calculated to be at 631 cm^{-1} is not really a zone frequency since the sum of two diagonal force constants is only 59 or 60 percent. However it is not a delocalized frequency either since the α diagonal force constant is 35 percent. We have chosen to list it as a zone frequency.

group frequency for CF_3OF, CF_3OCl, CF_3OOH, and CF_3OOD but changea to a zone frequency for CF_3OOF and a delocalized frequency for CF_3OOCl. This behsvior is consistent with (but not necessarily the explanation of) this mode having unexpectedly high infrared snd Raman intensities and low depolsrization ratios in CF_3OOF and CF_3OOCl. For CF_3OF, CF_3OCl, CF_3OOH, snd CF_3OOD but not for CF_3OOF and CF_3OOCl, the name is satisfactory in the sense that the large contributor is the diagonal force constant for the internal coordinate used to define the symmetry coordinate corresponding to the name (see Table 6, Section D). The intermediate frequency CF_3 deformation is s group frequency for CF_3OCl, CF_3OOD, and CF_3OOCl snd a zone frequency for CF_3OF, CF_3OOH, snd CF_3OOF. However, for CF_3OF snd CF_3OOH the mode is a zone frequency rather than a group frequency by only 1 percent. Then only CF_3OOF is far from a group frequency and the other five compounds are on the border between groups and zone frequencies. For CF_3OF, CF_3OCl, CF_3OOH, CF_3OOD snd CF_3OOCl but not CF_3OOF the name CF_3 deformation is sstisfactory in the sense thst the large contributor is the diagonal force constant for the internal coordinate used to define the symmetry coordinate corresponding to the nsme (aee Table 6, Section D).

Only the CO stretch and the COO bend fundamental modes are zone frequencies in all compounds. However, the lowest frequency CF_3 stretch, the OOX bend (COX bend for CF_3OX) and the lower frequency CF_3 rock sre zone frequencies for four or five of the compounds. The CO stretch is not s satisfsctory name becsuse the major contributor to the calculated frequency is the CF stretch force constant, so this mode is a CF stretch zone frequency snd there is no fundamental that is a CO stretch group frequency. In the COO bend, the force constants for changing the FCF snd FCO angles are lsrger contributors than the COO angle change so there is no fundamental

that is a COO bend group frequency. In the lowest frequency CF_3 stretch, the force constant for CO stretching is a somewhat larger contributor than the CF force constant but only for CF_3OCl is the difference large enough to qualify as a CO stretch group frequency. For the rest of the compounds, the lowest frequency CF_3 stretch is best viewed as a zone frequency for combined CO and CF stretching. The OOX bend is a zone frequency except for CF_3OOH and CF_3OOD where it is a group frequency due to its high frequency caused by the low H and D masses. In CF_3OF, CF_3OCl, CF_3OOF, and CF_3OOCl, the force constant for COX or OOX bending is second or lower in importance so the name OOX bend is satisfactory only in CF_3OOH and CF_3OOD. The lower frequency CF_3 rock is a zone frequency in CF_3OF, CF_3OCl, CF_3OOH, and CF_3OOD and a group frequency in CF_3OOF and CF_3OOCl. It is only a few percent short of a group frequency in CF_3OF and CF_3OOD. In CF_3OCl and CF_3OOH mixing with the COCl bend and OH torsion, respectively, prevent a group frequency. Except for CF_3OCl the name CF_3 rock is satisfactory in the sense that the large contributor is the force constant for the internal coordinate used to define the symmetry coordinate corresponding to the name (see Table 6, Section D).

The only fundamental mode that is a delocalized frequency for all compounds is the highest frequency CF_3 deformation. The name for this mode is not satisfactory in the sense that force constants for changes in the FCF and FCO angles are not the dominant contributors to the calculated frequency in each case. The only other delocalized frequency is the higher frequency CF_3 rock for CF_3OOCl. It is somewhat surprising that there are not more delocslized frequencies in view of the similar masses of all the atoms (except H and D) and similar values of some of the force constants.

The discussion of Table 17 (supplemented by Table 15) presented in

the last four paragraphs is summarized in Table 18. There a more accurate, new descriptive name is proposed for each fundamental mode based on the combined information from Tables 15 and 17. These new names in Table 18 may be compared to the descriptions of symmetry coordinates given in Table 6, Section D. Inspection of Tables 6 and 18 shows that for all the compounds the following four descriptions from Table 6 are so inappropriate that they have had to be completely replaced: rather than modified: symmetric CF_3 stretch, CO stretch, symmetric CF_3 deformation, and COO bend.

Table 18. New Descriptive Names of Fundamentals of CF_3OX and CF_3OOX Molecules. The Symbols G, Z and D refer to the Group, Zone and Delocalized Frequencies Defined in Table 17.

Number[a]		Symbol[b]	New Descriptive Name
1	1	a. ν_{CF_3}	G frequency for CF stretch
9	11	a. ν_{CF_3}	G frequency for CF stretch
2	2	s. ν_{CF_3}	Z frequency for combined CO and CF stretch (except G frequency for CO stretch in CF_3OCl)
3	3	ν_{CO}	Z frequency for CF stretch
	4	ν_{OO}	G frequency for OO stretch
4	5	ν_{OX}	G frequency for OX stretch (except Z frequency for OCl stretch in CF_3OCl)
5	6	s. δ_{CF_3}	D frequency for combined FCF, COO(COX), and FCO bend and some stretches
10	12	a. δ_{CF_3}	G/Z border line frequency for CF_3 deformation (FCF bend) for CF_3OCl, CF_3OOD, CF_3OOCl on G side and for CF_3OF and CF_3OOH on Z side by 1 percent; Z frequency for combined FCF, FCO and OOF bend for CF_3OOF.
6	7	a. δ_{CF_3}	G frequency for CF_3 deformation (FCF bend)
11	13	ρ_{CF_3}	G frequency for CF_3 rock (FCO bend) for CF_3OF, CF_3OCl, CF_3OOH, CF_3OOD; Z frequency for combined FCF and OOF bend for CF_3OOF; D frequency for combined FCF, OOCl, FCO bend for CF_3OOCl
	9	δ_{COO}	Z frequency for combined FCO, FCF, and COO bend
8	10	δ_{OOX}	Z frequency for combined FCF, FCO, and COF bend for CF_3OF, combined FCO and FCF bend and OCl stretch for CF_3OCl, combined FCO and OOX bend for CF_3OOF and CF_3OOCl; G frequency for OOX bend for CF_3OOH and CF_3OOD
7	8	ρ_{CF_3}	Z frequency for combined FCO and COX bend for CF_3OX, combined FCO and COO bend and OH torsion for CF_3OOH, combined FCO and

Table 18 continued:

Number[a]		Symbol[b]	New Descriptive Name
			and COO bend for CF_3OOD; G frequency for CF_3 rock (FCO bend) for CF_3OOF and CF_3OOCl
	14	τ_{OX}	G frequency for OX torsion for CF_3OOD, CF_3OOF and CF_3OOCl; Z frequency for combined OH torsion, FCO and COO bend for CF_3OOH
12	15	τ_{CF_3}	G frequency for CF_3 torsion

a. See Table 17 and Table 6, Section D. The numbers on the left refer to the CF_3OX series and the numbers on the right refer to the CF_3OOX series.

b. See Table 17 and Table 6, Section D. These symbols are a combination of the symbols and descriptions from Table 6. For the CF_3OX series δ_{OOX} becomes δ_{COX}.

Appendix A

Gas Phase Infrared Spectra of CF_3OX and CF_3OOX Compounds

This appendix contains six figures showing the gas phase infrared spectra of CF_3OX and CF_3OOX compounds recorded by Dr. D.D. DesMarteau and Dr. R.M. Hammaker using the Perkin Elmer Model 180 infrared spectrophotometer. These figures may be of interest while reading Section G on discussion of assignments. All spectra shown were recorded on IX scale expansion and the gas pressure used is shown. The infrared spectra from 4000 to 350 cm^{-1} were recorded using a 10 cm path length cell with AgCl windows. The infrared spectra from 650 to 160 cm^{-1} were recorded using a 15 cm path length cell with polyethylene windows.

The collections of compounds and spectral ranges for the aix figures are as follows:

1. Figure A-1... All compounds from 1400 to 1100 cm^{-1}.
2. Figure A-2... CF_3OOH, CF_3OOD, CF_3OF from 1000 to 500 cm^{-1}.
3. Figure A-3... CF_3OOCl, and CF_3OOF from 1000 to 500 cm^{-1}.
4. Figure A-4... CF_3OCl, CF_3OOH, and CF_3OOF from 1000 to 500 cm^{-1}.
5. Figure A-5... CF_3OF, CF_3OOH, and CF_3OOD from 650 to 160 cm^{-1}.
6. Figure A-6... CF_3OCl, CF_3OOF, and CF_3OOCl from 650 to 160 cm^{-1}.

All spectra were recorded with linear percent transmittance as the ordinate and linear frequency in cm^{-1} aa the abscissa.

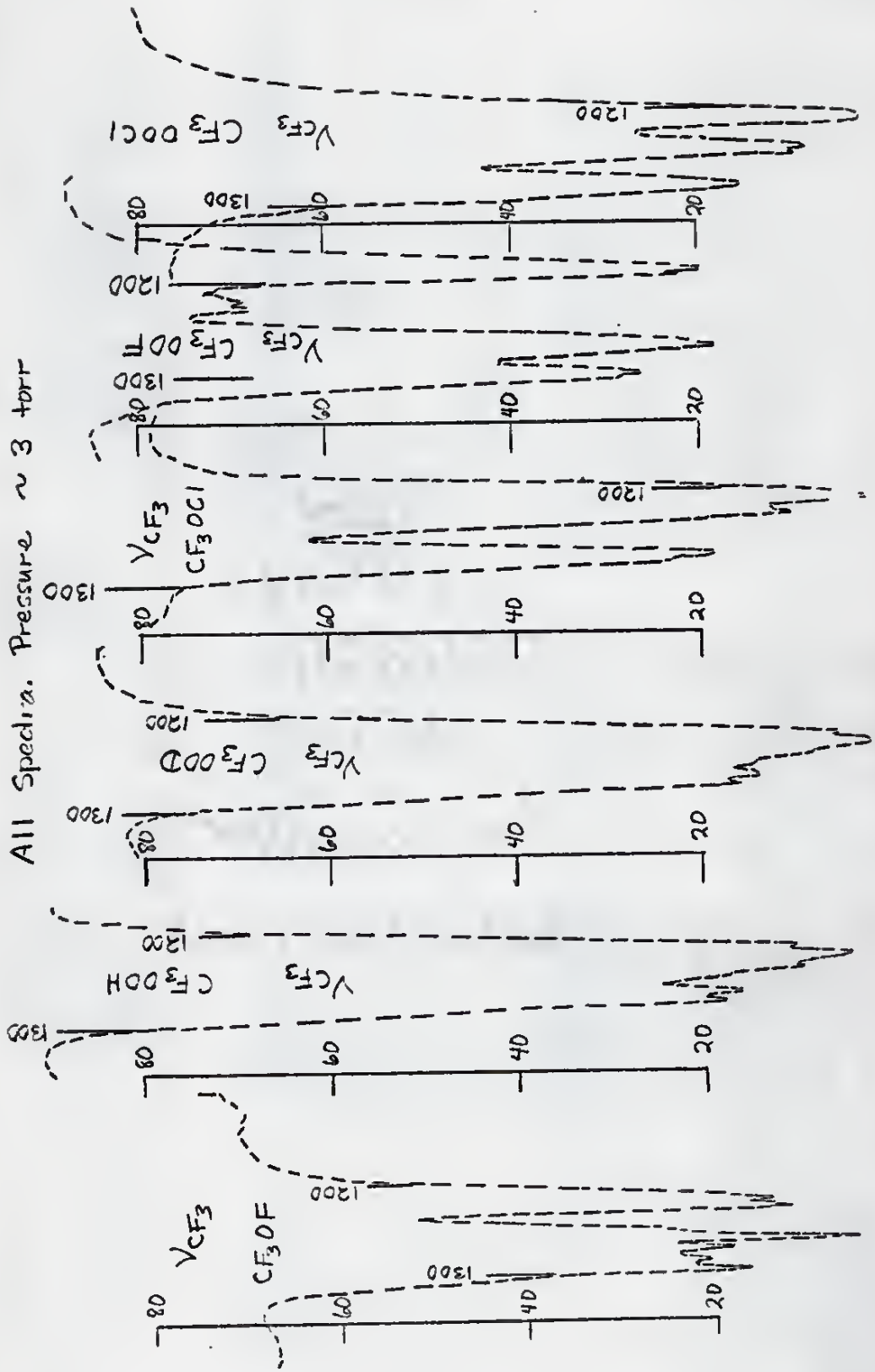
All Spectra. Pressure ~ 3 torr
ν_{CF_3} CF_3OH
ν_{CF_3} CF_3OD
ν_{CF_3} CF_3OCl
ν_{CF_3} CF_3OBr
ν_{CF_3} CF_3OF
1300
1200
80
60
40
20

Figure A-1

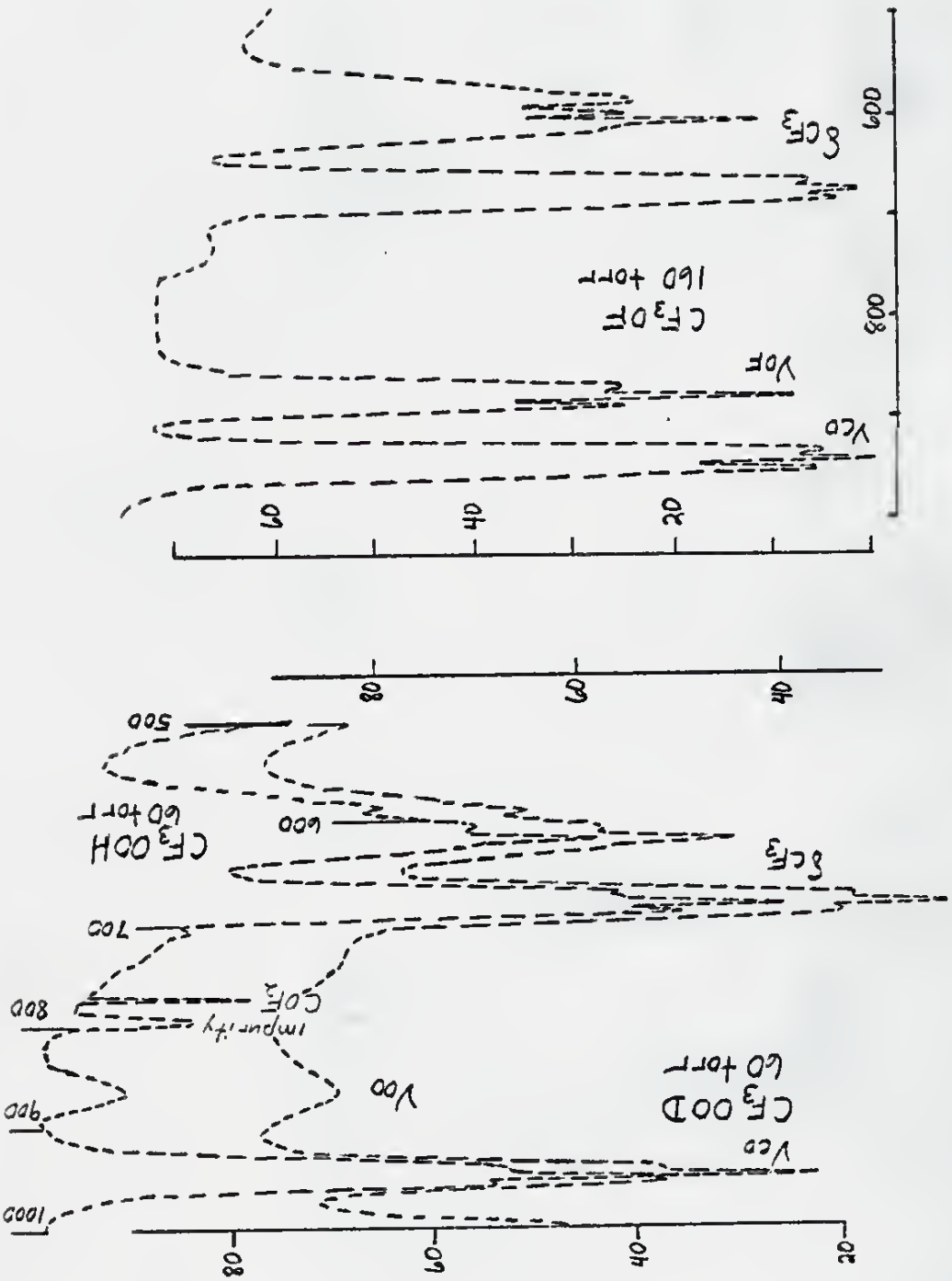
CF3OOD
60 torr
νCO
νOO
impurity
COF2
δCF3
CF3OOH
60 torr
νCO
νOF
CF3OF
160 torr
δCF3

Figure A-2

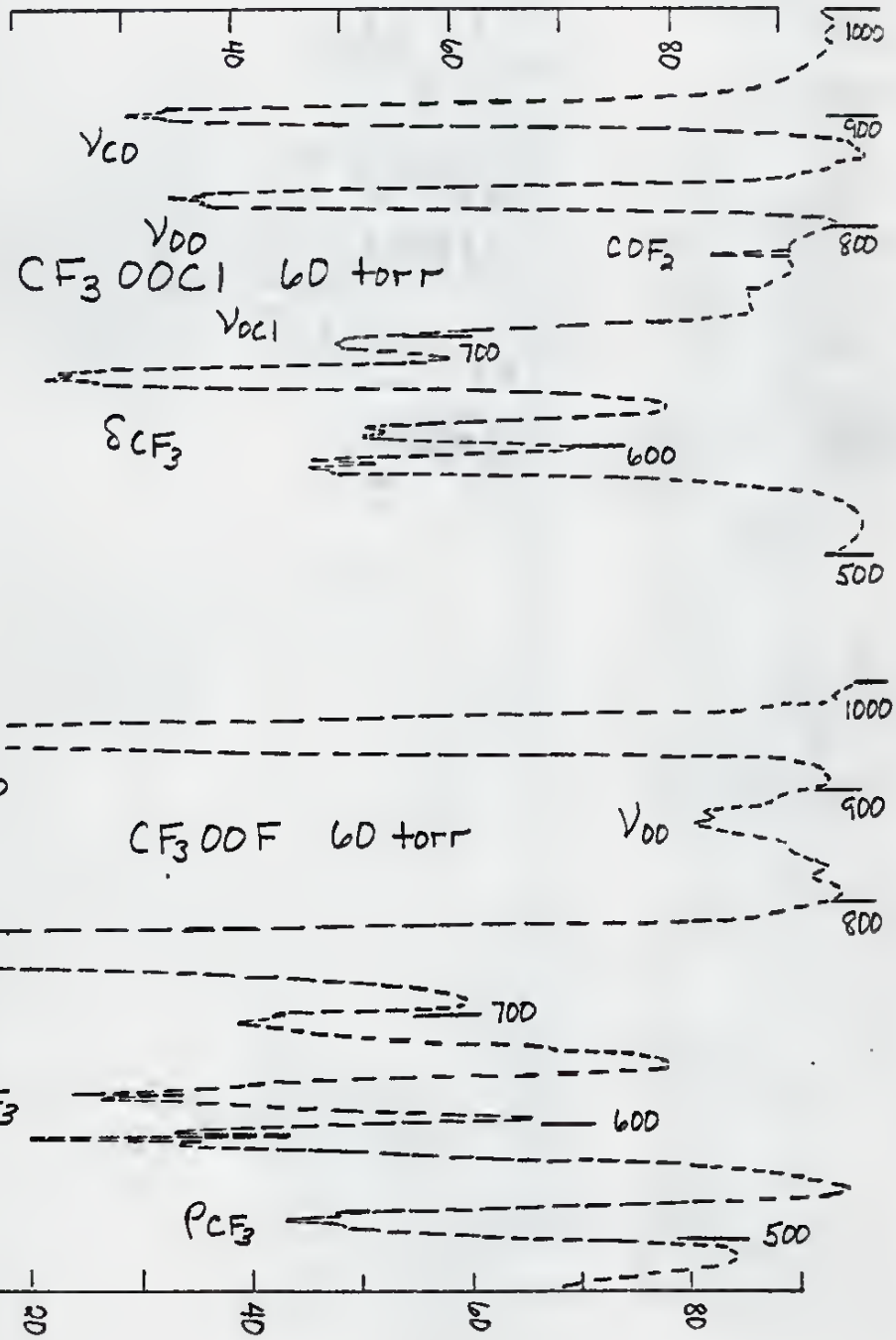
40
60
80
1000
900
800
700
600
500
ν_{CO}
ν_{OO}
CF_3OOCl 60 torr
COF_2
ν_{OCl}
δCF_3
CF_3OOF 60 torr
ν_{OO}
ν_{OF}
ρCF_3
20
40
60
80

Figure A-3

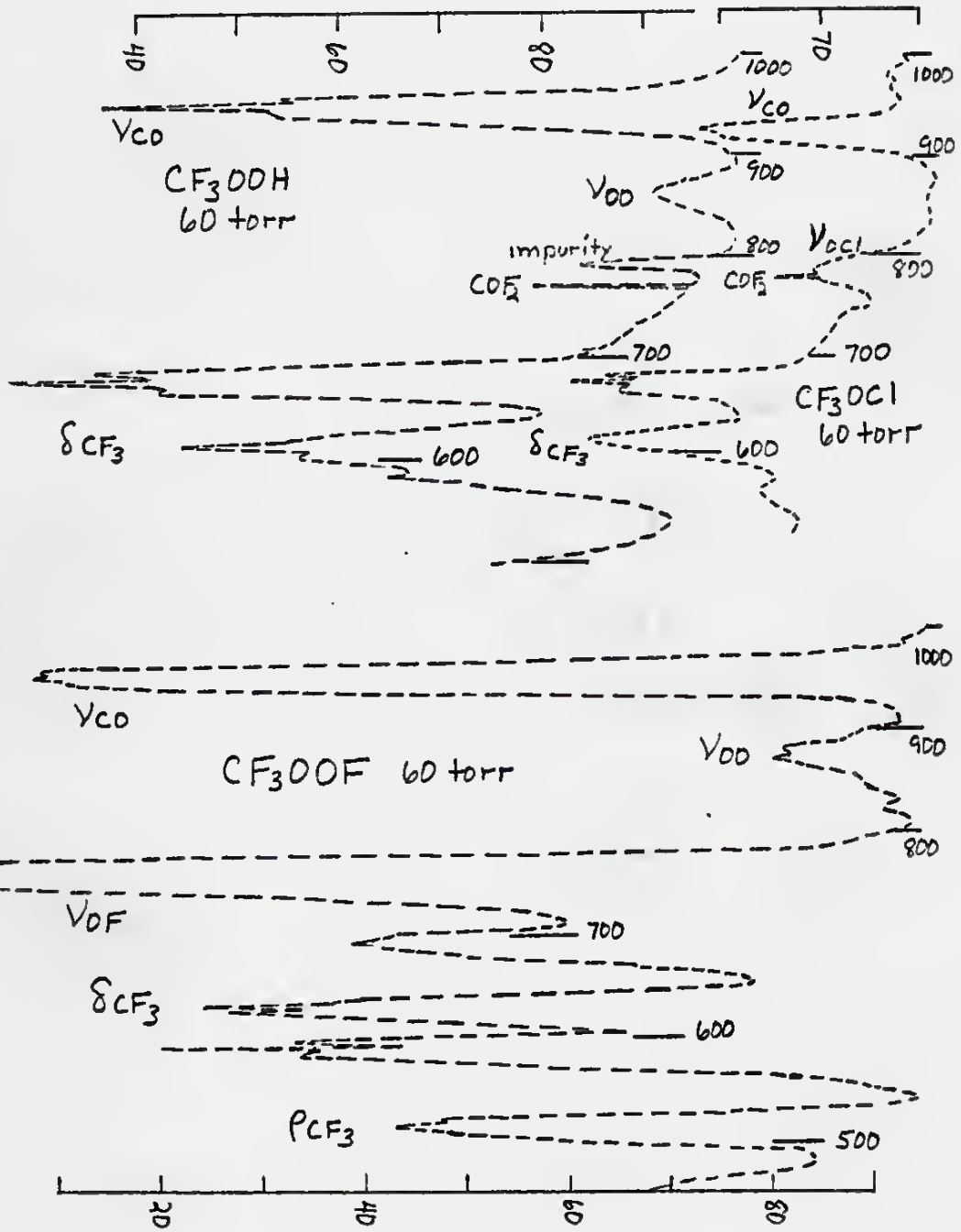
40
60
80
70
1000
1000
ν_{CO}
ν_{CO}
900
900
CF_3OOH
60 torr
ν_{OD}
impurity
800
ν_{OCl}
800
COF_2
COF_2
700
700
CF_3OCl
60 torr
δCF_3
600
δCF_3
600
1000
ν_{CO}
900
ν_{OD}
CF_3OOF 60 torr
800
ν_{OF}
700
δCF_3
600
ρCF_3
500
20
40
60
80

Figure A-4

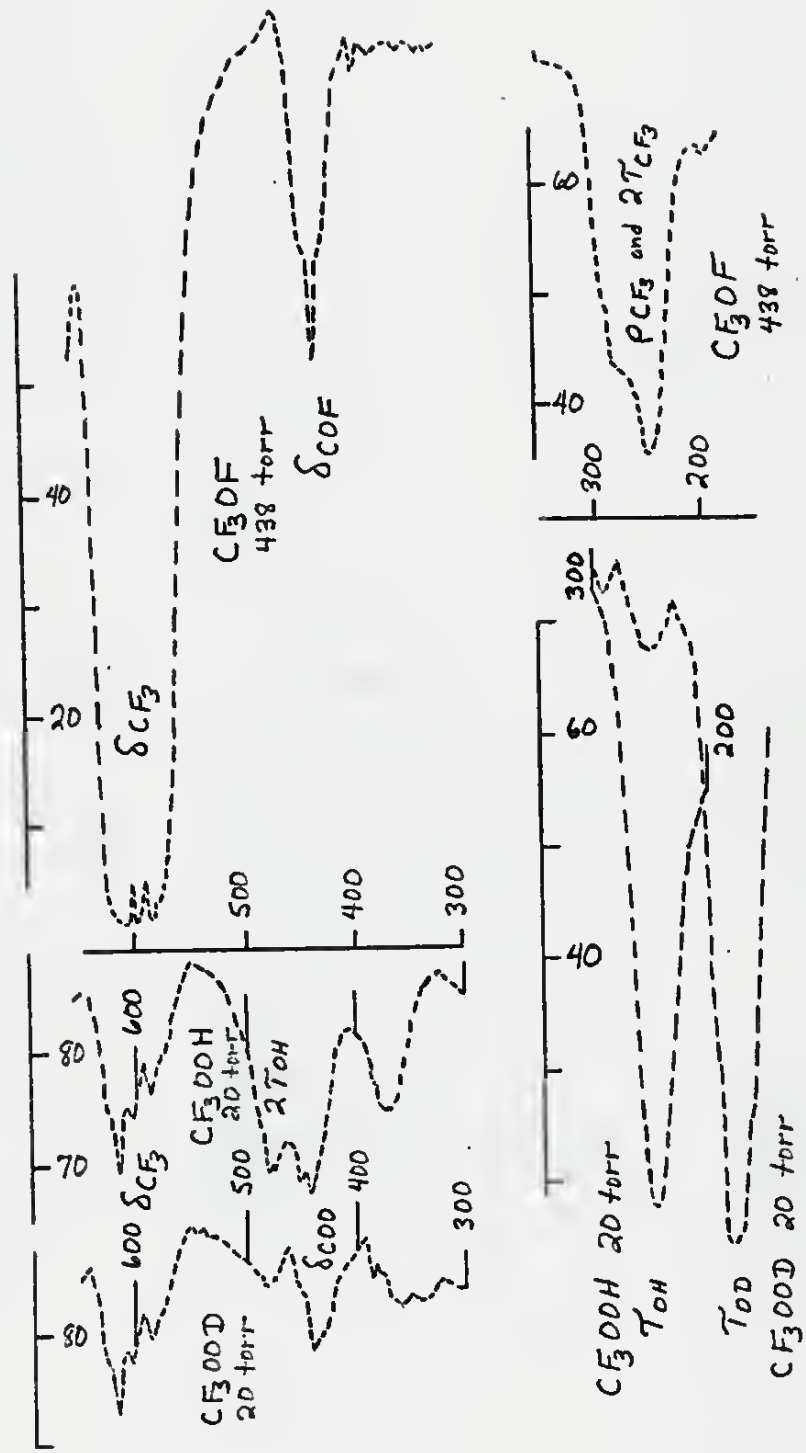
CF3OF
438 torr
δCF3
δCOF
500
400
300
40
20
CF3OOH
20 torr
2τOH
δCOO
CF3OOD
20 torr
80
70
600
τOH
τOD
CF3OOD 20 torr
CF3OOH 20 torr
60
200
PCF3 and 2τCF3
CF3OF
438 torr

Figure A-5

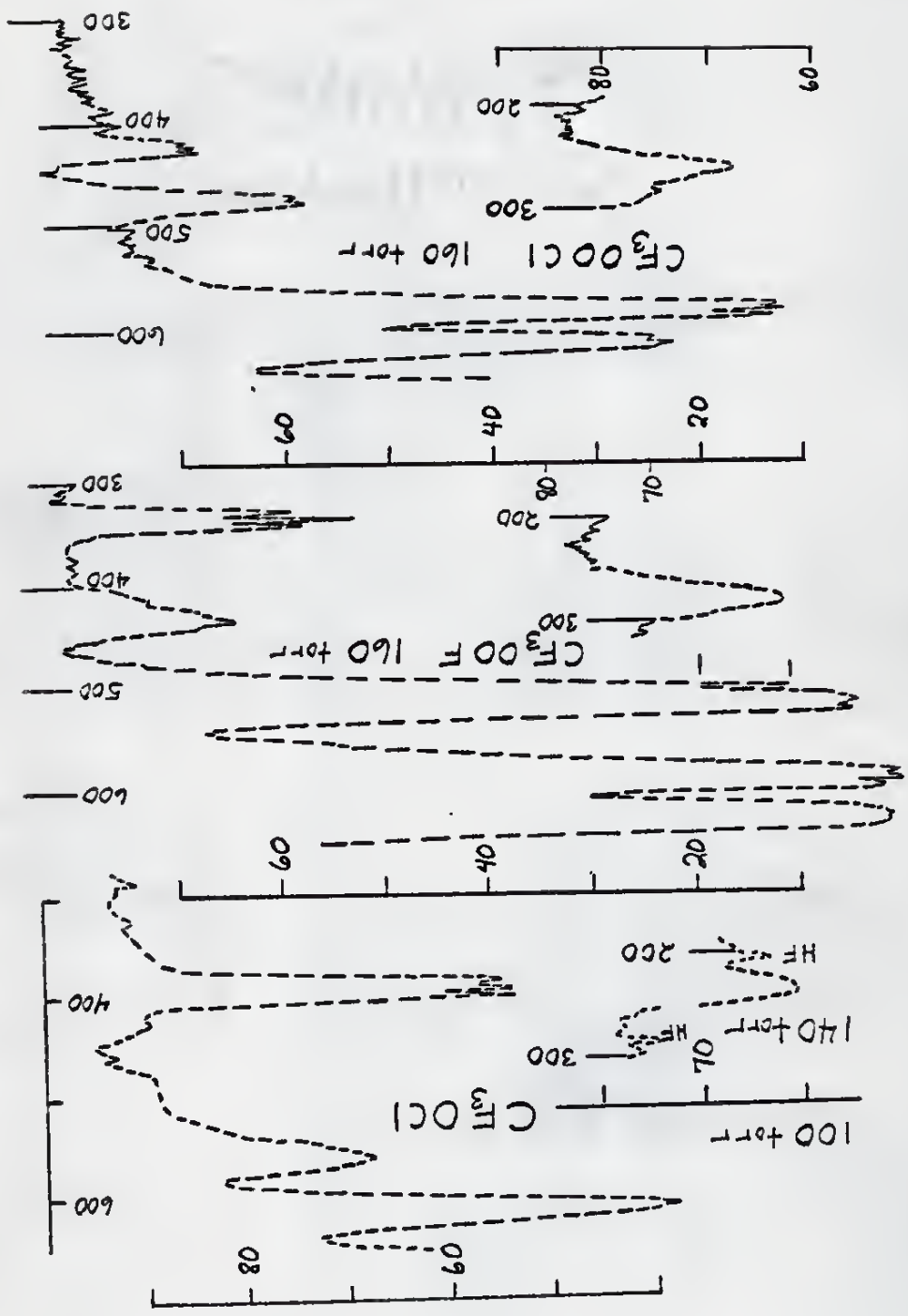

Figure A-6

Appendix B

Calculation of Torsional Barriers from Torsional Force Constants

The general term in the full form of the potential energy as a function of the internal torsional angle, τ, may be deduced from the expression on page 288 of the second item in reference (32) to be:

$$V(\tau) = \frac{V_n}{2}(1 - \cos(n\tau)) \tag{1}$$

For small values of the angle, x, a Maclaurin series expansion of cos(x) reduces to $\cos(x) = 1 - x^2/2$ or $1 - \cos(x) = x^2/2$. Thus, for small values of the torsional angle, τ, equation (1) becomes:

$$V(\tau) = Vn\,(n/2)^2\tau^2 \tag{2}$$

A simple harmonic potential where k_τ is a torsional force constant may be written as:

$$V(\tau) = (k_\tau/2)\tau^2 \tag{3}$$

Equating the coefficients of like terms between equations (2) and (3) gives:

$$V_n = (2k_\tau/n^2) \tag{4}$$

For $V(\tau)$ in kcal mole^{-1} and τ in radians, the units of V_n must be kcal mole^{-1} rad^{-2}. If k_τ is in units of mdyne Å rad^{-2} molecule^{-1}, a conversion factor of 287.9 must repalce the "2" on the right hand side of equation (4). This conversion factor is $2\text{x}1.439^{+}\text{x}10^2$ and the $1.439^{+}\text{x}10^2$ arises as follows:

(mdyne Å/rad^2 molecule) x (dyne/10^3 mdyne) x (cm/10^8 Å) x
(6.022x10^{23} molecules/mole) x (erg/dyne-cm) x (joule/10^7 erg) x
(cal/4.184 joule) x (kcal/10^3 cal) = 1.439^{+}x10^2 kcal mole^{-1} rad^{-2}

Thus, 1 mdyne Å rad^{-2} molecule^{-1} is equivalent to 1.439^{+}x10^2 kcal mole^{-1} rad^{-2}. The final working equation is:

$$v_n(\text{kcal mole}^{-1}\ \text{rad}^{-2}) = (287.9/n^2)k_\tau(\text{mdyne Å rad}^{-2}\ \text{molecule}^{-1}) \qquad (5)$$

The use of this equation with the force constant values in this work requires consideration of the details of the GMAT program (19) used in the normal coordinate analysis. For the CF_3 torsion where n = 3, the substitution n = 3 has already been taken into account in GMAT by having three rows for the τ_1 coordinate so n = 1 must be used to give $V_3 = 287.9k_\tau$ in equation (5). In the normal coordinate analysis done by Dr. Marsden at the University of Michigan the τ_1 values were nine times the values in Tables 9 and 16 and n = 3 would be used in equation (5). For the OX torsion GMAT has only one row for the τ_2 coordinate so n = 2 is used in equation (5) to give $V_2 = (287.9/4)k_\tau$. The V_3 and V_2 values calculated from equation (5) are presented in Table 16. This treatment contains the assumption that the torsional mode is 100 percent pure. Consequently, the results in Table 16 are only an approximation.

LITERATURE CITED

Gas Phase Raman Spectra of Some CF_3OOX Compounds (X = H,D,F,Cl)

1. R.L. Talbott, J. Org. Chem., 33, 2095 (1968).
2. P.A. Bernstein, F.A. Hohorst, and D.D. DesMarteau, J. Am. Chem. Soc., 93 3882 (1971).
3. D.D. DesMarteau, Inorg. Chem., 11, 193 (1972).
4. C.T. Ratcliffe, C.V. Hardin, L.R. Anderson, and W.B. Fox, J. Am. Chem. Soc., 93 3886 (1972).
5. N. Walker and D.D. DesMarteau, J. Am. Chem. Soc., 97,13 (1975).
6. P.A. Bernstein and D.D. DesMarteau, J. Fluorine Chem., 2, 315 (1973).
7. F.A. Hohorst and D.D. DesMarteau, Inorg. Chem., 13,715 (1974).
8. L.R. Anderson and W.B. Fox, J. Am. Chem. Soc., 89,4313 (1967); P.G. Thompson, ibid., 89,4316 (1967).
9. F.A. Hohorst, D.D. DesMarteau, L.R. Anderson, D.E. Gould, and W.B. Fox, J. Am. Chem. Soc., 95, 3866 (1973).
10. F.A. Hohorst and D.D. DesMarteau, J. Chem. Commun., 386, 1973 .
11. F.A. Hohorst, J.V. Paukstelis and D.D. DesMarteau, J. Org. Chem., 39,1298 (1974).
12. J.D. Witt, J.R. Durig, D.D. DesMarteau, and R.M. Hammaker, Inorg. Chem., 12, 807 (1973).
13. D.D. DesMarteau and R.M. Hammaker unpublished studies.
14. C.J. Marsden, D.D. DesMarteau, and L.S. Bartell, Inorg. Chem. 16, 2359 (1977).
15. R.R. Smardzewski and W.B. Fox, J. Fluorine Chem., 6, 417 (1975).
16. R.M. Hammaker and D.D. DesMarteau, Paper 451 Pittsburgh Conference on Analytical Chemistry and Applied Spectroscopy, Cleveland, Ohio, March 1976.

17. H.H. Claassen, H. Selig, and J. Shamir, Appl. Spectroacopy, 23, 8, 1969).

18. Jeng-chung Kuo, M.S. Thesis, Kanaas State University, Manhattan, Kansas (1978).

19. J.H. Schachtschneider, "Vibrational Analysis of Polyatomic Molecules V and VI," Tech. Repts No. 231-64 and 57-65, respectively, Shell Development Co., Houston, Texas.

20. P.M. Wilt and E.A. Jones, J. Inorg. Nucl. Chem., 30, 2933 (1968).

21. C.J. Schack and W.Maya, J. Am. Chem. Soc., 91, 2902 (1969).

22. J.D. Witt and R.M. Hammaker, J. Chem. Phys., 58, 303 (1973).

23. F.P. Diodati and L.S. Bartell, J. Mol. Structure, 8, 395 (1971).

24. J.R. Durig, W.E. Bucy, L.A. Carreira, and C.J. Wurrey, J. Chem. Phys., 60, 1754 (1974); J.R. Durig, W.E. Bucy, and C.J. Wurrey, J. Chem. Phys., 60, 3293 (1974); J.R. Durig, W.E. Bucy, C.J. Wurrey and L.A. Carreira, J. Phys. Chem., 79, 988 (1975).

25. R.M. Hammaker and D.D. DesMarteau, Raman Newsletter, 80, 7, August 1975.

26. P. Buckley and J.P. Weber, Can. J. Chem., 52, 942 (1974).

27. E.C. Tuazon, W.G. Fateley, and F.F. Bentley, Appl. Spectroacopy, 25, 374 (1971).

28. A.J. Melveger, L.R. Anderson, C.T. Ratcliff and W.B. Fox, Appl. Spectroscopy. 26, 381 (1972).

29. R.N. Dixon, J. Chem. Phys., 31 258 (1959).

30. E.L. Saier, L.R. Cousins, and M.R. Basila, J. Phys. Chem., 66, 232 (1962).

31. B.P. Stoicheff, Adv. Spectroscopy, 1, 91 (1959).

32. W.G. Fateley and F.A. Miller, Spectrochim Acta, 17 857 (1961); W.G. Fateley, F.A. Miller, and R.E. Witkowski, Technical Report AFML-TR-66-408, Air Force Materials Laboratory, Wright-Patterson Air Force Base, Ohio 45433.

33. M.M. Rochkind and G.C. Pimentel, J. Chem. Phys., 42, 1361 (1965).

34. L. Pierce, R. Jackson, and N. DiCianni, J. Chem. Phys., 35, 2240 (1961).

35. K.R. Loos, C.T. Goetschel, and V.A. Campanile, J. Chem. Phys., 52, 4418 (1970).

36. E. Hirota, J. Chem. Phys., 28,839 (1958); R.L. Redington, W.B. Olson, and P.C. Cross, J. Chem. Phys., 36, 1311 (1962).

37. A. Ruoff, H. Bürger, and S. Biedermann, Spectrochim. Acta, 27A 1359 (1971); R.W. Kirk and P.M. Wilt, J. Mol. Spectroscopy, 58, 102 (1975).

38. A. Müller and B. Krebs, J. Mol. Spectroscopy, 24, 180 (1967); B. Krebs, A. Müller, and A. Fadini, J. Mol. Spectroscopy, 24, 198 (1967); J.L. Duncan and I.M. Mills, Spectrochim. Acta, 20, 1089 (1964).

39. Page 28 in Tech. Report No. 57-65 reference 19.

40. H. Fuhrer, V.B. Kartha, K.G. Kidd, P.J. Kruger, and H.H. Mantsch, Computer Programs for Infrared Spectrophotometry XXXIX-XLI Volume V Normal Coordinate Analysis, National Research Council of Canada, N.R.C.C. Bulletin No. 15 (1976). pp 189-192.

41. J.R. Durig and D.W. Wertz, J. Mol. Spectroscopy, 25, 467 (1968).

ACKNOWLEDGEMENTS

I express deep appreciation to Professor Robert M. Hammaker for his guidence, energy, advice and valuable time during the course of this study.

I wish to express my gratitude to Dr. William G. Fateley for his guidance, support and invaluable encouragement during the course of this study.

I greatly acknowledge the contributions, help and advice of Dr. Darryl D. DesMarteau for doing the experimental work in this study. I am grateful to the members of my graduate committee for their cooperation and patience.

Thanks are due to Mr. Al Nielson for his excellent help and tremendous abilities to construct scientific instruments:
Mr. Mitsugi Ohno for his excellent glass design and work.

Acknowledgement is made to Kansas State University and to the United States Air Force, Wright - Patterson Air Force Base, for their financial support.

Finally, I wish to dedicate my work to my loving wife, Vanita and daughter, Monica.

VITA

The author was born on 2nd January 1950 in New Delhi, India.

He obtained his B.S. degree in Chemistry from University of Delhi, India in 1969 and then worked as Production/Research Chemist in D.C.M. Chemical works, New Delhi (India). He started his graduate study at Kansas State University in September 1974 and currently working towards his Ph.D. degree.

He is a member of American Chemical Society, Phi Lambda Upsilon and Society for Applied Spectroscopy.

1. SAMPLE ILLUMINATION OPTICS FOR RAMAN SPECTROSCOPY

by

AJIT SINGH MANOCHA

B.S. University of Delhi, 1969

AN ABSTRACT OF A MASTER'S THESIS

submitted in partial fulfillment of the

requirements for the degree

MASTER OF SCIENCE

Department of Chemistry

KANSAS STATE UNIVERSITY
Manhattan, Kansas

1978

ABSTRACT

1. Sample Illumination Optics for Raman Spectroscopy

Raman spectroscopy, being one of the most important tools for structural elucidation, has been of great interest to the fluorine chemistry group at Kansas State University. A Spex 14018 Double Monochromator and a detection system based on the RCA C31034 photomultiplier tube and Princeton Applied Research Model 1140AC Quantum Photometer were purchased. The sample illumination optics system was built in the Department of Chemistry shop.

The sources, prices and descriptions of various commercially available components have been listed. The designs of various parts of the sample illumination optics are presented in detail.

The completed system for Raman spectroscopy shows satisfactory performance for solids, liquids, and gases. Some examples are presented.

II GAS PHASE RAMAN SPECTRA FOR SOME CF_3OOX COMPOUNDS (X = H,D,F, AND Cl)

by

AJIT SINGH MANOCHA

B.S. University of Delhi, 1969

AN ABSTRACT OF A MASTER'S THESIS

submitted in partial fulfillment of the

requirements for the degree

MASTER OF SCIENCE

Department of Chemistry

KANSAS STATE UNIVERSITY
Manhattan, Kansas

1978

ABSTRACT

II Gas Phase Raman Spectra of Some CF_3OOX Compounds (X = H,D,F,Cl)

A major interest of the fluorine chemistry group at Kansas State University is the synthesis, physical properties, and reactions of fluorinated polyoxides. The CF_3OOX series is of particular concern because these compounds serve as the key reagents for the synthesis of many other highly fluorinated peroxides. Consequently, a detailed structural study of some CF_3OOX compounds was made including electron diffraction and the vibrational spectra reported here for the X = H, D,F,Cl members of the series.

The Raman spectra of liquid CF_3OOX compounds in a low temperature cell of conventional design and gaseous CF_3OOH and CF_3OOF in a conventional gas cell have been obtained using a Spex 14018 Double Monochromator and Spectra Physics Models 164 Ar^+ laser and 375 CW dye laser. The gas phase infrared spectra of these compounds in cells with AgCl and polyethylene windows were recorded from 4,000 to 160 cm^{-1} using a Perkin-Elmer Model 180 Infrared Spectrophotometer.

Assignments have been made to almost all the observed frequencies. Gas phase Raman spectra assist in assignments for CF_3 torsions and OX torsions and indicate significant frequency shifts on phase change for these modes consistent with CF_3OX compounds. Observed frequencies assigned to torsions are believed to correspond to $\Delta v = 1$ transitions rahter than $\Delta v = 2$ transitions. Normal modes expected to be common to all series members are assigned as follows: CF_3 stretching 1150 - 1300 cm^{-1}, CF_3 deformation 580 - 695 cm^{-1}, CF_3 rocking 250 - 300 cm^{-1} and 420 - 520 cm^{-1}, OO stretching 825 - 875 cm^{-1}, COO bending 420 - 445 cm^{-1}.

For the CF_3 torsion the range is $\sim$ 140 - 160 cm^{-1} (H,D), $\sim$70 - 80 cm^{-1} (F,Cl). Normal modes involving the O-X group are assigned as follows: stretching: OH $\sim$ 3575 cm^{-1}, OD $\sim$2640 cm^{-1}, OF $\sim$ 750 cm^{-1}, OCl $\sim$ 695 cm^{-1}; bending OOH $\sim$ 1385 cm^{-1}, OOD $\sim$ 1035 cm^{-1}, OOF $\sim$ 340 cm^{-1}, OOCl $\sim$ 295 cm^{-1}; torsions: OH $\sim$ 245 cm^{-1}, OD $\sim$ 179 cm^{-1}, OF $\sim$ 130 - 150 cm^{-1}, OCl $\sim$ 50 cm^{-1}??.

Final normal coordinate analysis was done at Kansas State University The electron diffraction study and preliminary normal coordinate analysis was done at the University of Michigan. The choices of fundamental frequencies were consistent with the normal coordinate analysis. However, the conventional designations for the normal modes appeared to be misleading descriptions of the motion for some normal modes.